

# Computer-Assisted Surgery of the Skull Base

Contributions to Guidance and Imaging



Brain Center  
Rudolf Magnus

Eduard Voormolen

# **Computer-Assisted Surgery of the Skull Base**

## **Contributions to Guidance and Imaging**

Eduard Voormolen

© E.H.J. Voormolen, Utrecht 2018 All rights reserved

ISBN: 978-94-6233-983-5

Cover: Photograph by Eduard Voormolen, an observer's view of the surgical field during a clinical experiment with EVADE

Designed and printed by: Gildeprint Drukkerijen

The printing of this thesis was financially supported by:

Wetenschappelijke Vereniging Neurochirurgen Utrecht, Brain Technology Institute, Brain Center Rudolf Magnus, Zeiss, Krijnen Medical, ChipSoft, ABN Amro Bank

# **Computer-Assisted Surgery of the Skull Base**

## **Contributions to Guidance and Imaging**

Computer Geassisteerde Schedelbasis Chirurgie:  
Bijdragen aan Beeldgeleiding en Beeldvorming

(met een samenvatting in het Nederlands)

Proefschrift ter verkrijging van de graad van doctor aan de Universiteit Utrecht  
op gezag van de rector magnificus, prof. dr. H. R. B. M. Kummeling,  
ingevolge het besluit van het college voor promoties  
in het openbaar te verdedigen  
op dinsdag 10 juli 2018 des ochtends te 10.30 uur.

door

Eduard Hendrik Joannes Voormolen  
geboren op 21 februari 1983  
te Leiden

Promotoren: Prof. dr. P. A. Robe  
Prof. dr. M. A. Viergever

Copromotoren: Dr. J.W. Berkelbach van der Sprenkel  
Dr. H.J. Noordmans

*Aan Anna Kalová, moje babička*



## Table of Contents

<b>Chapter 1:</b>	General Introduction	9
<b>Chapter 2:</b>	Determination of a Facial Nerve Safety Zone for Navigated Temporal Bone Surgery	19
<b>Chapter 3:</b>	Validation of Exposure Visualization and Audible Distance Emission for Navigated Temporal Bone Drilling in Phantoms	39
<b>Chapter 4:</b>	Benchmarking Distance Control and Virtual Drilling for Lateral Skull Base Surgery	63
<b>Chapter 5:</b>	Distance Control and Virtual Drilling Improves Anatomical Orientation during Anterior Petrosectomy	87
<b>Chapter 6:</b>	Implications of Extracranial Distortion in Ultra-High Field MRI for Image-Guided Cranial Neurosurgery	105
<b>Chapter 7:</b>	Summary & Discussion - A Manifesto for Computer Assisted Surgery of the Skull Base	121
<b>Appendix</b>	Nederlandse Samenvatting	135
	List of Publications	139
	Dankwoord	141
	Curriculum Vitae	147





# 1

## General Introduction



## General Introduction

The goal of this introduction is to provide fundamental information about the anatomy and concepts relevant to this thesis, while simultaneously providing a concise history of computer assisted surgery and skull base surgery. Moreover, the aims of this thesis are outlined.

The skull base is the most inferior area of the skull, composed of the endocranium and lower parts of the skull roof, on top of which the brain and the brain stem rests. It is generally known as a complex anatomical area because many important (cranial) nerves and blood vessels traverse the skull base.

The skull base is divided in anterior, lateral and posterior parts. This thesis will be mainly concerned with the lateral skull base, which consist for a large part of the temporal bone. The temporal bone is composed of four parts: the squamous, mastoid, petrous and tympanic bones. Of particular interest in this thesis is the mastoid (Chapter 3 and 4) and petrous bone (Chapter 5). Figure 1 illustrates this anatomy.

The lateral skull base is the habitat of both benign and malignant tumors. Tumors can occur extracranially inside the temporal bone (e.g. cholesteatoma and cholesterol granuloma), or intracranially, in spaces such as the cerebellopontine angle and petroclival area (e.g. schwannoma and meningioma).

Treatment of these tumors is a multi-disciplinary medical effort which combines the skills of neurosurgery, otolaryngology, radiation oncology, radiology, anesthesia, intensive care medicine, and physical and rehabilitative medicine. Therefore, treatments are usually only performed in centers which can offer such care through a skull base team.

Lateral skull base tumors are treated with either surgery or radiotherapy, or a combination of both modalities. Currently, drug therapies have a subsidiary role in treatment. The goal of radiotherapy (or radiosurgery) is to stop further tumor growth. The goal of surgery is tumor removal or tumor mass reduction and obtaining a tissue diagnosis. The process of lateral skull base surgery can be divided into two distinct surgical stages. First, drilling an approach through the bone of the skull base, and second, removal of the tumor. During drilling, the aim is to create a large enough bony exposure to facilitate tumor removal, while preventing iatrogenic injury to important normal anatomical structures which traverse the bone (e.g. the facial nerve, the sigmoid sinus, the cochlea, and the internal carotid artery).

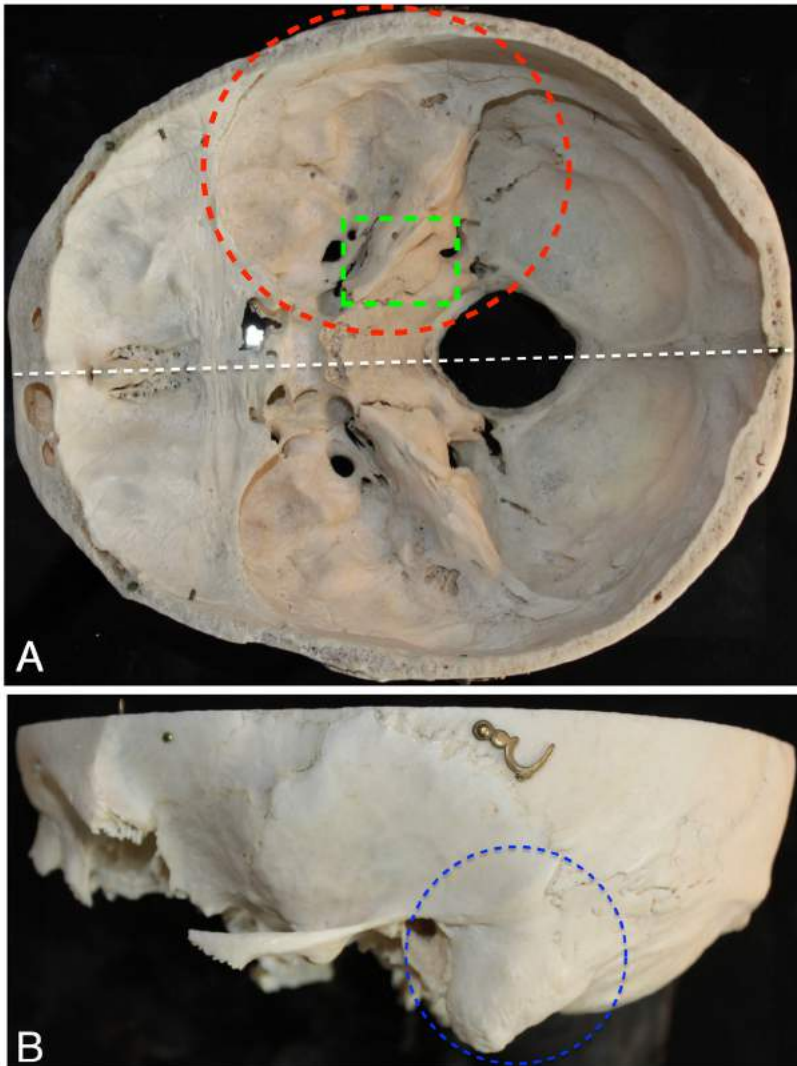


**Figure 1.1: Skull Base Anatomy**

This Figure displays the bone anatomy of interest in this thesis. Frame A shows the inner skull base from a superior view. The white line stresses the left-right symmetry present in the skull base (relevant for Chapter 5). The red circle designates the lateral skull base. The green square indicates the petrous bone (Chapter 5).

Frame B shows the left lateral skull base from a lateral view. The blue circle contains the mastoid portion of the temporal bone (Chapters 3-4).

Legend:

A = anterior

Ca = caudal

Cr = cranial

L = left

R = right

P = posterior

Considering surgery in general, localization of a tumor within the human body, with the aim that it can be approached and removed without damage to surrounding normal tissues, is essential. Especially in complex and delicate anatomical areas, such as the lateral skull base, precise localization of tumor with respect to important normal anatomical structures is of importance for successful surgery. Therefore, the maturation of surgery of the skull base as a specialty, and innovations in localization technology have gone hand-in-hand.

Before the invention of X-rays in the 1890s, skull base tumor localization was based on the patients' symptoms correlated with anatomical atlases based on dissections. In the early 20th century, two-dimensional air-injected X-ray images of the skull (pneumoencephalography) improved tumor localization. The birth of 'digital imaging', or computer-based three-dimensional X-ray imaging (i.e. computed tomography or CT), in the early 1970s, was probably the most important innovation with regards to anatomical localization. Furthermore, the ongoing development of magnetic resonance imaging (MRI) since the 1980's, provides ever improving soft tissue contrast in images, making localization increasingly accurate.

The advantage of modern digital image acquisition techniques, such as CT and MRI, is that besides tumor localization, the normal anatomical structures around the tumor and along potential surgical approaches, are imaged simultaneously. Another advantage is that these images can be analyzed after acquisition with image segmentation methods, to further improve anatomical localization. Image segmentation is the process of partitioning a digital image into multiple segments. Since the invention of digital imaging, segmentation methods are continually developed and refined to locate anatomical structures within images (e.g. tumor vs normal tissue) with increasing accuracy. Chapter 2 provides an example of a new segmentation method.

In the early 20th century, neurosurgeons developed stereotaxy (from Greek: στερεος = three-dimensional, τασσω = to probe). Stereotaxy is the application of mathematical methods to anatomy: a method of assigning a (three-dimensional) coordinate system to a volume of anatomy. The goal of applying stereotaxy during surgery, is to be able to locate items within the anatomical volume (e.g. normal structures vs. tumor). In the early days, stereotaxy was based on anatomical atlases. With the invention of digital imaging it became possible to relate a coordinate system imposed on a patient's cranium, usually in the form of a metal frame fixed to the skull, to an image volume of that patient's specific anatomy. Because frame-based stereotaxy suffered from practical inconveniences during surgery, technology was developed to surgically apply frameless stereotaxy, in the mid-eighties of the 20th century [1].

Frameless stereotactic surgery works by mathematically co-registering a coordinate system applied to a patient's cranium through a reference arc, to the coordinate system of a pre-operatively acquired image on the basis of corresponding sample points or surfaces (i.e. patient-image registration). The positions of the reference arc and surgical tools in the operating room are measured in real-time by either infrared optical tracking (passive or active), or by electromagnetic triangulation. The positions are transferred to a computer which calculates the co-registration, and subsequently displays the anatomical image and image positions of surgical tools on a screen during surgery.

Since the inception of frameless stereotactic surgery, more than three decades of refinements in its hardware and software have passed. It is nowadays better known as 'neuronavigation', or more generally, as 'image guidance'. Image guidance is considered to be one of several components of computer assisted surgery, as will be explained below.

The described advancements in imaging and image guidance improved tumor and healthy tissue localization over the last forty years, and by that means were key to the rise of lateral skull base surgery. Moreover, these computer-based innovations occurred in synergy with numerous other inventions: vascular reconstruction techniques for bypass [2], cranial nerve grafting repair [3], innovations in closure techniques to prevent cerebrospinal fluid leaks [4], introduction of the endoscope [5], and the gradual realization that sub-maximal tumor resection leads to improved patient outcomes even in the best of hands, especially when combined with radiosurgery.

All in all, before the 1970s, a skull base tumor implied for the majority of patients a poor prognosis, leading to severe functional impairment and probable death, either from natural progression or surgical efforts. Today, patients treated for lateral skull base tumors have near normal life expectancies in the majority of cases [6]. However, preventing iatrogenic morbidity (e.g. neurologic deficits such as cranial nerve palsy) due to surgery, remains a crucial issue [7]. It is the primary concern of this thesis.

The chief hypothesis of this thesis is that application of computer assistance during skull base surgery reduces iatrogenic morbidity. Accordingly, the overall aim of this thesis is to improve the standard of care of patients with lateral skull base tumors by advancing the field of Computer Assisted Surgery of the Skull Base (CASSB).

In general, within the scientific field of CASSB, nine principal components of investigation can be identified:

- 1) Preoperative Imaging
- 2) Treatment planning
- 3) Decision making
- 4) Patient-Image Registration
- 5) Patient positioning
- 6) Execution of surgery
- 7) Image Guidance
- 8) Intraoperative imaging
- 9) Follow-up Imaging

## **This Thesis**

The scientific objective of this thesis is to present improvements in preoperative imaging and image guidance.

### **Contributions to Preoperative Imaging**

Chapter 2 discusses NerveClick, a semi-automated segmentation technique of the facial nerve centerline in high resolution CT-images, specifically developed for lateral skull base surgery. Chapter 6 describes the evaluation of the spatial accuracy of ultra-high field 7T MRI images for patient-image registration and image guidance.

### **Contributions to Image Guidance**

Chapters 3-5 describe the development and evaluation of EVADE. EVADE is novel software incorporating segmentation methods (e.g. NerveClick) to pre-operatively segment normal anatomical structures in the (lateral) skull base and has an active assistance function that augments image guidance with audiovisual feedback. Its key feature is that it pro-actively warns when the surgeon is drilling in too close proximity of a segmented normal anatomical structure.

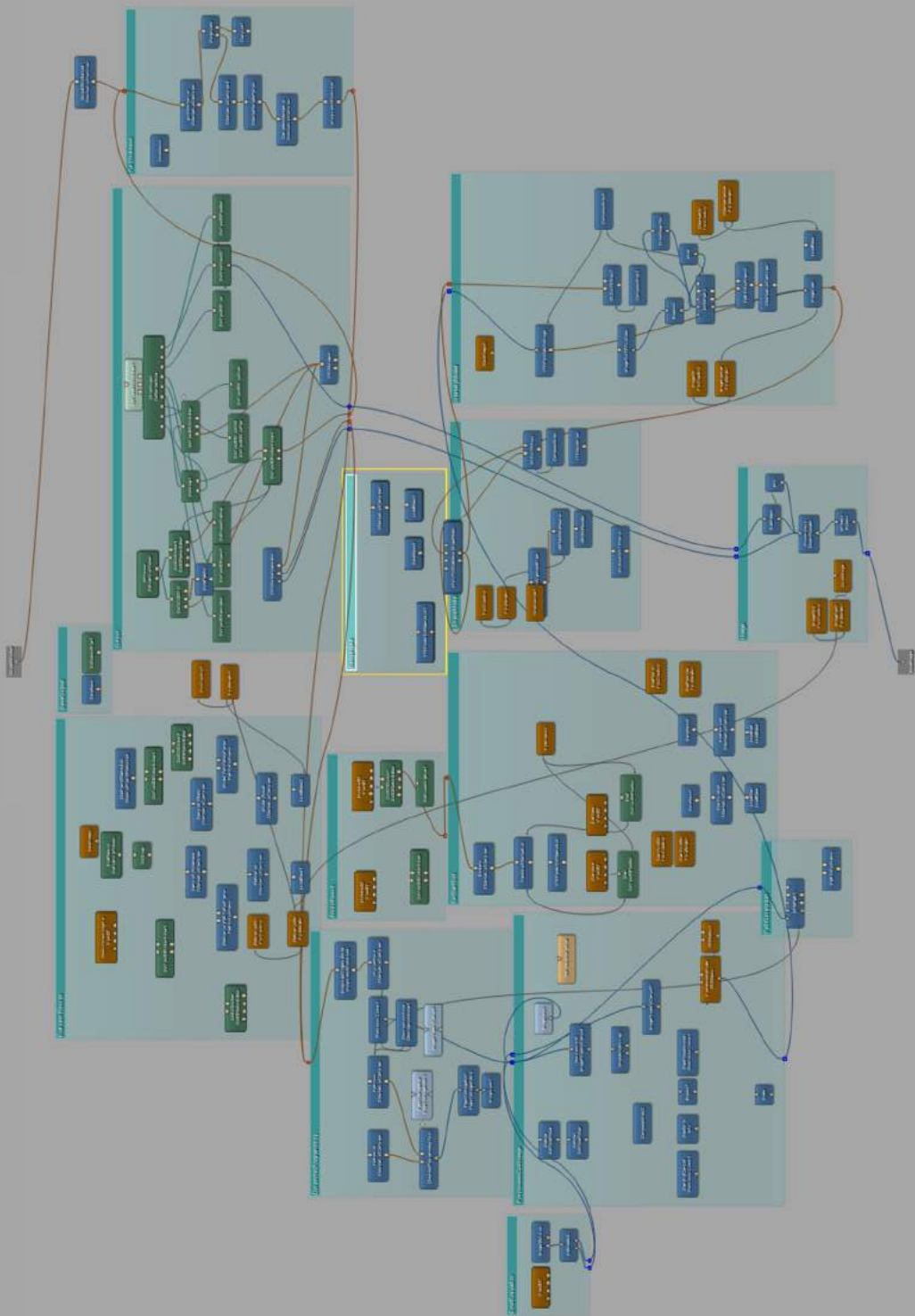
Chapter 7 summarizes the thesis and outlines the principal author's vision for the future of CASSB, describing how the role of the computer should be changed from a passive assistant during surgery to a full-fledged 'member' of the multidisciplinary skull base team.



## References

1. Woerdeman PA: Frameless image-guided neurosurgery in motion. 2008 PhD Thesis University of Utrecht
2. Kalavakonda C, Sekhar LN: Cerebral revascularization in cranial base tumors. *Neurosurg Clin N Am* 12:557–574, viii–ix, 2001
3. Sekhar LN, Lanzino G, Sen CN, Pomonis S: Reconstruction of the third through sixth cranial nerves during cavernous sinus surgery. *J Neurosurg* 76:935–943, 1992
4. Jones NF, Schramm VL, Sekhar LN: Reconstruction of the cranial base following tumour resection. *Br J Plast Surg* 40:155–162, 1987
5. Jho HD, Carrau RL: Endoscopic endonasal transsphenoidal surgery: experience with 50 patients. *J Neurosurg* 87:44–51, 1997
6. Di Maio S, Ramanathan D, Garcia-Lopez R, Rocha MH, Guerrero FP, Ferreira M, et al: Evolution and Future of Skull Base Surgery: The Paradigm of Skull Base Meningiomas. *World Neurosurgery* 78:260–275, 2012
7. Schick B, Dlugaczky J: Surgery of the ear and the lateral skull base: pitfalls and complications. *GMS Curr Top Otorhinolaryngol Head Neck Surg* 12:2013 Available: <https://www.ncbi.nlm.nih.gov/pmc/articles/PMC3884540/>.





## **Determination of a Facial Nerve Safety Zone for Navigated Temporal Bone Surgery**

***Authors:***

Eduard H. J. Voormolen, Marijn van Stralen, Peter A. Woerdeman, Josien P.W. Pluim, Herke Jan Noordmans, Max A. Viergever, Luca Regli, Jan Willem Berkelbach van der Sprenkel

Based on the publication in:  
Neurosurgery 2012 70[ONS Suppl 1]:ons50–ons60

## Abstract

**Background:** Trans-temporal approaches require surgeons to drill the temporal bone to expose target lesions while evading critical structures contained within it: the facial nerve and other neurovascular structures. We envision a novel protective neuronavigation system that continuously calculates the 'drill-tip-to-facial nerve' distance intra-operatively and produces audiovisual warnings if the surgeon drills too close to the facial nerve. Two major problems need to be solved before such a system can be realized.

**Objective:** Solving the problems of 1) facial nerve segmentation and 2) calculating a safety zone around the facial nerve in relation to drill tip tracking inaccuracies.

**Methods:** We specially developed a new algorithm, called NerveClick, for semi-automatic segmentation of the intra-temporal facial nerve centerline from temporal bone CT images. We evaluated NerveClick's accuracy in an experimental setting on healthy, neuro-otologic and neurosurgical patients. Three neurosurgeons used it to segment 126 facial nerves, which were compared to the gold standard: manually segmented facial nerve centerlines. The centerlines are used as a central axis around which a tubular safety zone is build. The zone's thickness incorporates the drill tip tracking errors. The system will warn when the tracked tip crosses the safety zone.

**Results:** Neurosurgeons using NerveClick could segment facial nerve centerlines with a maximum error of  $0.44 \pm 0.23$  mm (mean standard deviation) on average compared to manual segmentations.

**Conclusion:** Neurosurgeons using our new NerveClick algorithm can robustly segment facial nerve centerlines to construct a facial nerve safety zone, which potentially allows timely audiovisual warnings during navigated temporal bone drilling despite tracking inaccuracies.

## Introduction

During temporal bone approaches, the skull base surgeon drills the temporal bone to expose target pathology in the cerebellopontine angle or petrous apex. Meanwhile, the surgeon aims to preserve critical structures like the sigmoid sinus, jugular bulb, and facial nerve. It can be challenging to maintain optimal orientation during drilling due to high variation in temporal bone anatomy [1], and the fact that surgical landmarks are frequently eroded by inflammation, tumor, or previous surgery. Diminished orientation entails a higher risk of harming critical structures.

Fortunately, neuronavigation offers skull base surgeons modern means of improving their intra-operative orientation [2] by showing the position of a pointer on a scan of the patient's anatomy acquired pre-operatively. Such usage of navigation has led to improved surgical confidence [3-6] and increased speed of surgery [3,4].

Additionally, neuronavigation technology can be used in another way: the surgeon delineates important structures within pre-operative scans and the navigator tracks the tip of a surgical instrument showing its position in relation to these delineated structures. Such usage is useful to help surgeons evade vital structures during temporal bone drilling. Thus, we envision enhancing standard neuronavigation with a protective warning system that continuously calculates the 'drill tip to critical structure' distance and gives off audiovisual warnings notifying the surgeon when he/she is drilling in (too) close proximity to the structure.

At the moment, however, there are two practical problems that hamper such an audiovisual warning framework from being build. First, delineation, or segmentation, of vital structures on commercially available neuronavigation systems can generally only be performed by either using simple techniques (e.g. intensity thresholding) which are insufficient for segmentation of complex temporal bone structures, or by manually drawing around the structures of interest which is time consuming and labor intensive. Second, even in the temporal bone, where tissue shift that notoriously hampers navigation accuracy intracranially [5-8] is non-existent, neuronavigation suffers from position-tracking inaccuracies [2,9,10], which prevent clinically reliable warnings when nearing critical structures because of inaccurate 'drill tip to critical structure' distance calculation.

In this article we present solutions to these two problems for one of the temporal bone critical structures: the facial nerve. Our solutions will allow augmentation of standard neuronavigation with an audiovisual warning framework for the intra-temporal segment of the facial nerve.

We chose the facial nerve because clinically it is important to preserve the nerve during surgery; even minor structural damage to it causes significant morbidity to patients from resulting hemifacial paresis and its complications (e.g. synkinesis, corneal ulceration, drooling, and feeding and speech difficulties) [11]. Injuries to the intra-temporal part of the facial nerve still occur in our own experience and in other clinics [12,13], generally, in 3.6% of new surgical cases and 4 -10% of revision surgeries [14]. These injuries are often caused by aberrant facial nerve anatomy or dehiscence of the fallopian canal [15].

Moreover, technically, the facial nerve is probably the most challenging temporal bone structure to segment from temporal bone computed tomography (CT) scans. Segmentation is very difficult because the facial nerve is a structure with large inter-patient variation in shape and intensity, unclear edge definitions between structure and environment, changing intensity values along its structure and a complexly curved shape (Figure 1). Therefore, most available purely intensity based (e.g. region growing, simple snakes or level-set methods) or shape based (e.g. atlas mask projection) segmentation methods do not suffice. As was established previously by Noble et al. [18], prior information about the facial nerve's intensity pattern and shape needs to be incorporated: Noble et al. extended their 'standard' temporal bone atlas-based method with an optimal path finding algorithm using spatially dependent feature values based on a priori geometric information. Their resulting fully automatic full-structure facial nerve segmentation algorithm method performs well in anatomically unaltered temporal bones. However, since Noble et al.'s atlas and facial nerve geometric model were constructed with and evaluated on normal temporal bones [18], their method possibly will not work on neuro-otological and neurosurgical patients with skull base tumors and/or disrupted temporal bone anatomy.

Therefore, we propose and evaluate a new semi-automatic intra-temporal facial nerve centerline segmentation technique that uses a statistical model constructed with normal and pathologically altered temporal bones of the nerve's centerline shape and its surrounding image intensities (the texture), referred to as 'NerveClick' segmentation. Subsequently, we explain how the nerve's centerline is used to implement a safety zone that may allow for a reliable audiovisual warning system despite position tracking inaccuracies.

## Materials & Methods

This section will describe the methods needed to implement and evaluate the performance of the NerveClick segmentation algorithm. NerveClick is a semi-automated method that finds the facial nerve centerline after the user has designated the start and end point of the intra-temporal facial nerve by two mouse-clicks in a temporal bone CT scan.

### ***Model Training Population & Scan Parameters***

The NerveClick segmentation algorithm employs a statistical model that is based on facial nerves of twenty consecutive patients who received a temporal bone CT-scan over a two-month period in the end of 2008. Patients were at least 18 years of age. We included 8 female and 12 male patients, with a mean age of 53 years (range 23 – 86 years). Patients suffered from a variety of diseases; nine patients showed no structural abnormalities, eleven suffered from a broad spectrum of temporal bone deformations including fluid in mastoid cells, tumors with ingrowths in the mastoid and the fallopian canal, and one patient had received a mastoidectomy (Table 1). All patients were scanned according to the same CT protocol on a Philips single slice CT-scanner. Patients were positioned head first in the scanner and axial slices through the cranium were obtained from the cranial base caudally to the end of the mastoid part of the temporal bone cranially. Scan parameters were set to 120 kV and 400 mAs. This yielded images with a matrix size of 512x512x30 with voxels of 0.313 x 0.313 x 1.0 mm<sup>3</sup>.

### ***NerveClick Segmentation***

#### *NerveClick Facial Nerve Start and End Point Definition*

NerveClick segmentation is initiated by two mouse-clicks within the temporal bone CT scan; one at the start position where the intracranial facial nerve enters the fallopian canal through a small porus in the lateral part of the internal acoustic meatus, i.e. the very start of the labyrinthine segment of the facial nerve (Figure 1). And another at the end position where the mastoid section of the facial nerve leaves the mastoid bone through the stylomastoid foramen (Figure 1).

#### *NerveClick's Facial Nerve Model Construction*

NerveClick's statistical model construction involved several steps (explained in detail in Figure 2): First, after assuring low inter - and intra-rater variability (see below), one author trained in facial nerve anatomy by a radiologist specialized in temporal bone anatomy, manually segmented all forty facial nerves by drawing contours slice by slice. Second, centerlines from



these segmented facial nerves were obtained. Third, a statistical shape and texture model was constructed from the extracted centerline shapes and texture profiles (mirrored to incorporate all in one model). This model was used to find the facial nerve centerline of a new patient.

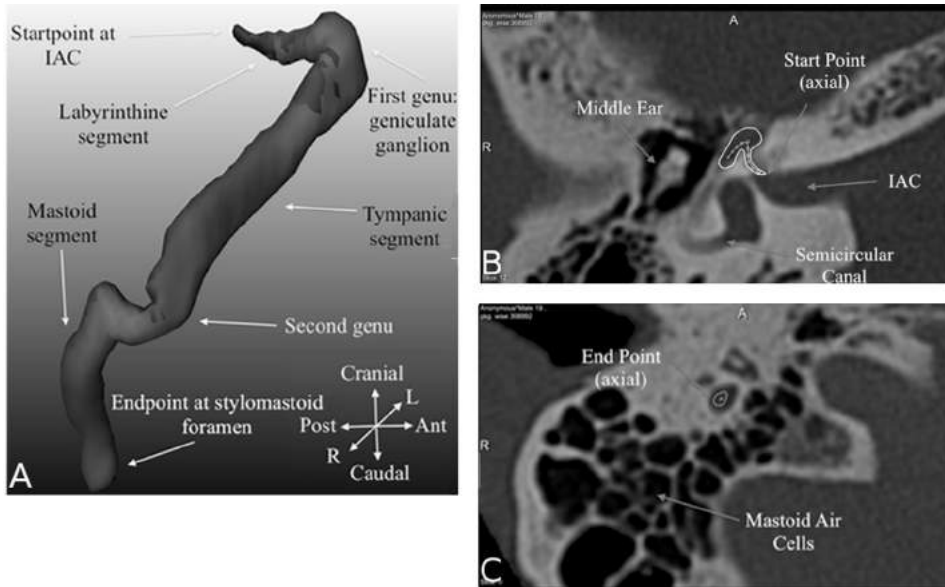


**Figure 2.1: Facial Nerve Anatomy and Start & End Point Definitions**

3D anatomy of the intra-temporal segment of the facial nerve (Figure 1A) surrounded by axial images showing where surgeons should designate the start point (Figure 1B) in the internal acoustic canal (IAC), and end point at the stylomastoid foramen (Figure 1C). Also note the manual facial nerve segmentation contours drawn on the axial slices with in the center the extracted centerline, used as gold standard in the evaluation and as a basis to build NerveClick’s model.

#### *NerveClick’s Facial Nerve Centerline Delineation in a New Patient*

To delineate the facial nerve centerline in a new patient, NerveClick begins with a rough estimate of the shape and subsequently optimizes this shape to eventually match the shape of the patient’s facial nerve centerline. The initial rough estimate was the model’s average facial nerve shape positioned between start and end points as designated by the surgeon’s mouse clicks. Then, a patient specific estimate was computed by looking for areas where the estimated texture corresponded best to the model’s average facial nerve texture. Subsequently, these improved estimates were restricted according to the statistical variation allowed by our model. These restricted shape and texture estimates were then used to compute a final unrestricted optimized facial nerve shape for the new patient. These steps are explained in detail in Figure 3. A detailed technical description of the NerveClick methodology is described in Voormolen et al. (2011) [16].

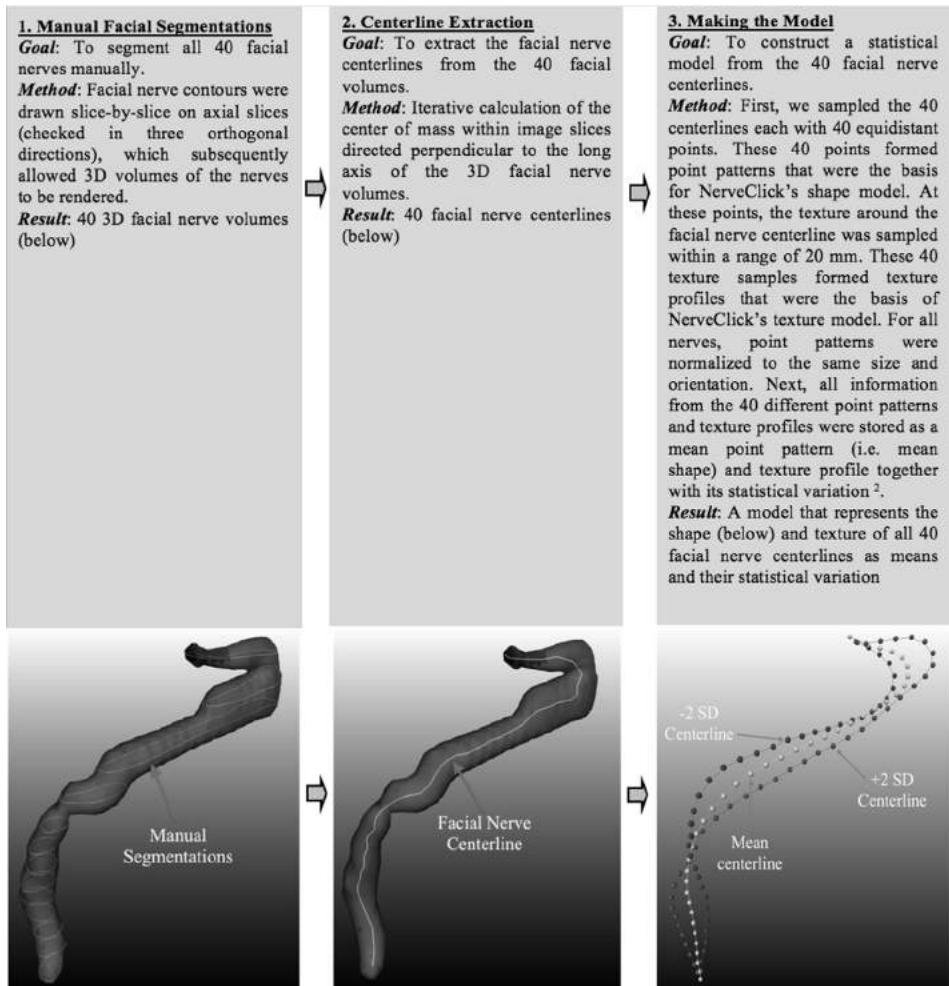
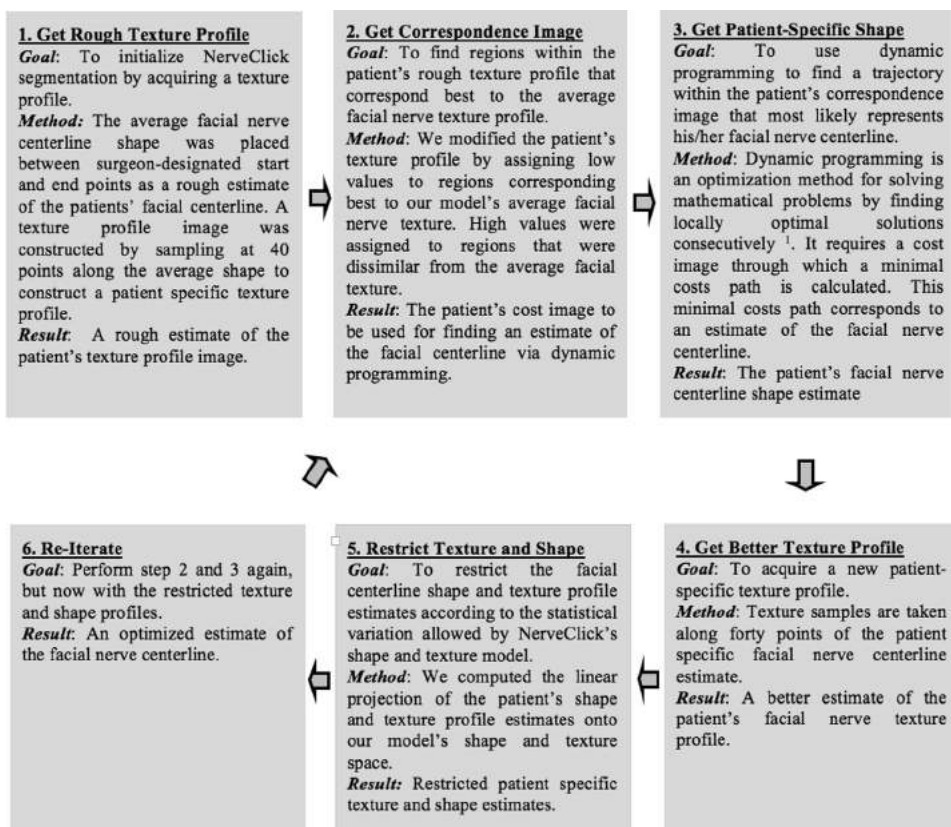


Figure 2.2: Constructing NerveClick's Statistical Model



**Figure 2.3: Performing NerveClick's Model-Based Facial Nerve Centerline Segmentation in a New Patient**

### *Intra- & Inter-rater Variability of Manual Segmentations for NerveClick's Model*

We assessed the intra- and inter-rater variability of the manual facial nerve centerline segmentations used for NerveClick's model in 5 patients (10 facial nerves). Facial nerves were manually drawn slice by slice and centerlines were extracted (as described in Figure 4, step 2) and subsequently compared in terms of root mean square difference and maximum difference. These measures are computed in the same fashion as the root mean square error and maximum error (see definitions below). A period of eight months passed between the first and second segmentation used to assess intra-rater variability. Inter-rater variability was evaluated between two raters: the principal author and a staff neurosurgeon (non-author).

### *Evaluation of NerveClick Performance*

We tested the performance of NerveClick facial nerve centerline segmentation by 'leave-one-out' cross-validation on our training population. This means that NerveClick's statistical model

was constructed using data from 38 facial nerves from 19 patients and we subsequently performed and evaluated the segmentation on the patient that was not included in the model. Three different neurosurgeons (two staff members and one resident) used our segmentation method to segment facial nerves in twenty patients. Beforehand, they received a brief instruction and saw one example of how to designate start and endpoints correctly. Each surgeon used NerveClick to segment 40 facial nerves, i.e. 120 segmentations were performed in total.

Additionally, a neurosurgeon used NerveClick on six extra test facial nerves to evaluate how the technique performs in patients with skull base tumors and/or with major disruption of the peri-facial nerve anatomy. These patients were scanned on other CT scanners with image acquisition parameters different from the training populations scans (Table 1 and Figure 6). Case 1 is a 56-year old male with a right-sided vestibular schwannoma likely to be scheduled for surgery. Case 2 is a 74-year old male presenting with a symptomatic petrous apex cholesterol granuloma on the left side. Case 3 is a 49-year old male with a large recurrence of a previously resected clear cell meningioma (World Health Organization grade II) of the left skull base. This patient had undergone an extended middle fossa approach previously. His temporal bone CT scan showed a beam-hardening artifact from a metal clip (clipping the superior petrosal sinus) in the temporal bone area. Case 4 is 50-year old male with a right-sided jugular paraganglioma invading the mastoid segment of the facial nerve canal. Case 5 is a 40-year old female who had previously undergone a right-sided translabyrinthine and retrosigmoid craniotomy for a large cholesteatoma. Case 6 is a 72-year old male that suffered high energy trauma and had a fracture of the right temporal bone traversing the facial nerve canal.

### *Segmentation Quality Measures*

The segmentation performance was quantified by comparing the centerlines found by our semi-automatic segmentation method to the gold standard, i.e. centerlines extracted from manual segmentations; both facial nerve centerlines were sampled with 500 equidistant points along their trajectory (achieving a sample resolution of approximately 0.05 mm) and the closest distance between points on the segmented centerline to points on the reference centerline was calculated in terms of 1) the *root mean square error (RMSE)* and 2) the *maximum error per centerline*. Lower error values correlate with better segmentation performance.

### *Manual Correction Option*

After the surgeons completed their segmentations, an expert observer (the principal author) evaluated their segmentations qualitatively by visually assessing whether the nerves were located exactly in the center of the fallopian canal. If the centerlines were judged even a

fraction off-center by the observer the surgeons had to manually correct their centerline. Manual correction was performed by dragging any of 40 equidistant markers spread along the segmented centerline to the desired position with the mouse in.

### *Software*

To develop the NerveClick segmentation algorithm we used and extended the MeVisLab visual programming environment (version 2.0, Mevis Medical Solutions, Bremen, Germany) available from [www.mevislab.de](http://www.mevislab.de).

## Results

### *Manual Segmentations to Build NerveClick's Facial Nerve Model*

The average time to segment one facial nerve manually was 92 minutes (mean standard deviation). Intra-rater variability assessment yielded an average root mean square difference of  $0.19 \pm 0.07$  mm with a maximum difference of  $0.37 \pm 0.15$  mm between manually obtained centerlines. Inter-rater variability evaluation showed an average root mean square difference of  $0.21 \pm 0.09$  mm and a maximum difference of  $0.38 \pm 0.14$  mm between manual segmentations of two neurosurgeons.

### *NerveClick Segmentation Performance*

Three different neurosurgeons used NerveClick to segment 40 facial nerves each. On average they took  $50 \pm 24$  seconds to select start and end points. It took on average  $70 \pm 2$  seconds of runtime to perform one NerveClick segmentation on a laptop computer (2.67 Ghz CPU, 2.0 GB RAM, 32-Bit Microsoft Windows). The expert observer judged parts of 31 of the 120 centerlines (26%) off center and therefore in need of manual correction (Figure 5). Inspection and manual correction of these 31 segmentations took on average  $57 \pm 35$  seconds. The surgeons' average RMSE with NerveClick (without manual correction) was  $0.28 \pm 0.17$  mm. The maximum error (without manual correction) measured along a centerline was on average  $0.42 \pm 0.22$  mm (Figure 4).

Additionally, for the six extra test cases with skull base tumors and/or with major disrupted temporal bone anatomy, the RMSE and maximum error (without manual correction) was  $0.38 \pm 0.08$  mm and  $0.78 \pm 0.23$  mm respectively (Table 2). Two of these six facial nerve centerlines (case 3 and 6) were judged partly off center and therefore needed manual correction.

### *Using NerveClick's Facial Nerve Centerline Segmentation for Determination of a Safety Zone*

The solution we present here uses the centerline of the facial nerve as a central axis to construct a tubular safety mantle zone around it following its contours exactly (Figure 7). The thickness of the safety mantle can be adjusted to compensate for spatial inaccuracies during tracking of the drill. The system works as follows: It keeps track of the drill tip continuously intra-operatively and knows when the drill tip penetrates the safety mantle; then it gives off a distinct audiovisual warning notifying the surgeon that he/she is drilling in (too) close proximity of the facial nerve. The surgeon hears the warning without having to discontinue drilling to look at the monitor, and can take appropriate actions (e.g. release

pressure on the drill, drill in a different direction, change the drill bit, etc.). At our hospital, we have implemented this framework and verified its feasibility in temporal bone phantom models (unpublished data).

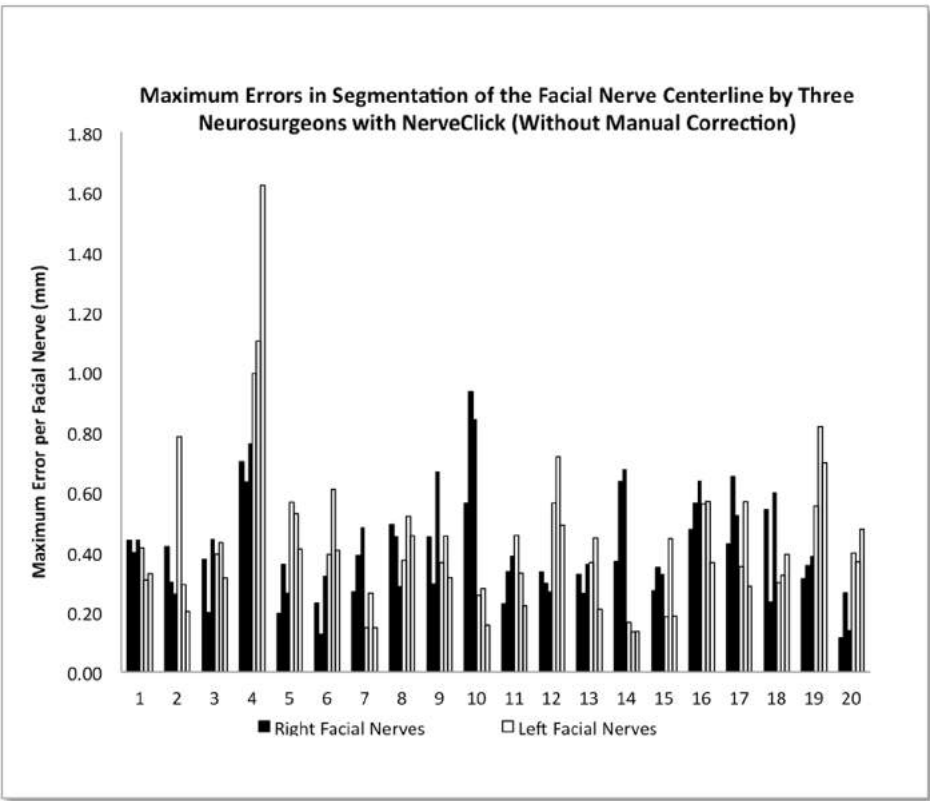


**Figure 2.4: Neurosurgeon’s Segmentation Accuracy Using NerveClick**  
Graphs plotting the maximum error (mm) obtained by three neurosurgeons using NerveClick to segment the intra-temporal facial nerve as compared to manual centerline segmentations for each of the twenty patients divided in right and left facial nerves.

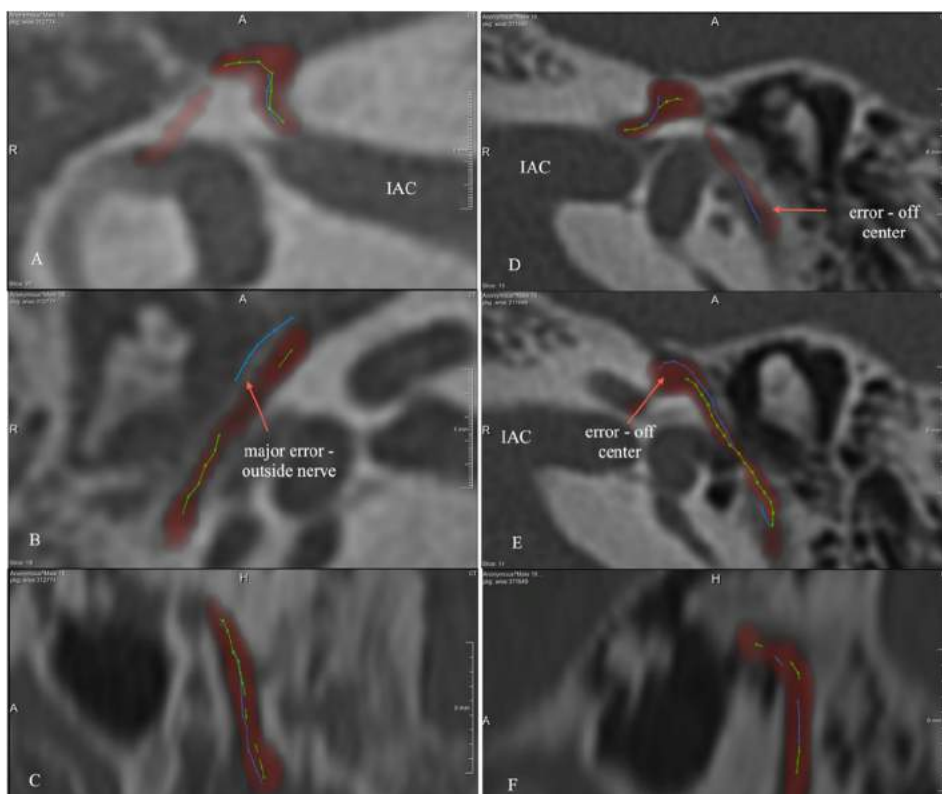


**Figure 2.5: Examples of Facial Nerve Centerline Segmentation Errors Requiring Manual Correction**

Segmentation results of two patients are displayed showing the labyrinthine segment (figures 5A and 5D) in axial cuts, the tympanic segment (Figures 5B and 5E) in axial cuts, and the mastoid segment (Figures 5C and 5F) in sagittal cuts. Figures 5A, 5B, and 5C show a right sided facial nerve, and Figures 5D, 5E, and 5F show a left sided facial nerve. The red area denotes manual segmentations of the facial nerve. The green line designates the obtained manual centerline (the gold standard). Blue is the centerline as found by a staff neurosurgeon using NerveClick. These results were considered poor and needed manual correction after automated segmentation.





**Figure 2.6: Test Patients with Skull Base Tumors and Disrupted Temporal Bone Anatomy**

This figure shows scans of the additional test patients on which NerveClick was evaluated. These cases represent likely neurosurgical candidates and/or have extensive aberration of the peri-facial nerve anatomy. Every sub-figure shows representative images of each case's underlying disease/temporal bone abnormality (on MRI or CT), next to the NerveClick segmentation results overlaid on temporal bone CT. The red area denotes manual segmentation of the full facial nerve. The green line designates the obtained manual centerline (the gold standard). Blue is the facial nerve centerline as found by a neurosurgeon using NerveClick.

Figure 6A shows a 56-year old male (case 1) with a right-sided vestibular schwannoma on T2-weighted MRI (left). NerveClick results for the labyrinthine segment are displayed (right) on axial CT scan. Figure 6B displays a 74-year old male (case 2) presenting with a petrous apex cholesterol granuloma (PACG) on the left side on T1-weighted MRI (left). Next to it (right) an axial CT scan showing the segmented part of the labyrinthine facial nerve centerline. Figure 6C shows a 49-year old male with a large recurrence of a previously debulked (extended middle fossa approach) clear cell meningioma of the left skull base on contrast enhanced T1-weighted MRI (left). Note that his temporal bone CT scan (top right) shows a beam-hardening artifact from a metal clip (clipping the superior petrosal sinus) disrupting the image around the temporal bone. The axial CT (bottom right) shows segmentation results for the labyrinthine and tympanic facial nerve. Figure 6D shows a contrast enhanced T1-weighted MRI of a 50-year old male with a right-sided jugular paraganglioma (case 4). The axial CT (right) shows segmented centerline next to tumor invasion of the mastoid segment of the facial nerve canal. Figure 6E displays a cranial CT scan (left) of a 40-year old female who had previously undergone a right-sided translabyrinthine and retrosigmoid craniotomy for a cholesteatoma (case 5) with next to it NerveClick results overlaid on temporal bone CT (right). Figure 6E shows a 72-year old male (case 6) on cranial CT, that suffered high energy trauma and had a fracture of the right temporal bone traversing the facial nerve canal. Next to it a temporal bone CT axial slice (top right) and coronal slice (bottom right) showing centerline segmentation results in the area of fracture.

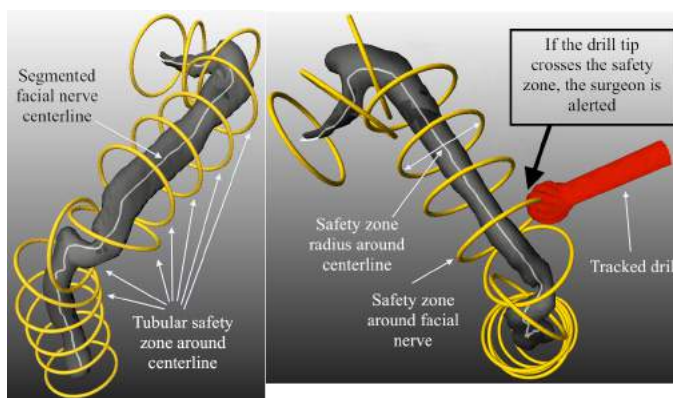


**Figure 2.7: Intra-Temporal Facial Nerve Safety Zone Solution Using NerveClick's Segmentations**

Figure 7A shows a schematic illustration of our safety zone mantle solution around a segmented facial nerve centerline. Note that the safety zone is represented as discrete rings, while in practice it is a continuous tube following the contours of the structure. Figure 7B demonstrates how this can potentially protect the facial nerve from iatrogenic damage from a navigated drill by giving audiovisual warnings when the drill tip crosses the safety zone.

## Discussion

The purpose of this article was twofold. First, we present and evaluate a new semi-automatic method for delineation of the intra-temporal facial nerve centerline: NerveClick. Second, we describe how the obtained facial nerve centerline segmentation could be used during surgery to implement a protective audiovisual warning system extending the possibilities of current neuronavigation.

We demonstrate that neurosurgeons can use NerveClick segmentation robustly, since their segmentations deviated maximally 0.44 mm (on average) from the true facial nerve centerline. This accuracy result is satisfactory since the diameter of the intra-temporal facial nerve varies between 1-2 mm [17].

Besides obtaining good results in healthy and neuro-otologic patients (with endolymphatic sac tumor, cholesteatoma, fibrous dysplasia, otosclerosis, opacified mastoid air cells), results from the six additional test cases indicate that NerveClick also works well in patients with skull base tumors (vestibular schwannoma, cholesterol granuloma, jugular paraganglioma, and meningioma) who might require neurosurgical treatment. Moreover, the technique appears to be robust in spite of extensive structural abnormalities of the peri-facial nerve anatomy, like prior surgery (e.g. extended middle fossa, translabyrinthine, or retrosigmoid craniotomies), destruction by tumor growth (e.g. tumor invasion into the facial canal) and traumatic temporal bone fracture (with a fracture through the facial canal). Also, it seems NerveClick's performance is not heavily influenced by CT scanner and image acquisition parameters.

In approximately three quarters of patients NerveClick performs excellently, and in the other quarter the surgeon can easily manually correct any deviation from the centerline. We strongly believe the surgeon should always thoroughly check and correct the NerveClick result because this minor inconvenience is compensated by increased accuracy of the audiovisual warnings and thus less risk of iatrogenic harm during subsequent surgery.

Furthermore, NerveClick is significantly less labor intensive and faster than manual segmentation; requiring about 2 – 4 minutes (including start and endpoint selection, computer runtime and correction if needed) compared to 7 – 11 minutes for manual facial nerve segmentation. In our experience NerveClick enjoys a steep learning curve, requiring only one demonstration ('see one') and one assisted attempt ('do one'), before neurosurgeons knew where to click

for facial nerve start and endpoints. More research in a larger population of neurosurgeons is necessary to thoroughly evaluate NerveClick's learning curve.

Another advantage of NerveClick segmentation is that it is a self-learning algorithm that may further improve its accuracy during clinical use. Optionally, each found and checked centerline can be included in model construction thereafter. This means that each time our segmentation method is used the statistical model may be based on a larger sample than before and can theoretically become more accurate. For this to work, surgeons must assure that only accurately segmented facial nerve centerlines are included.

A clear disadvantage of the NerveClick segmentation algorithm is that it only segments the intra-temporal facial nerve within the fallopian canal. The surgically important cisternal and intracranial segments are not segmented because they are not visible on temporal bone CT images. This entails that audiovisual warnings will not be protecting the intracranial facial nerve if opening of the internal acoustic canal is necessary.

Theoretically, the envisioned safety mantle thickness should be at least as large as the maximum facial nerve radius plus the navigation system position tracking error (which depends on the type of fiducials used), plus the segmentation error. We estimate these values at 1 mm (facial nerve radius) + 2 mm (position error when using bone implantable screw fiducials<sup>2</sup>) + 0.5 mm (segmentation error). Therefore, our current estimation for an adequate safety zone radius is 3.5 mm around the facial nerve centerline (i.e. 2.5 mm from the edge of the fallopian canal).

This safety zone implementation is conceptually superior to working the other way around; defining a safe workspace outside the facial nerve resembling a mastoidectomy cavity, as was performed by Strauss et al. [19] previously. The advantages of a safety mantle compared to a workspace definition are that it is much easier to: 1) safeguard a large part of the facial nerve instead of only the mastoid section, 2) incorporate position tracking inaccuracies systematically into the safety mantle, and 3) allow 'drill tip to facial nerve' distance calculations and coupled audiovisual warnings. Therefore, our safety zone solution is to be preferred over workspace definitions for the facial nerve, but also for critical structures in general.

Another item that could be incorporated in a safety mantle is 'response time', which depends on the audiovisual warning system's latency (the time between drill tip position updates plus the run time necessary to do calculations and output an audiovisual signal), and the surgeon's

response time (the time needed for the surgeon's brain to receive and process the audiovisual signal, and let his/her muscles take appropriate actions). The response time could be translated into extra safety mantle thickness by multiplying it by the drill tip movement speed. Measurements of response times and drill tip movement speeds are necessary to investigate the magnitude of such an extra 'response margin'. Clearly, future audiovisual warning systems should strive to reduce system latency to a minimum.

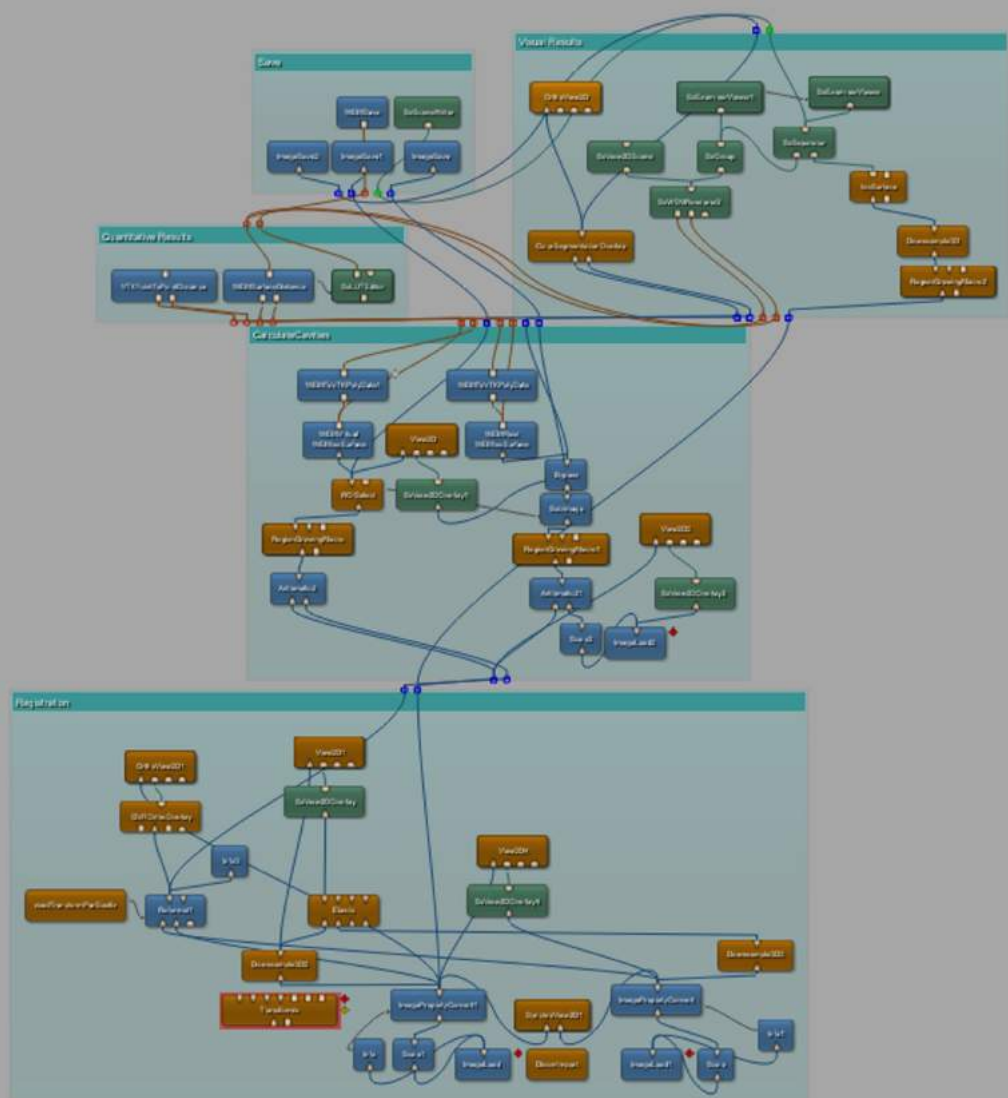
Overall, NerveClick segmentation is fast, simple, and allows neurosurgeons to adequately segment facial nerve centerlines. It solves the practical hurdle of performing a manual segmentation, and our safety mantle implementation potentially allows safeguarding the intra-temporal facial nerve with an audiovisual warning system during navigated trans-temporal surgery. In the near future, temporal bone model and cadaver studies will be performed to investigate whether the hypothesized 3.5 mm thickness of the safety mantle is adequate, and if audiovisual warnings can indeed prevent the facial nerve from getting harmed.

## Conclusion

We demonstrate that neurosurgeons can segment the intra-temporal facial nerve centerline robustly using the NerveClick segmentation algorithm in healthy and neuro-otologic patients, and patients with skull base tumors. Furthermore, we present the concept of using the acquired centerline as a basis for a safety zone, which may allow protection of the facial nerve from iatrogenic injury during navigated trans-temporal approaches by extending standard neuronavigation with an audiovisual warning framework. This result paves the way for additional research evaluating the protective capacity of such warning system in cadaver heads.

## References

1. Day JD, Tschabitscher M. Anatomic position of the asterion. *Neurosurgery*. Jan 1998;42(1):198-199.
2. Pillai P, Sammet S, Ammirati M. Application accuracy of computed tomography-based, image-guided navigation of temporal bone. *Neurosurgery*. 2008;63(4 Suppl 2):326-332.
3. Staecker H, O'Malley BW, Eisenberg H, Yoder BE. Use of the LandmarX trade mark Surgical Navigation System in Lateral Skull Base and Temporal Bone Surgery. *Skull.Base*. 2001;11(4):245-255.
4. Gharabaghi A, Rosahl SK, Feigl GC, et al. Image-guided lateral suboccipital approach: part 2-impact on complication rates and operation times. *Neurosurgery*. 2008;62(3 Suppl 1):24-29.
5. Roberts DW, Hartov A, Kennedy FE, Miga MI, Paulsen KD. Intraoperative brain shift and deformation: a quantitative analysis of cortical displacement in 28 cases. *Neurosurgery*. Oct 1998;43(4):749-758; discussion 758-760.
6. Nimsky C, Ganslandt O, Cerny S, Hastreiter P, Greiner G, Fahlbusch R. Quantification of, visualization of, and compensation for brain shift using intraoperative magnetic resonance imaging. *Neurosurgery*. Nov 2000;47(5):1070-1079; discussion 1079-1080.
7. Dorward NL, Alberti O, Velani B, et al. Postimaging brain distortion: magnitude, correlates, and impact on neuronavigation. *J.Neurosurg*. 1998;88(4):656-662.
8. Woerdeman PA, Willems PWA, Noordmans HJ, Tulleken CAF, van der Sprenkel JWB. The Impact of Workflow and Volumetric Feedback on Frameless Image-Guided Neurosurgery. *Neurosurgery*. 2009;64(3).
9. Woerdeman PA, Willems PWA, Noordmans HJ, Tulleken CAF, Berkelbach van der Sprenkel JW. Application accuracy in frameless image-guided neurosurgery: a comparison study of three patient-to-image registration methods. *J Neurosurg*. 2007;106(6):1012-1016.
10. Vrionis FD, Foley KT, Robertson JH, Shea JJ, III. Use of cranial surface anatomic fiducials for interactive image-guided navigation in the temporal bone: a cadaveric study. *Neurosurgery*. 1997;40(4):755-763.
11. Ryzenman JM, Pensak ML, Tew JM, Jr. Facial paralysis and surgical rehabilitation: a quality of life analysis in a cohort of 1,595 patients after acoustic neuroma surgery. *Otol Neurotol*. May 2005;26(3):516-521; discussion 521.
12. Asma A, Marina MB, Mazita A, Fadzilah I, Mazlina S, Saim L. Iatrogenic facial nerve palsy: lessons to learn. *Singapore Med J*. Dec 2009;50(12):1154-1157.
13. Green JD, Jr., Shelton C, Brackmann DE. Iatrogenic facial nerve injury during otologic surgery. *Laryngoscope*. Aug 1994;104(8 Pt 1):922-926.
14. Wiet RJ. Iatrogenic facial paralysis. *Otolaryngol Clin North Am*. Nov 1982;15(4):773-780.
15. Weber PC. Iatrogenic complications from chronic ear surgery. *Otolaryngol Clin North Am*. Aug 2005;38(4):711-722.
16. Voormolen EH, Stralen van M, Woerdeman PA, et al. Intra-temporal facial nerve centerline segmentation for navigated temporal bone surgery. *Proceedings of SPIE Medical Imaging 2011*; Lake Buena Vista, FL, USA. 7964-1C
17. Lin AL, Qin SZ, Gong J, Xu GZ, Li J, Yao GJ. [Neuronavigation-assisted microanatomical study of the facial nerve canal through the transpetrosal approach]. *Di Yi.Jun.Yi.Da.Xue.Xue.Bao*. 2004;24(6):659-661.
18. Noble JH, Warren FM, Labadie RF, Dawant BM. Automatic segmentation of the facial nerve and chorda tympani in CT images using spatially dependent feature values. *Med.Phys*. 2008;35(12):5375-5384.
19. Strauss G, Koulechov K, Hofer M, et al. The navigation-controlled drill in temporal bone surgery: a feasibility study. *Laryngoscope*. 2007;117(3):434-441.



# **Validation of Exposure Visualization and Audible Distance Emission for Navigated Temporal Bone Drilling in Phantoms**

***Authors:***

Eduard H. J. Voormolen, Peter A. Woerdeman, Marijn van Stralen, Herke Jan Noordmans,  
Max A. Viergever, Luca Regli, Jan Willem Berkelbach van der Sprenkel

Based on the publication in:

PLoS One. 2012;7(7):e41262. doi: 10.1371/journal.pone.0041262



## Abstract

**Background:** A neuronavigation interface with extended function as compared with current systems was developed to aid during temporal bone surgery. The interface, named EVADE, updates the prior anatomical image and visualizes the bone drilling process virtually in real-time without need for intra-operative imaging. Furthermore, EVADE continuously calculates the distance from the drill tip to segmented temporal bone critical structures (e.g. the sigmoid sinus and facial nerve) and produces audiovisual warnings if the surgeon drills in too close vicinity.

**Objective:** The aim of this study was to evaluate the accuracy and surgical utility of EVADE in physical phantoms.

**Methods:** We performed 228 measurements assessing the position accuracy of tracking a navigated drill in the operating theatre. Five neurosurgeons each drilled two temporal bone phantoms, once using EVADE, and once using a standard neuronavigation interface. Furthermore, we compared the distances between surface meshes of the virtual drill cavities created by EVADE to actual drill cavities.

**Results:** A mean target registration error of  $1.33 \pm 0.61$  mm with a maximum error of 3.04 mm was found. While using standard neuronavigation the surgeons damaged three modeled temporal bone critical structures. No structure was hit by surgeons utilizing EVADE. Surgeons felt better orientated and thought they had improved tumor exposure with EVADE. The average maximum errors between virtual and real drill cavities were  $2.54 \pm 0.49$  mm and  $-2.70 \pm 0.48$  mm.

**Conclusions/Significance:** These results demonstrate that EVADE gives accurate feedback which reduces risks of harming modeled critical structures compared to a standard neuronavigation interface during temporal bone phantom drilling.

## Introduction

Surgical approaches through the temporal bone require some form of temporal bone drilling to create an adequate access towards the surgical target. Skull base surgeons need to be thoroughly oriented during temporal bone drilling to optimize access creation while minimizing bone removal and evading critical structures, such as the facial nerve and sigmoid sinus. Anatomical landmarks are the traditional means of orientation during temporal bone drilling; however, these are subject to high inter-individual variability [1] and can be eroded by tumor, inflammation or previous surgery. Neuronavigation (i.e. frameless image guidance) techniques offer surgeons alternative modern means of intra-operative orientation during temporal bone surgery [2,3,4,5,6,7,8].

Neuronavigation systems display the location of the tip of a tracked drill on a navigation map of the patient's anatomy imaged pre-operatively. Contemporary neuronavigation systems offer 'point in space' feedback, which has limitations: The navigation scan is not updated while the patient's anatomy is altered by drilling, so the surgeon remains visually uninformed in regards to the relationship of the size of the surgical approach as compared to the size underlying tumor. Furthermore, standard neuronavigation does not adequately notify the surgeon about where he/she is drilling in relation to surrounding temporal bone critical structures.

In order to improve these aspects, we designed and implemented a novel neuronavigation interface that augments the information relay to the surgeon (Figure 1). Our interface has two special characteristics: First, it shows the bone drilling process virtually in real time, providing feedback on the entire progress of bone drilling. So, the surgeon can see the extent of his drill cavity at all times. Second, it allows (semi-automatic) segmentation of temporal bone critical structures (such as the facial nerve [9,10]) and continuously updates the distance of the tracked drill to these structures and emits audiovisual warnings [11] when the drill tip comes in (too) close proximity. Our interface is referred to as EVADE: 'Exposure Visualization and Audible Distance Emission' (Video S1).

Here we evaluate the accuracy and surgical utility of EVADE in phantom models. The aim of this article is threefold. First, we assess whether it is possible to track a drill tip with sufficient accuracy. Second, it is investigated whether EVADE is able to show virtual bone excavation truthfully. Third, we conduct a trial to test EVADE's added surgical value by comparison with a standard neuronavigation system.

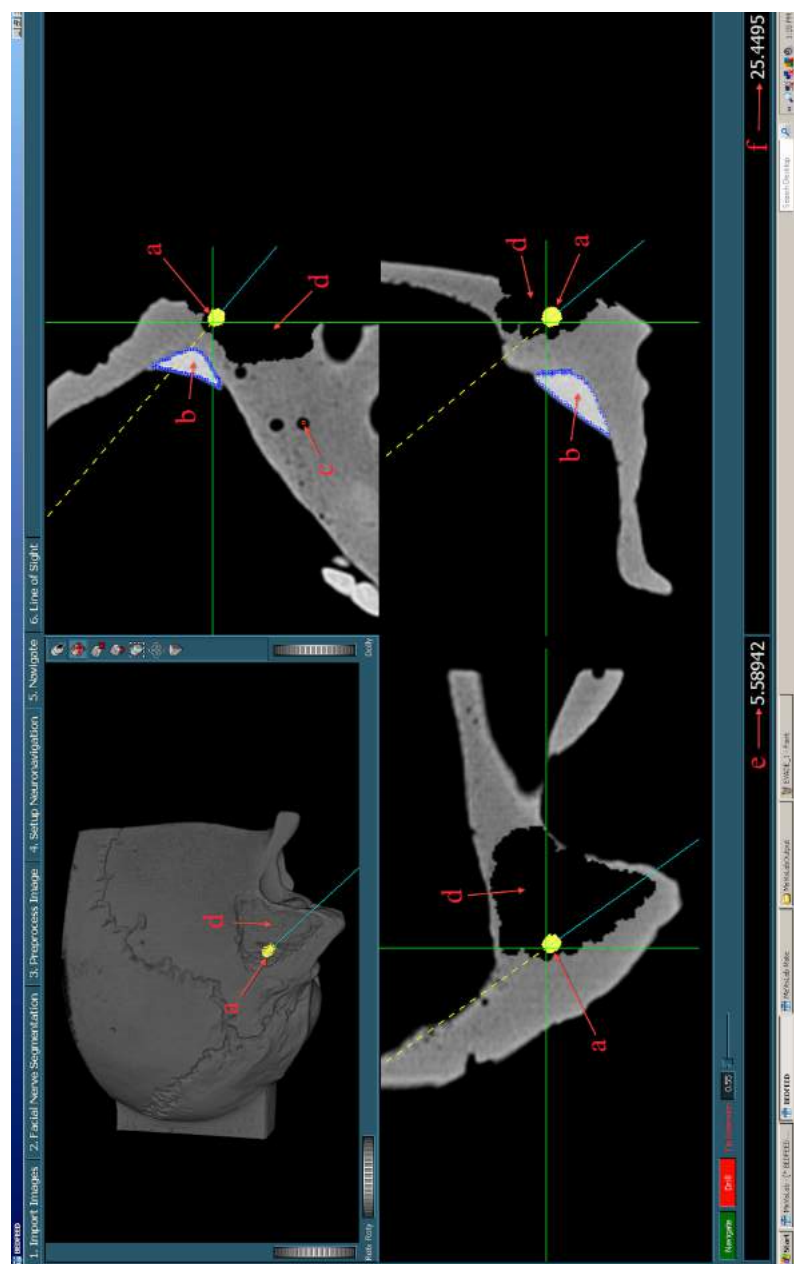


**Figure 3.1 The EVADE Interface**

The EVADE interface is shown. Figure annotations (a-f) are displayed in red. In the upper left corner, a 3D rendering of the anatomy (in this case a temporal bone phantom) is shown, and around it are three orthogonal sections. The green cross designates the current position of the drill tip. The yellow shape represents the drill bit being used (a). The modeled sigmoid sinus (b) and facial nerve (c) are outlined in blue and orange respectively. The virtually drilled cavity is displayed both in 3D as in 2D (d). The two numbers on the bottom give the current distance to the sinus (e) and facial nerve (f).

## Material and Methods

### Hardware

The EVADE system's hardware consists of a Stealth Treon navigation machine (Medtronic Inc. Boulder CO, USA) used for its optical tracking capabilities and patient-to-image registration algorithm, and a separate laptop computer (Apple Inc. Cupertino CA, USA) running Windows XP (Microsoft Corp. Redmond WA, USA) connected via a network cable. The laptop outputs its display to a 21.30 sized display monitor. A SureTrak™ frame (Medtronic Inc. Boulder CO, USA) was attached to the drill allowing the navigation machine to track it. The phantoms were fixed to the operating table with a Mayfield head clamp (Integra LifeSciences Corp. Cincinnati OH, USA). A reference frame (Medtronic Inc. Boulder CO, USA) was attached to the Mayfield clamp to translate drill coordinates recorded in camera space to coordinates in image space.

### Software

The commercial software StealthLink (Version 1.0, Medtronic Inc. Boulder CO, USA) was used to interface between the navigation machine and our custom-made software (build with MeVisLab Programming Environment 2.0, MeVis Research, Bremen, Germany; [www.mevislab.de](http://www.mevislab.de)). The necessary custom-made software modules are available at request from the principle author) running on the laptop computer. Drill tip and hind positions and resulting drill shaft orientations were calculated (in image space) on the laptop computer from information provided via StealthLink.

### Drill Calibration

The system needs to know the relation between the tracking frame and the tip and hind of the drill to calculate the image space positions. Therefore, it needs to be calibrated before surgery. The calibration procedure involves three steps: First, the pointer is placed into a divot within the reference frame with its shaft parallel to the long axis of the divot. Second, the drill is placed within the same divot with its shaft positioned analogously to the pointer in the previous step. Third, the drill is placed next to the divot directly on the reference frame while keeping its shaft in the same orientation as during the previous step. This is to compensate for the fact that some drill bits are large and cannot reach the bottom of the divot. Effectively, their tip does not reach the exact location where the pointer tip was located during the first calibration step, which leads to inaccuracies. To adjust for this, the difference in drill tip distance along the drill's shaft between being in the divot and just next to the divot is calculated. Subsequently, the difference between the drill tip distance and the divot depth is added to

the tip of the drill. The drill hind is calculated to be at a fixed point 10 cm above the drill tip along the drill shaft.

### Phantoms

Two different phantoms were used for our experiments. A cylinder and ball phantom (Figure 2) was used to assess the accuracy of tracking a drill. The phantom consisted of 19 cylinders of different lengths spread across its base, on top of which hollow balls could be placed. The centers of these balls correspond to the top center points of the cylinders, which locations are designated with a small divot. The phantom was fitted with four metal screws to serve as fiducial markers.



**Figure 3.2: Drill Tracking Accuracy Experimental Setup**

The setup in the operating room during drill tracking accuracy experiments on the cylinder and ball phantom (a) is shown. Note the head clamp (b) and reference frame (c). Registration of the phantom was performed via four rigidly attached screws that served as fiducial markers. The top of the cylinders were touched with the drill (d) with attached tracking frame and pointer (e) and the image coordinates were recorded and compared with the actual positions to yield target registration errors.

Furthermore, we used temporal bone phantoms constructed from drillable plastic (Sawbones Europe AB, Malmö, Sweden). In each model a straight canal was drilled by hand to resemble the mastoid section of the facial nerve canal and silicone gel was applied on the intra-cranial side to model the sigmoid sinus and a vestibular schwannoma tumor (Figure 3). This ensured that each model was slightly different from the next. Six divots were drilled into each of these models to serve as fiducial markers.

#### Scan Parameters

The cylinder and ball phantom was scanned on a 64-slice Philips CT scanner. Scan parameters were set to 120 kVp and 200mAs, which yielded images with a matrix size of 512x512x207 with voxels of 0.48x0.48x1.0 mm<sup>3</sup>. The temporal bone phantoms were scanned on either a 64- or 256-slice Philips CT scanner. Two different protocols were used. For models 1–3 we scanned with 120 kVp, 300 mAs acquiring images with a matrix size of 712x712x168 and anisotropic voxel sizes of 0.18x0.18x1.0 mm<sup>3</sup>. Models 4–10 were scanned with the following parameters: 120 kVp, 400 mAs, matrix size of 512x512x281 with voxel sizes of 0.34x0.34x0.4 mm<sup>3</sup>. All models were re-scanned post-operatively using the same scan protocol as pre-operatively.

#### Exposure Visualization Implementation

EVADe's virtual drilling relies on knowledge of the drill tip location and the orientation of its shaft which information is acquired approximately every 0.16 seconds through StealthLink. The drill bit is represented as a collection of points (3D point cloud) sampled from a prior ultra-high-resolution CT image of the drill bit with matrix sizes of 768x768x45 with voxel sizes of 0.096x0.096x0.35 mm<sup>3</sup>. We constructed point clouds of 3, 4 and 5 mm drill bits (Figure 4). Within these point clouds the tip point and hind point were designated to be aligned with the drill's axis shaft. The point clouds were of higher resolution than the phantom's CT images. Every point is interpolated to the closest voxel through nearest-neighbor interpolation. Subsequently, these voxels are accessed and their voxel value is set to match the background (air) intensity. A drill bit shape is effectively 'removed' from the model's image. During surgery, many consecutive drill tip position updates create a virtual drill cavity within the model's image.

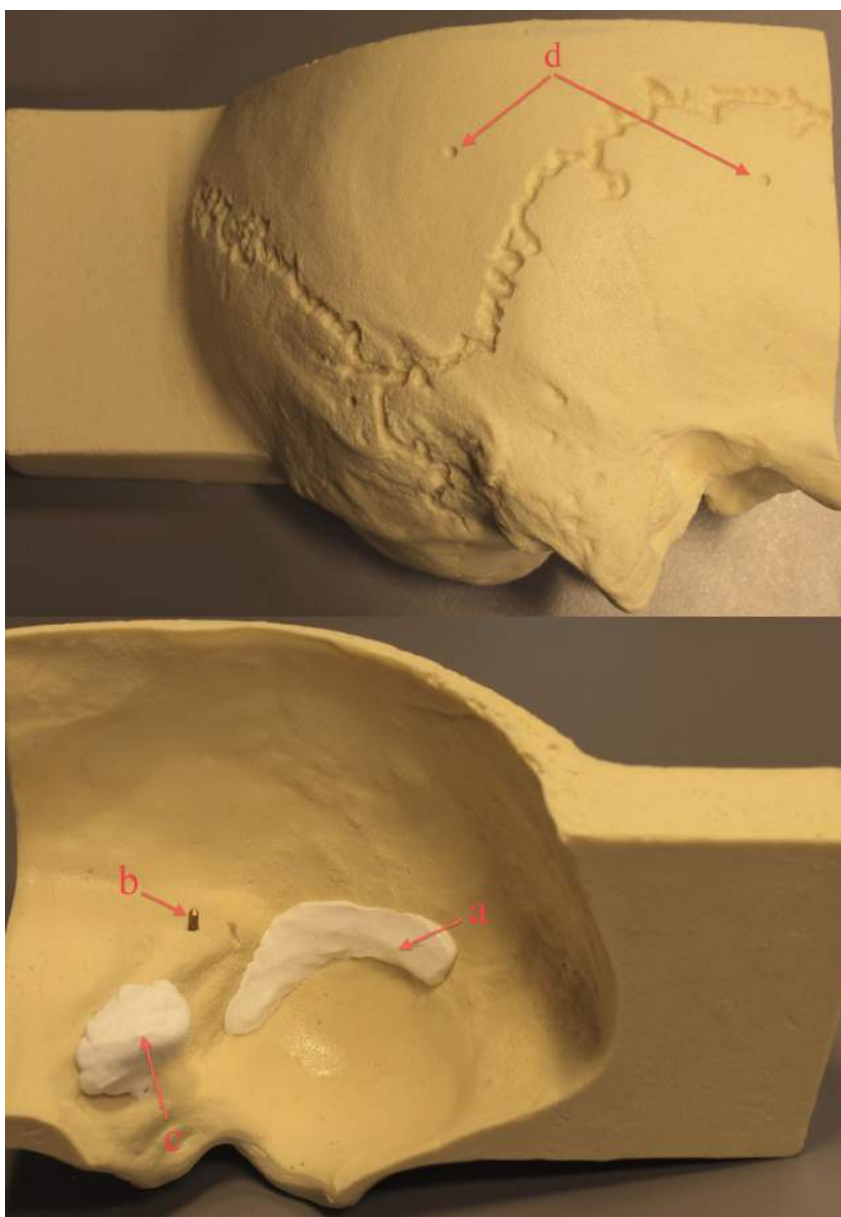


**Figure 3.3: Temporal Bone Phantoms**

This Figure shows an example of a plastic temporal bone phantom. On the outside divots (d) were drilled to be used as fiducial markers for registration. On the inside a modeled silicon sigmoid sinus (a) and tumor resembling a vestibular schwannoma (c) were placed. Also, a straight canal was drilled in which a metal rod was placed serving as a modeled facial nerve (b).

### Critical Structure Segmentation

To make audible distance emission work the system needs to learn the image positions of critical structures. Therefore, these structures were designated on individual images of the phantoms acquired pre-operatively via manual segmentation: it required the surgeon to draw contours around the structures slice-by-slice. Subsequently, 3D volumetric images of the structures were generated by adding all contours. The 3D volumes were transformed into point clouds by sampling the surfaces at a resolution of 0.1 mm. In this way, EVADE learned the position of the facial nerve and sigmoid sinus for each phantom.

### Audible Distance Emission Implementation

EVADE's audible distance emission feature works as follows: the system calculates the Euclidian distance from the drill bit tip coordinate to the closest points on the critical structure point clouds continuously. If this distance becomes less than a particular predefined distance, known as the safety mantle thickness, it gives off a distinct audiovisual warning notifying the surgeon that he/ she is drilling in (too) close proximity of the critical structure. So effectively, a safety mantle that follows the contours of the segmented critical structures is imposed, and EVADE tracks the drill tip continuously during drilling to warn when the drill tip penetrates this safety mantle (Figure 5) [9]. The surgeon hears the warning without having to discontinue drilling to look at the monitor, and can take appropriate actions (e.g. release pressure on the drill, drill in a different direction, change the drill bit, etc.). The thickness of the safety mantle determines how 'early' EVADE produces warnings. All surgeons used the same safety mantle thickness of 3 mm.

### Experiment Protocols

Two different experiments were performed. First, we assessed how accurate the EVADE system could track the drill tip on the cylinder and ball phantom. A high-resolution CT image of the phantom was acquired, after which the phantom was taken to the operating room, placed in a Mayfield head clamp and registered. Subsequently, the drill tip was positioned at the small divots at the top center points of the 19 cylinders, and the 19 image positions were saved. This experiment was conducted four times (each instance requiring a new setup and registration) using 3, 4, and 5 mm cutting drill tips, amounting to a total of 228 measurements. We also acquired image positions for the standard navigation pointer to obtain a reference accuracy measure.



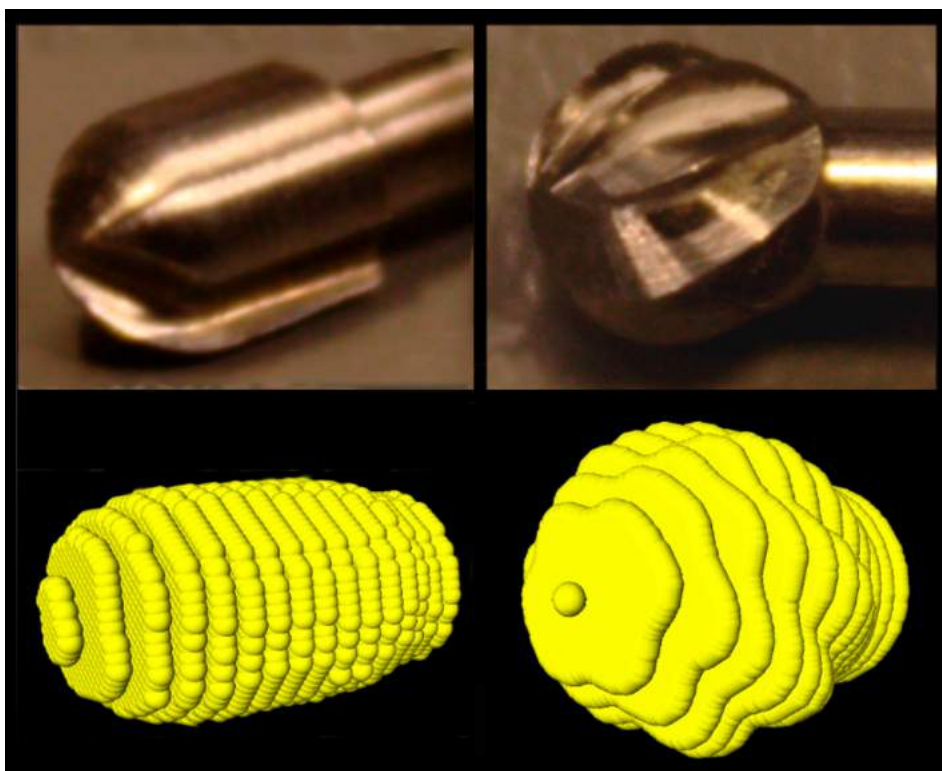


**Figure 3.4: Virtual Drill Bits**

Drill bits were scanned with high resolution CT and represented as 3D point clouds. On the left is displayed a 3 mm match-head drill bit and on the right a 4 mm drill bit can be seen.

Second, ten temporal bone phantoms were scanned with high- resolution CT. The modeled facial nerve canal and sigmoid sinus were segmented. Subsequently, the phantoms were taken to the operating room, placed in a Mayfield head clamp and registered (Figure 6). The fiducial registration error calculated by the neuronavigation system was stored. Five different neurosurgeons were asked to each perform a trans-labyrinthine approach to the modeled vestibular schwannoma on two phantoms, for the interface trial comparing EVADE to a standard navigation interface. In half of the cases the surgeons were exposed to the augmented feedback EVADE offers (i.e. real time drill cavity updates and distance feedback with audible warnings of the modeled facial nerve and sigmoid sinus) and in the other half they used standard navigation while EVADE was running silently in the background (calculating a virtual drill cavity). The order of whether or not EVADE was used, was decided randomly. Time between the first and second surgery was on average  $260 \pm 177$  days. The surgeons used one drill bit per surgery. The virtually drilled image of the temporal bone phantom created by EVADE was saved after the surgeons stopped drilling. The decision to stop surgery was made by

the surgeons. They were instructed to stop once they thought they had achieved their best exposure of the modeled tumor. The drilled phantoms were re-scanned post-operatively with high resolution CT.

#### Data Analysis

Target registration errors (TRE) of tracking a drill with attached SureTrak™ on the cylinder and ball phantom were calculated in the follow way. We obtained the true image position of the top center of the cylinders via image analysis on the model's CT image: each ball, positioned on top of one of the nineteen cylinders, was segmented (using a 3D region growing algorithm) and its center of mass was calculated which corresponded to the true image position of the cylinder top center. The TRE was calculated as being the Euclidian point-to-point distance between the true image positions of the cylinder top center and the measured image position while the drill was touching that cylinder's top center divot. Obtained TREs were averaged to yield the main outcome measure for this experiment: mean TRE.

Furthermore, we performed image processing to compare images of the temporal bone model drill cavities virtually 'erased' by EVADE to images of the corresponding real drill cavities. For each temporal bone model, the post-operative CT image of the drilled model was registered globally with a fully automated mutual-information based affine registration algorithm to its original CT image [16]. The virtually drilled model was not registered because its world matrix (i.e. its scaling, position, and orientation) was identical to the original model image. Both virtual and real drilled model images were subtracted from the original model image. Drill cavities were segmented in the subtraction images using a 3D region growing algorithm to obtain images of the virtual and real drill cavity. The virtual and real cavity images were overlaid and converted to 3D surface meshes without loss of resolution (i.e. with nodes at every voxel). The region of the cavity surfaces corresponding to the area where the surgeon started drilling on the outer surface of the temporal bone phantom was excluded from analysis. Inclusion would bias results because here correspondence between cavities was optimal. The mean and signed maximum Euclidian surface-to-surface distances between the real and virtual drill surface were calculated.

The resulting surface-to-surface distances were a measure of the virtual drilling error: if the distance is zero, there is perfect overlap and the virtual drilling corresponds exactly to the real drilling. If the distance is non-zero, EVADE either overestimated or underestimated the cavity compared to reality. To visualize the location and magnitude of the virtual drilling errors, and to depict areas of over- and underestimation, 3D error-to-color coded surface maps were generated (Figure 7).

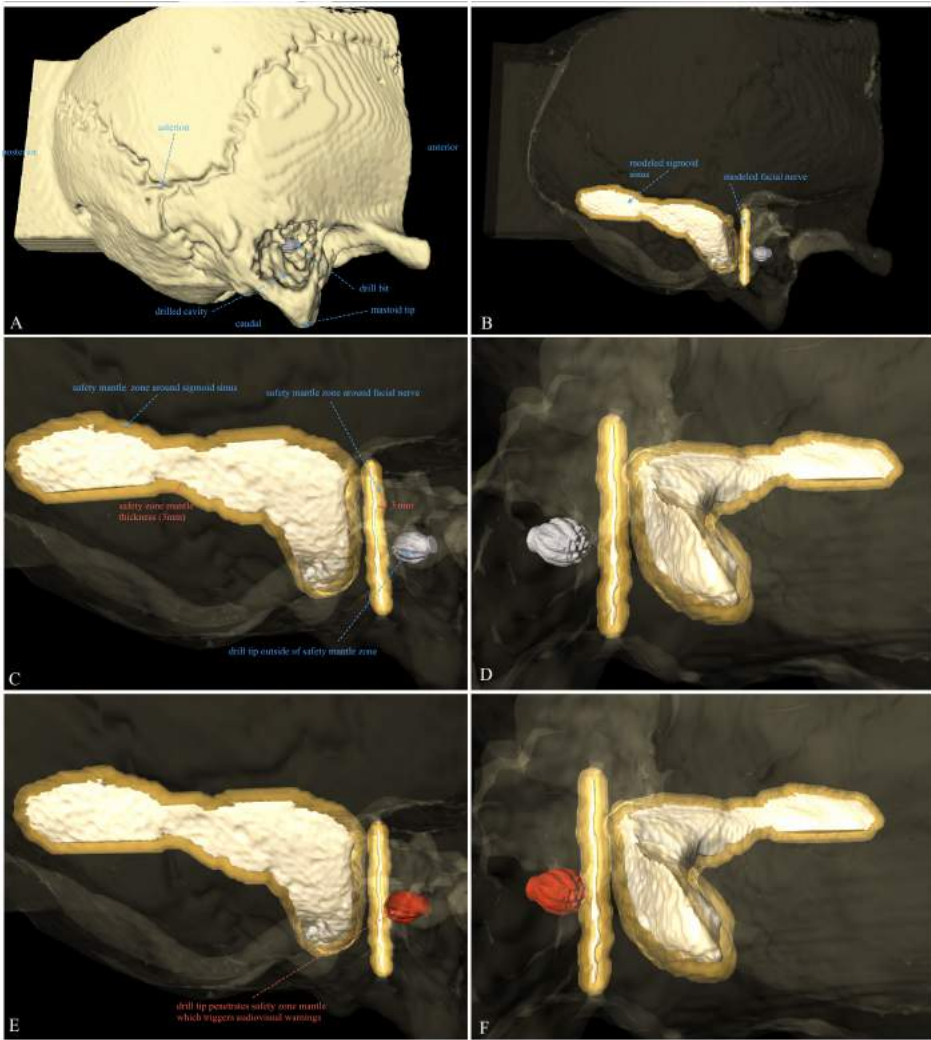


**Figure 3.5. Illustration of Critical Structure Safety Mantle Implementation.**

This Figure illustrates the principle of the critical structure safety mantle implementation which EVADE uses to generate timely audiovisual warnings in spite of drill tracking inaccuracies of the navigation machine. Figure 5A shows the temporal bone phantom for purposes of anatomical orientation. In Figure 5B the bone phantom has been rendered translucent to show the drill bit (in grey) and modeled critical structures; the sigmoid sinus and the facial nerve. Figure 5C is a zoomed in view on the critical structures (in white) in which the safety mantle (the orange-golden translucent area) is visible around the critical structures. Note that the safety mantle thickness measured from the surface of the structures is 3 millimeters. Figure 5D shows the same situation from a different angle. The drill bit is still outside of the safety mantle. In Figure 5E the surgeon has continued drilling and the drill bit tip (now in red) has entered the safety mantle around the facial nerve. EVADE is triggered to provide audiovisual warnings. Figure 5F shows the situation as in 5E from a different angle.



**Figure 3.6: Intra-Operative Setup during Temporal Bone Surgery**

This Figure shows the typical situation during a trans-labyrinthine approach with a navigated drill (a) on the temporal bone phantoms (b) in the operating room. The surgeon used either the EVADE interface (c) or the standard navigation interface (d). Note the infra-red camera (e) used for tracking.

#### Trial Neurosurgeons

Five different trial surgeons participated in the interface trial. Three surgeons were neurosurgical staff members with extensive experience in skull base surgery (over fifty approaches) and two were neurosurgical residents who had participated in five or less skull base approaches.

#### Trial Outcome Measures

Four outcome measures were acquired for the interface trial. The surgeon's impressions of the navigation system were noted via a standardized questionnaire. Two questions were asked: 1) How satisfied are you with the exposure of the tumor? 2) How well do you think your surgical orientation was during surgery? The questionnaire allowed answers to be given on a five-point scale with 1 reflecting a very poor verdict and 5 an outstanding verdict. The surgeons used common sense, their clinical training and experience to form an opinion of the surgical exposure of the modeled tumor.

Furthermore, the phantoms were assessed visually post-operatively for damage to the modeled facial nerve and sigmoid sinus. We also measured the time required by the surgeon to perform a satisfactory exposure.

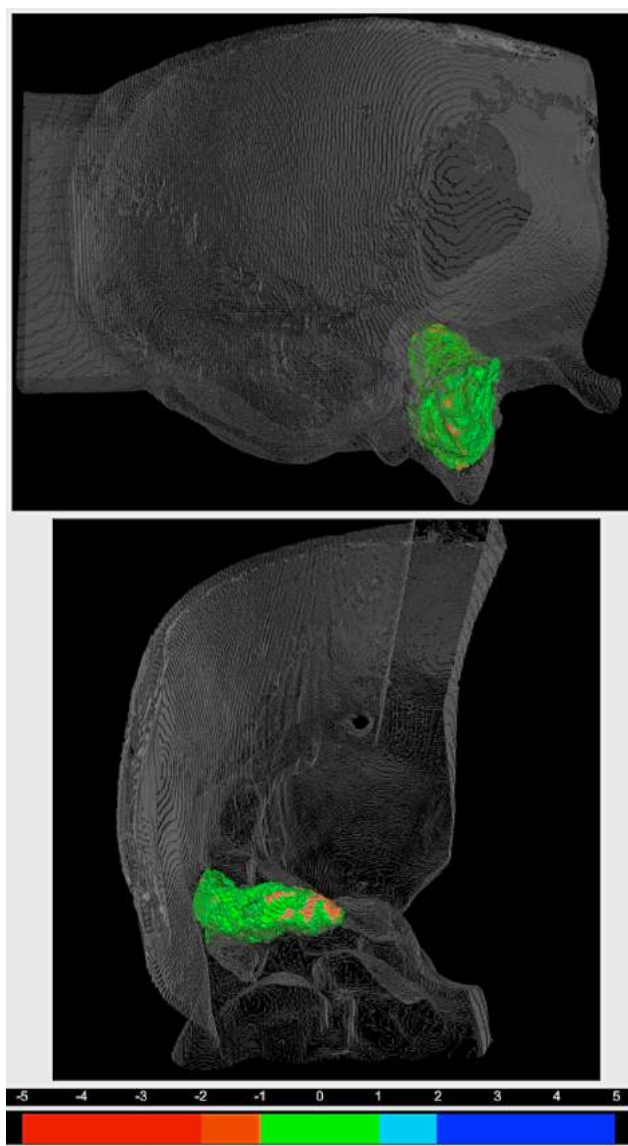


**Figure 3.7: Illustration of Drill Cavity Overlap Error**

The error-to-color coded surface to surface distance map of drill cavity index number 6 is displayed in a 3D rendering of the corresponding temporal bone. The top view is from lateral and the bottom view shows the cavity from anterior. The legend for the error-to-color representation is provided under the 3D renderings. Note the green areas within the distance map denote errors of under 1 mm, and the orange areas represent virtual underestimation errors of between 1 and 2 mm.

## Results

The accuracy of tracking a drill tip while navigating a cylinder and ball phantom was assessed by measuring the target registration error (TRE). The mean TRE was  $1.33 \pm 0.61$  mm (Table 1). The maximum TRE measured was 3.04 mm, which was obtained with a 5 mm drill bit.

Next, it was investigated how accurate the EVADE interface could virtually depict the drilling process (Figure 8). All five neurosurgeons had the qualitative impression during surgery that the displayed virtual drill cavity was correct. The average real-to-virtual drill cavity overlap, i.e. surface-to-surface distance (mean surface-to-surface distance averaged over ten temporal bone models), measured  $0.67 \pm 0.66$  mm. The average virtual maximum overestimation and underestimation was  $3.25 \pm 0.91$  mm and  $3.18 \pm 1.06$  mm respectively. An error-to-color coded map of a drill cavity is provided in Figure 3. Subgroup analysis showed that for the first three models (indices 1–3) the average mean surface-to-surface distance was  $0.98 \pm 0.09$  mm with maximum over- and underestimations of  $4.58 \pm 0.41$  mm and  $4.37 \pm 0.55$  mm. The last seven models (indices 4–10), which were imaged at higher resolution, showed an average mean surface-to-surface distance of  $0.53 \pm 0.18$  mm with  $2.54 \pm 0.49$  mm and  $-2.70 \pm 0.48$  mm over- and underestimation respectively.

**Table 3.1: Optical Tracking Accuracy**

Experiment	Pointer	SD	3 mm	SD	4 mm	SD	5 mm	SD
1	0.85	0.48	1.02	0.51	1.13	0.65	1.21	0.59
2	1.13	0.33	1.59	0.33	1.47	0.67	1.26	0.56
3	1.25	0.46	1.75	0.51	1.32	0.52	1.92	0.59
4	-	-	1.19	0.53	0.85	0.40	1.64	0.53
<b>Average (mm)</b>	1.05	0.45	1.36	0.57	1.17	0.59	1.47	0.63
<b>Maximum (mm)</b>	2.34		2.83		3.01		3.04	

This table displays results for four separate tracking accuracy experiments on the cylinder and ball phantom in the operating room. Average target registration errors are given in millimeters for the "Pointer" and a drill with "3 mm", "4 mm" or "5 mm" drill bits attached, for each experiment. Additionally, overall average and maximum target registration errors for each of the instruments are displayed in millimeters in the row "Average" and "Maximum" respectively. "SD" means standard deviation.

Furthermore, a trial was performed that compared the clinical efficacy of a standard navigation interface vs. the EVADE interface during temporal bone phantom drilling. While using the standard navigation interface the average fiducial registration error (displayed on the navigation machine) was  $0.70 \pm 0.14$  mm. The surgeons in this group required an average of  $33 \pm 11$



minutes to perform the surgery. The modelled facial nerve was hit on two occasions. Once by an experienced staff surgeon and once by a resident. The modelled sigmoid sinus was damaged once by a staff neurosurgeon. The average qualitative scores for surgeon satisfaction with intraoperative orientation and the resulting exposure were 3.6/5.0 and 2.8/5.0 respectively. During usage of EVADE navigation the fiducial error registration error was  $0.82 \pm 0.18$  mm. The average time required for exposure was  $31 \pm 7$  minutes. The modelled facial nerve and the sigmoid sinus were not hit by any surgeon. The scores for satisfaction with intraoperative orientation and resulting exposure with EVADE were 5.0/5.0 and 4.4/5.0 respectively. Results of statistical comparisons between trial groups were deemed unreliable because of small sample size and therefore were not included.

**Video 3.1 Demonstration of EVADE's Novel Feedback Characteristics.**

This video shows surgeons performing a trans-labyrinthine craniotomy on a temporal bone phantom while using EVADE neuronavigation. It provides an illustration of how the 'exposure visualization' and 'audible distance emission' features of the interface can be used in the operating theatre. Link: <https://doi.org/10.1371/journal.pone.0041262.s001>

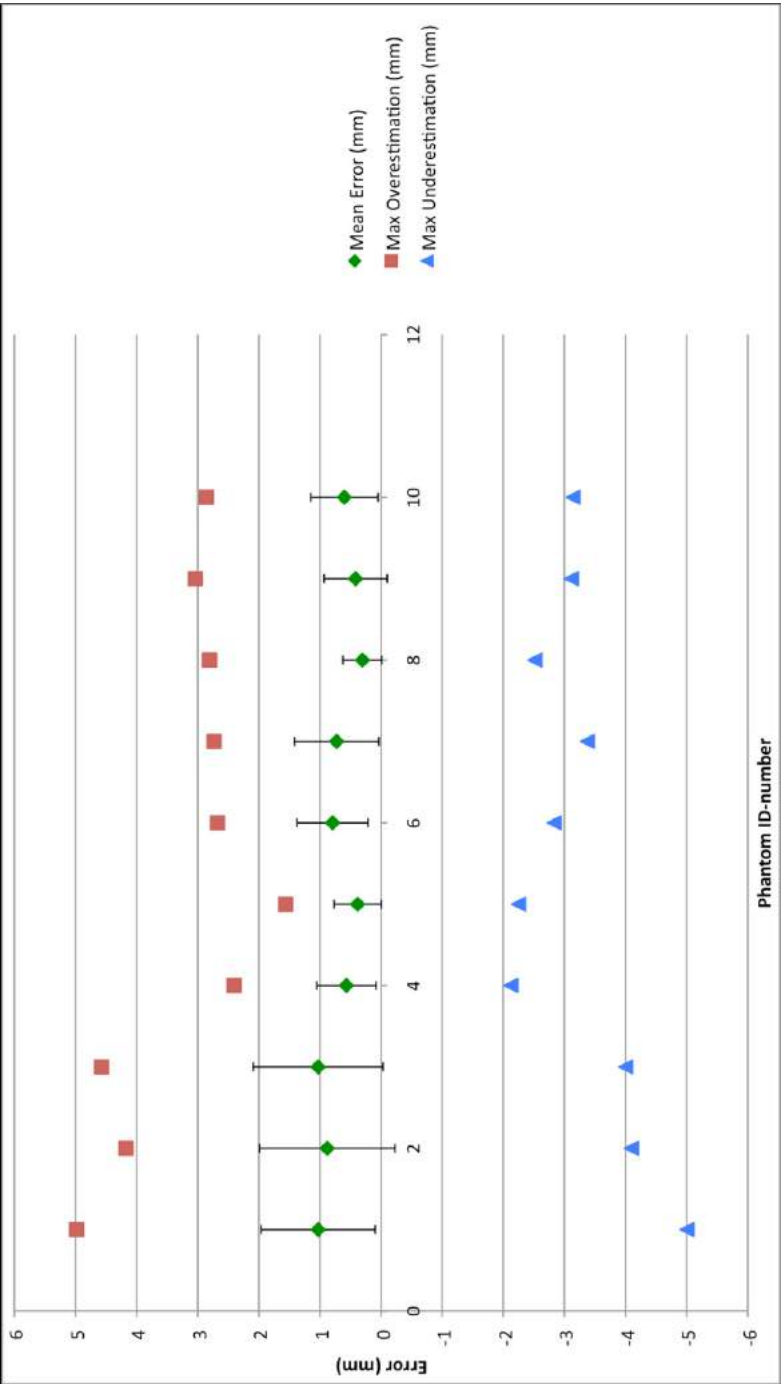


**Figure 3.8: Exposure Visualization Accuracy Results**

The mean and maximum over- and underestimation errors in virtually representing the drill cavity (i.e. the surgical exposure) are presented in millimeters (on the y-axis) for each temporal bone phantom (whose index is displayed on the x-axis). Note the differences in errors between the first three models and the last seven models in which higher resolution CT scans were used.



## Discussion

The purpose of EVADE is to augment standard neuronavigation adding audiovisual feedback to further aid the surgeon in performing trans-temporal surgery. The absence of soft-tissue shift in the temporal bone makes it possible to maintain high spatial tracking accuracy of a tracked drill throughout the whole approach.[12,13] To the best of our knowledge we are the first to confirm that a commercial neuronavigation system can indeed track a drill with attached tracking frame at high accuracy on a high-resolution CT image, with corresponding mean TRE of 1.3 mm and maximum TRE of 3 mm. We believe this accuracy to be sufficient for temporal bone neuronavigation since the error is not larger than the average distance between temporal bone critical structures (i.e. the area that needs to be navigated).

EVADE harnesses drill tracking information to give online intra-operative image updates of the drill cavity without the need for intra-operative imaging and associated radiation. Previous work concerning the use of navigation interfaces with such 'exposure visualization' features has been done by Wurm et al. (2008) [14] and at our institute by Woerdeman et al. (2009) [15]. Like EVADE, these neuronavigation feedback modes adjust voxel intensities around a tracked instrument tip. The difference is that EVADE uses geometric models of drill bits to erase voxels to simulate drilling, while the earlier encompassed simple spheres. The major problem of simulating drilling with spheres is its inherent inaccuracy should the surgeon use non-spherical drill bits (such as the 3 mm match head drill bit in Figure 4). In such case, we postulate that the drill cavity will not be represented truthfully. Instead, when using geometric model (in the exact shape of the non-spherical drill bit) for voxel erasing the accuracy of depicting the drill cavity is improved.

Here, we demonstrate that the EVADE interface truthfully represents surgeon-made drill cavities, with maximum errors of approximately 3 mm.

In general, neuronavigation tracking errors can be caused by inaccuracy in:

- 1) designating fiducial points in the image
- 2) designating fiducial points on the patient (or phantom)
- 3) patient-to-image fiducial point calculations
- 4) measuring the tracking frame position in space
- 5) drill tip-tracking frame calibration errors

The above sources of inaccuracy cause the errors observed in the cylinder and ball phantom experiments. Furthermore, the implementation of EVADE's virtual drilling adds more sources of imprecision due to:

- 6) drill cavity sampling due to (low) image resolution
- 7) modelling of the drill bit geometry

We investigated whether these additional sources of inaccuracy contribute to the total neuro-navigation error in the temporal bone phantom experiments. The location of neuronavigation errors were visualized on 3D error-to-color coded surface maps. In the first three phantoms, we observed that errors were systematically largest along the axis of lowest image resolution (the z-direction). These errors were caused by drill cavity sampling inaccuracy. Therefore, we changed the imaging protocol to isotropic scans with a higher z-resolution. Consequently, in the last seven models such a distinct error pattern was not identified and consistently lower error values were observed. These error values corresponded to the errors we found during the cylinder and ball phantom experiments. So, we can conclude that modelling of the drill bit geometry does not contribute to the neuronavigation error. Moreover, we stress the importance of using EVADE with an isotropic high-resolution image to improve designation of fiducials in the image and drill cavity sampling.

The error color-coded maps show the location of signed errors (Figure 7). Positive errors represent areas where the EVADE interface overestimates the size of the drill cavity. Overestimation errors cause the system's monitor to display particular anatomy as absent, while it is still present within the operating field. This may lead the surgeon to mistrust and eventually discard the system.

Conversely, negative errors represent 'under-estimation' errors of the drill cavity. Underestimation errors could potentially be dangerous since the surgeon gets the impression from the system's monitor that he/she might drill further to arrive at a particular target while in fact it has already been reached. In a worst-case scenario, erroneous drill cavity underestimation might contribute to iatrogenic injury of temporal bone critical structures.

EVADE was primarily designed to prevent such adverse events by its audible distance warning mechanism (see Methods section; Audible Distance Emission Implementation). The special attribute of this warning mechanism is the safety mantle imposed around critical structures (Figure 5). The thickness of the safety mantle can be adjusted to compensate for drill tracking

errors.[9] Therefore, this safety mantle implementation uncouples the magnitude of the position tracking error from the size of segmented critical structures. Even if the tracking error is larger than the critical structure size, EVADE still gives timely audiovisual warnings. Our phantom results indicate that for this to work properly the safety mantle thickness should be 3 mm when using optical tracking, high resolution isotropic CT images and a drill with attachable tracking frame. We wish to validate this safety mantle thickness value further in the context of real human temporal bone anatomy with realistic critical structures. Therefore, cadaver head experiments are currently being performed. These experiments are part of the second and final pre-clinical phase, after which EVADE will be ready for testing in patients.

It is important to emphasize that audible distance emission will work only if temporal bone critical structures have been delineated accurately in individualized pre-operative images. EVADE incorporates a semi-automated method to segment the facial nerve in CT scans of patients (NerveClick) [9,10]. We are currently developing algorithms for automated segmentation of other temporal bone structures. However, these algorithms are tuned to find structures within images of patients. Since the phantoms had very different image characteristics compared to patients, we could not use these segmentation algorithms for this study. Instead, we used manual segmentation to designate the positions of modeled critical structures within each individual phantom's image (see Methods section; Critical Structure Segmentation). The results of the interface trial indicate that EVADE reduces the risks of iatrogenic injury to critical structures and improves the intra-operative surgical orientation and exposure of the tumor in comparison to a standard neuronavigation interface.

Note that temporal bone drilling was conducted on phantoms which had far less bony landmarks for surgical orientation than a real temporal bone. Moreover, the modeled critical structures just approximated the shapes of actual temporal bone structures. So, instead of relying on anatomical knowledge the surgeons had to depend heavily on the feedback received from the neuronavigation interface to find a safe approach to the tumor.

The disadvantage of the phantom design is that it hampers surgical realism. Therefore, the trial results do not necessarily forebode that EVADE will improve surgery on actual patients. On the other hand, the phantom design does allow for testing the surgical usefulness of the navigation information (i.e. the amount of anatomical insight) provided during surgery. Therefore, the trial results demonstrate that EVADE is a superior surgical navigation interface as compared to the current standard interface. We anticipate that EVADE will aid the surgeon in difficult clinical cases with aberrant temporal bone anatomy due to extensive pathology or

prior surgery. In such cases, it is our experience that neither bony landmarks nor conventional neuronavigation provide enough information for accurate surgical orientation.

Besides the phantom design, this study has several other limitations. The sample size for the interface trial was small and rendered statistical analyses unreliable. Therefore, we did not include statistical test results. Another disadvantage that impedes extrapolating the trial results to the actual clinical situation was that not all trial surgeons were experienced skull base surgeons. Interestingly, two of three critical structures were hit by an experienced skull base surgeon (using a standard neuronavigation setup).

## Conclusion

Our results demonstrate that the EVADE neuronavigation interface is accurate. Furthermore, we show that EVADE's intra-operative feedback reduces risks of harming modeled critical structures compared with using a standard neuronavigation interface during translabyrinthine surgery of temporal bone phantoms. Further pre-clinical validation of EVADE in cadaver heads is necessary to confirm that the technical benefits observed in the present phantom study can be extended to patients receiving temporal bone surgery.

## References

1. Gharabaghi A, Rosahl SK, Feigl GC, Liebig T, Mirzayan JM, et al. (2008) Image-guided lateral suboccipital approach: part 1-individualized landmarks for surgical planning. *Neurosurgery* 62: 18–22.
2. Gharabaghi A, Rosahl SK, Feigl GC, Safavi-Abbasi S, Mirzayan JM, et al. (2008) Image-guided lateral suboccipital approach: part 2-impact on complication rates and operation times. *Neurosurgery* 62: 24–29.
3. Pillai P, Sammet S, Ammirati M (2009) Image-guided, endoscopic-assisted drilling and exposure of the whole length of the internal auditory canal and its fundus with preservation of the integrity of the labyrinth using a retrosigmoid approach: a laboratory investigation. *Neurosurgery* 65: 53–59; discussion 59.
4. Staecker H, O'Malley BW, Eisenberg H, Yoder BE (2001) Use of the LandmarX trade mark Surgical Navigation System in Lateral Skull Base and Temporal Bone Surgery. *Skull Base* 11: 245–255.
5. van Havenbergh T, Koekelkoren E, de Ridder D, van de Heyning P, Verlooy J (2003) Image guided surgery for petrous apex lesions. *Acta Neurochir(Wien)* 145: 737–742.
6. Nemec SF, Donat MA, Mehra S, Friedrich K, Krestan C, et al. (2007) CT- MR image data fusion for computer assisted navigated neurosurgery of temporal bone tumors. *Eur J Radiol* 62: 192–198.
7. Miller RS, Hashisaki GT, Kesser BW (2006) Image-guided localization of the internal auditory canal via the middle cranial fossa approach. *Otolaryngol Head Neck Surg* 134: 778–782.
8. Sure U, Alberti O, Petermeyer M, Becker R, Bertalanffy H (2000) Advanced image-guided skull base surgery. *Surg Neurol* 53: 563–572.
9. Voormolen EH, van Stralen M, Woerdeman PA, Pluim JP, Noordmans HJ, et al. (2011) Determination of a Facial Nerve Safety Zone for Navigated Temporal Bone Surgery. *Neurosurgery*. In Press.
10. Voormolen EH, Stralen van M, Woerdeman PA, Pluim JPW, Noordmans HJ, et al. (2011) Intra-temporal facial nerve centerline segmentation for navigated temporal bone surgery. In: Wong KHHI, D., editor. *Proceedings of SPIE. Lake Buena Vista, FL, USA*.
11. Woerdeman PA, Willems PW, Noordmans HJ, van der Sprenkel JW (2009) Auditory feedback during frameless image-guided surgery in a phantom model and initial clinical experience. *J Neurosurg* 110: 257–262.
12. Kral F, Riechelmann H, Freysinger W (2011) Navigated surgery at the lateral skull base and registration and preoperative imagery: experimental results. *Arch Otolaryngol Head Neck Surg* 137: 144–150.
13. Pillai P, Sammet S, Ammirati M (2008) Application accuracy of computed tomography-based, image-guided navigation of temporal bone. *Neurosurgery* 63: 326–332.
14. Wurm J, Bohr C, Iro H, Bumm K (2008) Intra-operative image update: first experiences with new software in computer-assisted sinus surgery. *IntJMedRobot* 4: 202–209.
15. Woerdeman PA, Willems PW, Noordmans HJ, Tulleken CA, van der Sprenkel JW (2009) The impact of workflow and volumetric feedback on frameless image-guided neurosurgery. *Neurosurgery* 64: 170–175.
16. Klein S, Staring M, Murphy K, Viergever MA, Pluim JP (2010) Elastix: a toolbox for intensity-based medical image registration. *IEEE Trans Med Imaging* 29: 196–205.





## **Benchmarking Distance Control and Virtual Drilling for Lateral Skull Base Surgery**

***Authors:***

Eduard H. J. Voormolen, Sander J. Diederer, Marijn van Stralen, Peter A. Woerdeman, Herke Jan Noordmans, Max A. Viergever, Luca Regli, Pierre A. Robe, Jan Willem Berkelbach van der Sprenkel

Based on the publication in:  
World Neurosurg. 2018 Jan;109:e217-e228. doi: 10.1016/j.wneu.2017.09.142.



## Abstract

**Background:** Novel audiovisual feedback methods were developed to improve image guidance during skull base surgery by providing audiovisual warnings when the drill tip enters a protective perimeter set at a distance around anatomic structures ("distance control") and visualizing bone drilling ("virtual drilling").

**Objective:** To benchmark the drill damage risk reduction provided by distance control, to quantify the accuracy of virtual drilling, and to investigate whether the proposed feedback methods are clinically feasible.

**Methods:** In a simulated surgical scenario using human cadavers, 12 unexperienced users (medical students) drilled 12 mastoidectomies. Users were divided into a control group using standard image guidance and 3 groups using distance control with protective perimeters of 1, 2, or 3 mm. Damage to critical structures (sigmoid sinus, semicircular canals, facial nerve) was assessed. Neurosurgeons performed another 6 mastoidectomy, translabyrinthine, and retrolabyrinthine approaches. Virtual errors as compared with real postoperative drill cavities were calculated. In a clinical setting, 3 patients received lateral skull base surgery with the proposed feedback methods.

**Results:** Users drilling with distance control protective perimeters of 3 mm did not damage structures, whereas the groups using smaller protective perimeters and the control group injured structures. Virtual drilling maximum cavity underestimations and overestimations were  $2.8 \pm 0.1$  and  $3.3 \pm 0.4$  mm, respectively. Feedback methods functioned properly in the clinical setting.

**Conclusion:** Distance control reduced the risks of drill damage proportional to the protective perimeter distance. Errors in virtual drilling reflect spatial errors of the image guidance system. These feedback methods are clinically feasible.

## Introduction

Lateral skull base approaches can be used to approach pathology in the cerebellopontine angle or at the petrous apex. The initial part of these approaches involves temporal bone drilling during which several critical structures (i.e., facial nerve, semicircular canals, sigmoid sinus, and jugular bulb) must be preserved.

To accomplish this, an intimate understanding of skull base anatomy and adequate orientation during drilling are key. Anatomic landmarks are traditionally used to help locate critical structures. These landmarks can, however, vary between individuals and are frequently altered[1] because of inflammation, tumor development, congenital malformations, or previous surgery. Therefore, even experienced surgeons may have difficulties in recognizing anatomic structures, which results in damage of critical structures during drilling. [2-5]

Expectations for contemporary skull base dissection are high, especially for preservation of facial movement and serviceable hearing. [6] Image guidance can be used as a tool to aid the surgeon with orientation during surgery, but the technology is unable to provide real-time feedback while the surgeon is drilling.

Recently, several methods have been introduced that provide augmented feedback during navigated drilling of the skull base. The first method is navigated control, which shuts down the drill as soon as the drill tip ventures outside a safe space predefined (e.g., a segmented mastoidectomy cavity) in the patient's scan. [7-9] Another method is distance control, which provides audiovisual warnings when the drill tip comes within a certain distance of a predefined area (a segmented anatomical structure, such as the semicircular canals) on the patient's scan.

Luz et al. [10] compared both methods and found that the distance control method has the same effect on improving surgical performance (i.e., reducing the risk of accidentally damaging an anatomical structure with the drill) as navigated control, but it has fewer adverse effects, such as prolonging the duration of surgery and increasing the subjective workload of the surgeon. Moreover, the subjective workload experienced by surgeons with distance control was even lower than in a manual control condition without image guidance. [10] Therefore, in theory, a distance control image guidance system could be a useful tool during skull base surgery. However, the amount of risk reduction such a system offers has never been quantified in a realistic surgical setting.

Distance control was first implemented in 2011, specifically for endoscopic sinus surgery by Strauss et al. [11] It was also developed separately by us and later by Cho et al. in 2012 for open (lateral) skull base surgery. [12,13] Our software, called EVADE, has additional features as compared with the implementation of Cho et al., which supplies the surgeon with distance feedback to one structure—the facial nerve.

EVADE is an acronym for Exposure Visualization and Audible Distance Emission. The software provides surgeons with two types of feedback. First, it offers distance control for multiple structures at the same time (8 different structures in the current software implementation), instead of just the facial nerve. The audio warning consists of a beep followed by a voice stating the name of the structure (Figure 1). Second, it updates the preoperative CT scan in near real time to show bone drilling virtually, enabling the surgeon to see the current extent of the drill cavity during surgery (Figure 1). [14] This feature is called virtual drilling.

Virtual drilling is similar to commercially available software from BrainLab (Munich, Germany) called Eraser; it draws spheres of different user-adjustable sizes at the tip of a navigated instrument. [15] The disadvantages of Eraser are that it cannot handle non-spherical shapes (e.g., a match-head shaped drill bit) and that a published result of evaluation of its accuracy is lacking. EVADE's virtual drilling was validated and as accurate to within approximately 3 mm in a study conducted earlier by our group. [12] However, these experiments were performed in rudimentary plastic temporal bone phantoms with modeled critical structures and drill bits of one given size and type.

The current investigation has three goals. First, we sought to set a benchmark for distance control image guidance systems, quantifying the method's potential for risk reduction of drill damage. Our hypothesis was that the protective perimeter distance was inversely proportional to the amount of risk. Drill damage risk was evaluated in an anatomically realistic test condition in which bias through diverging surgical skills or anatomic knowledge was minimized. Inexperienced users (medical students) performed a first-time mastoidectomy on human cadaveric heads, divided into 3 groups of decreasing protective perimeters, with a control group that did not have distance control. Second, we tested whether virtual drilling could reach similar accuracy in human cadaveric skulls, during realistic skull base approaches (multiple drill bit types and sizes were used), as during previous phantom experiments. Third, we investigated the clinical feasibility of the combined distance control and virtual drilling system EVADE.

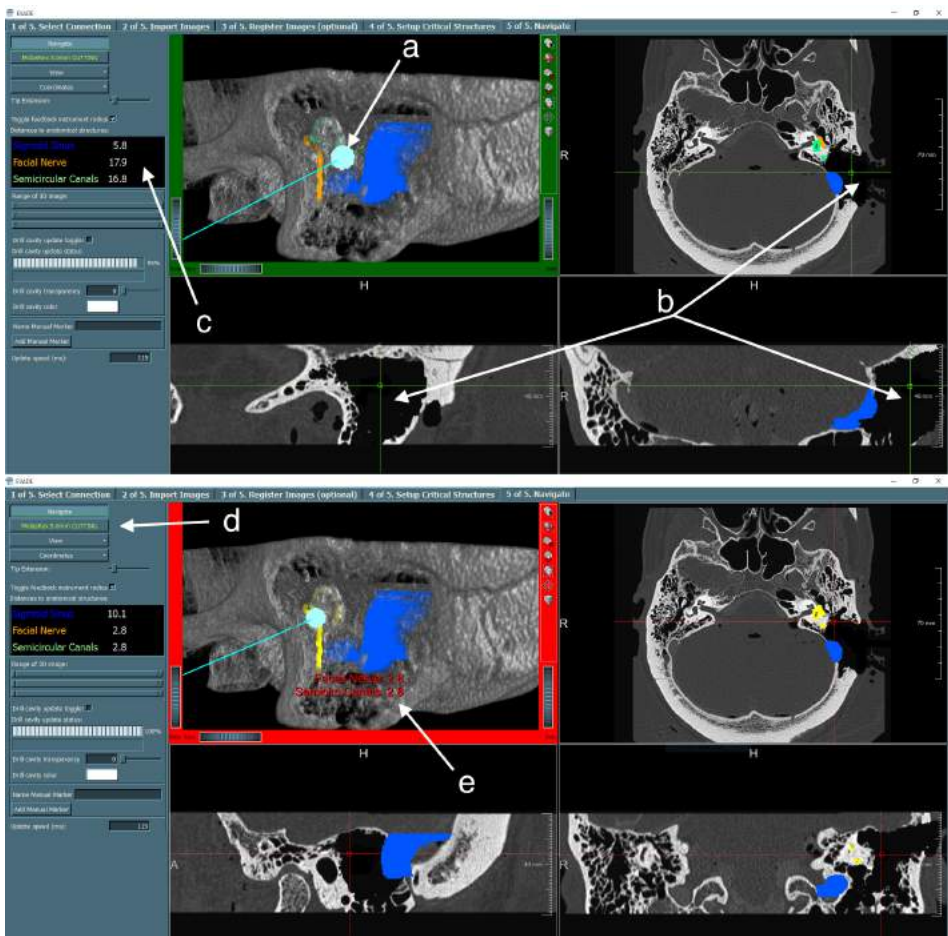


**Figure 4.1: The EVADE Interface**

The EVADE software interface is shown twice. The top image shows the interface in normal conditions. The bottom frame shows the interface when it gives an audiovisual warning because the drill entered the protective perimeter of critical structures. Figure annotations are displayed in white and are not part of the software. The cross designates the current position of the drill tip. The light blue shape at (A) represents the drill bit on the tip of the drill. The type and size of the drill bit can be selected at (D). The sigmoid sinus is shown in blue, the semicircular canals are shown in green, and the facial nerve is outlined in orange. The virtually drilled cavity is shown on the anatomic images in black in 3D and in 2D (B). The current distances to critical structures are displayed in the textual information panel at (C). The bottom panel shows a moment during surgery when the distances to the facial nerve and semicircular canals are 2.8 mm from the drill bit, which is below the set protective perimeter of 3 mm. Therefore, the system gives the surgeon a visual warning changing colors of the interface from green to red. In addition, a text is displayed over the 3D rendering stating the names of the structures and the distance to these structures at (E). Moreover, an audio warning is given at the same time.

## Material and Methods

### Test Subjects

Twelve medical students (9 men, 3 women, mean age 25 years) volunteered to participate in this study. Students were not associated with the authors or their departments in any way at the time the experiments were conducted. These students drilled cavities in the mastoid on prepared cadaver heads. The students were in their final year of medical school and had no surgical experience or extensive anatomic knowledge of the temporal bone. None of the students had performed a mastoidectomy beforehand. Each student performed only 1 mastoidectomy.

### Cadaver Heads

Nine formalin-fixed human cadaveric heads supplied by our institute's pathology department were used for this study. The cadaver heads were fitted with 8 bone-mounted screw fiducial markers for registration purposes. They were placed 4 cm off midline along the convexity of the skull on both sides (Figure 2).

### Scans

Subsequently, two computed tomography (CT) scans were acquired per head. One scan of lower resolution depicted the whole head, including all fiducial markers; this scan was used for cadaver head-image registration for image guidance. The other scan had a high resolution but only showed the temporal bone anatomy; this scan was used to designate temporal bone critical structures. The heads were moved slightly between scans to mimic movement of the patient between subsequent scans. Both scans were acquired on either a 64- or a 256-slice Philips CT scanner. Scan parameters were set to 120 kVp, 200 mAs, with a voxel size of 0.48 0.48 1.0 mm<sup>3</sup> for the image guidance scan and 0.20x0.20x0.30 mm<sup>3</sup> or 0.20x0.20x0.40 mm<sup>3</sup> for the temporal bone scan.

### Experimental Setup

The cadaver heads were fixed using 4 table-mounted screws. A reference frame (Medtronic, Boulder, Colorado, USA) was attached to the cadaver head. Each head was registered with its corresponding image-guidance CT scan. Segmented structures of the corresponding head were loaded into the EVADE interface. The drill was calibrated as described previously. [12]

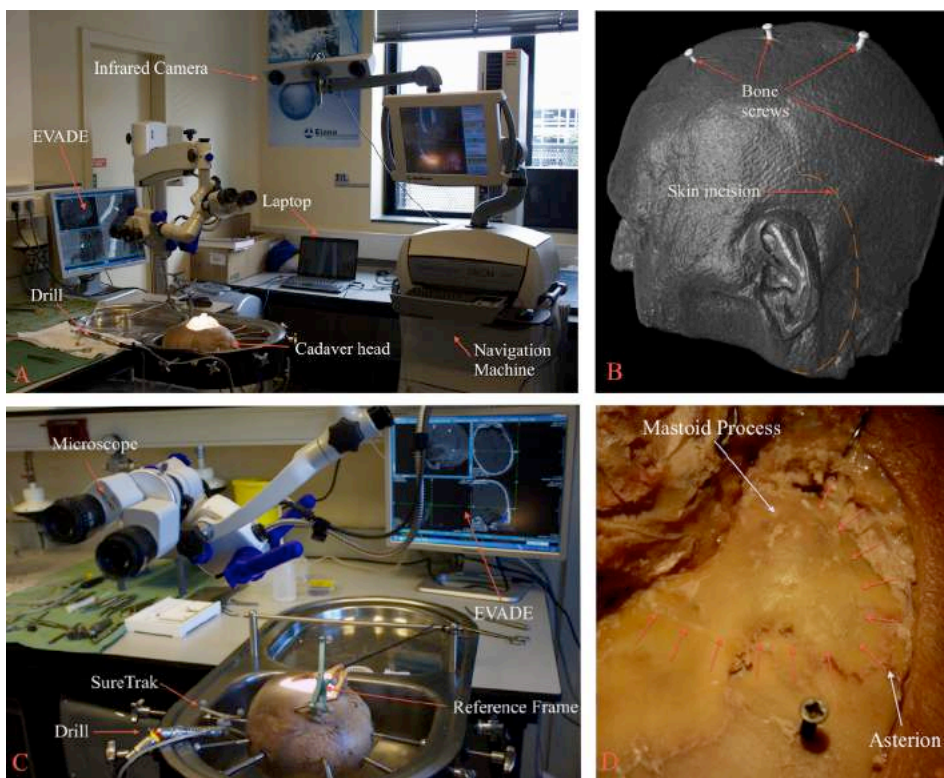


**Figure 4.2: Experimental Setup**

(A, C) The experimental setup for lateral skull base surgery using a navigated drill and the EVADE interface. (B) The position of the bone screws used for cadaver head-image registration and the approximate position of our skin incision for the student mastoidectomies on a 3D volume rendering of a cadaver head computed tomographic scan. (D) The typical engraved outline of a mastoidectomy (designated by the red arrows), which guides the students to drill the correct part of the skull base.

### Critical Structure Segmentation

Before segmentation, the temporal bone scan was registered to the image guidance scan using an image intensity-based rigid registration algorithm [16] for each particular cadaver head, of which the following structures were segmented: facial nerve, sigmoid sinus, jugular bulb, and semicircular canals delineated by experienced neurosurgical residents (authors E.V. or S.D.). The facial nerve was segmented using software integrated into EVADE, called Nerve-Click [17], extended with a function that projects a tubular shape around the facial nerve centerline (representing the diameter of the facial nerve). If necessary, centerlines were manually corrected. The other structures were delineated manually. Contours were drawn slice by slice in the axial direction and checked in sagittal and coronal directions and in three dimensions.

## Hardware and Software

Optical tracking was achieved with a Stealth Treon or S7 image guidance system (Medtronic). The image guidance machine was connected to a computer (Apple, Cupertino, California, USA) running Windows 7 (Microsoft Corp. Redmond WA, USA). The drill was tracked using a SureTrak frame (Medtronic). The EVADE interface was used; it is custom-made software programmed with the MeVisLab Programming Environment versions 2.0 to 2.3.1 (MeVis Research, Bremen, Germany). StealthLink (Medtronic) software enabled the EVADE interface to use the (x, y, z) coordinates provided by the image guidance system to calculate the drill position within the anatomic image. The position update frequency of the whole system varies between 6 and 15 Hz.

## EVADE

The EVADE user interface consists of multiple tabs for setup, registration, and segmentation of structures. There is a separate tab for setting the protective perimeter distance for each of the segmented structures individually (up to 8 structures). The protective perimeter distance can be changed during surgery. The image-guidance tab (Figure 1) used during surgery consists of a control and textual information panel on the left side. Located next to this is a panel with image information. In the top left corner of this image information panel, a 3-dimensional (3D) volume rendering of the anatomic image is shown. Three 2-dimensional (2D) orthogonal slices of the anatomic image are located around the 3D rendering. A cross designates the current position of the drill tip. The positions of the drill and drill bit are also shown in the 3D volume rendering. The type (e.g., manufacturer, diamond vs. cutting) and size of the drill bit is selected manually by the surgeon with a button that opens a popup menu. Virtual drilling cavities are created automatically if the system sees a navigated drill and rendered in near-real time in 2D and 3D in the image information panel. The current distances to segmented anatomic structures are displayed in the textual information panel. If the system gives a warning, the cross designating the current drill position becomes red. In addition, a text is displayed over the 3D rendering stating the names of the structures and the distance to these structures, while a red outline is displayed around the 3D rendering. Moreover, at the same time, a beep sound is produced and subsequently a voice states the name of the structure whose protective perimeter is crossed.

## Objective 1: Efficacy of Audiovisual Warnings

The following experiments were conducted in a simulated surgical setting using human cadaveric heads. One of the authors (E.V. or S.D.) performed a retro-auricular incision, and a myocutaneous flap was retracted anteriorly to expose the temporal bone underneath. Mus-



cles were freed from the mastoid process. A superficial outline on the cortical bone was made corresponding approximately to MacEwan's triangle to designate the area to be drilled by the students. The goal was to make the students perform a crude canal wall up cortical mastoidectomy. See Figure 2 for an overview of the experimental setup. Preoperatively, an introduction with a PowerPoint presentation (Microsoft) was given to every student; it covered the basics of a mastoidectomy, image guidance, and EVADE.

Twelve different medical students were asked to drill all bone within the outline on the mastoid bone without harming critical structures. Nine students used the EVADE interface during drilling. Three students in the control group used standard image guidance. If a student used EVADE, the sigmoid sinus, facial nerve, and semicircular canals received distance-controlled audiovisual warnings throughout the procedure. The virtual drilling feedback method was disabled. Protective perimeter distances were set to 1, 2, or 3 mm. Each perimeter setting was used by 3 different students; this resulted in 4 groups of 3 users per group:

1. A control group that used standard image guidance
2. A 3-mm perimeter EVADE group
3. A 2-mm perimeter EVADE group
4. A 1-mm perimeter EVADE group

Students used either a Hilan surgical drill with a 4.5 mm round cutting drill bit (B. Braun AG, Melsungen, Germany) or a Midas Rex surgical drill with a 4 mm round cutting drill bit. A drill-mounted irrigation system provided irrigation during drilling. The goal was to create the largest and deepest cavity possible within the outline, drilling as close as possible to the critical structures without damaging them. Users were instructed to stop the experiment when they thought no further drilling was possible without damaging critical structures. Time data were not recorded because it was not deemed a meaningful measure because of the experimental setup.

Postoperatively, the cadaver heads drilled by the medical students using EVADE were rescanned using a high-resolution CT scan protocol. Subsequently, the postoperatively acquired temporal bone scans were registered to the corresponding preoperative temporal bone scans. The drilled cavities were then delineated manually (slice by slice in the axial direction and checked in three orthogonal dimensions). The delineations were converted to 3D surface meshes without loss of resolution (i.e., with nodes at every voxel). For each of the 9 approaches performed by the students, the minimum unsigned Euclidian point-to-point distances be-



tween the meshes of the postoperative cavities and the segmented critical structures were calculated. A color-coded surface map of the temporal bone critical structures was made (Figure 3).

#### Objective 2: Accuracy of Virtual Drilling

The following experiments were conducted in a simulated surgical setting using human cadaveric heads. An experienced user (neurosurgeon) performed 2 canal wall-up cortical mastoidectomies, 2 translabyrinthine, and 2 retrolabyrinthine approaches using the operating microscope and EVADE. Different cutting and diamond drill bit sizes ranging 2-5 mm were used. A drill-mounted irrigation system provided irrigation during drilling. Spatulas and micro-instruments were used. All approaches were inspected for damage to critical structures after completion by the senior author (J.W.B.).

During the mastoidectomy, the distance control system was enabled for the sigmoid sinus, facial nerve, and semicircular canals. A protective perimeter of 3 mm was used during the initial gross dissection. During translabyrinthine and retrolabyrinthine approaches, the audiovisual warnings for the sigmoid sinus were switched off once it was adequately exposed. Switching off the warnings enabled a focus on protecting the semicircular canals and facial nerve. For the translabyrinthine approaches, the warnings for the semicircular canals were switched off when drilling through the canals to find the internal auditory canal.

The mean and signed maximal Euclidian surface-to-surface distances (i.e., the errors) between EVADE's "virtually" drilled cavity and the real cavity were calculated for the lateral skull base approaches. Both these cavities were delineated manually, and surface meshes were constructed from these delineations. The resulting surface-to-surface distances are a measure of the virtual drilling error; if the distance is zero, there is perfect overlap and the virtual drilling corresponds exactly to the real drilling. If the distance is nonzero, EVADE either overestimated or underestimated the virtual cavity as compared with reality (Figure 4). The mean distance, standard deviation, maximum underestimation error, and maximum overestimation error were calculated per approach. We used the same methods as described in our previous phantom article [12], where we found that the maximum intrinsic target registration error of the navigation system was 3 mm when using a navigated drill, and virtual drilling in phantom models had maximum errors of 1.6-3.4 mm. Our hypothesis was that the system could also obtain errors in these ranges in human cadaveric heads.

### Objective 3: Clinical Feasibility

Ethics approval from the institutional review board of the University Medical Center Utrecht and written informed consent the patients were obtained. In all cases, patient-image registration was performed with a preoperatively obtained CT-scan using 4 bone-anchored skull fiducial markers. Patient 1 was a 61-year-old man with progressive walking disability and right-sided facial nerve paresis (House-Brackmann grade 2) with a petroclival meningioma that underwent subtotal resection through a right-sided combined retrolabyrinthine-middle fossa approach. Surgery was performed by a neurosurgeon.

Patient 2 was a 36-year-old man with tinnitus and vertigo and a left-sided superior semicircular canal dehiscence who underwent transmastoid plugging of the superior semicircular canal.

Patient 3 was a 59-year-old man with vertigo and a left-sided superior semicircular canal dehiscence who underwent transmastoid plugging of the left superior semicircular canal. Both surgeries on patients 2 and 3 were performed by an otolaryngologist.

Before surgery, we checked that the software was working properly. We also checked whether scans loaded in the commercial image guidance system corresponded to the scans loaded into EVADE; whether the tool position of the commercial image guidance system and EVADE was identical; whether EVADE emitted audiovisual warnings to all segmented structures, by setting the protective perimeter temporarily to a great distance (e.g., 30 cm) and moving the navigated drill close to the head of the patient; and whether virtual drilling was working, by touching the skin of the patient with the drill and observing that the system created a virtual “cavity” in the skin. Furthermore, we asked the surgeon during surgery whether he or she received the audiovisual information and whether it was comprehensible. Lastly, we interviewed the surgeons about the added feedback methods postoperatively.

## Results

### Efficacy of Audiovisual Warnings

Surgically inexperienced users (medical students) using EVADE with a protective perimeter of 3 mm approached 9 of 9 (100%) critical structures to within 3 mm and did not damage any critical structures (0% risk). In the 2-mm group, users approached 7 of 9 structures to within 2 mm, and the sigmoid sinus was damaged once (1/7 amounts to 11% risk of damaging approached structures). Users in the 1-mm group came within 1 mm proximity of structures 6 of 9 times, and the sigmoid sinus was damaged twice (2/6 or 33% risk). The facial nerve and semicircular canals were approached closely in 14 of 18 cases and not injured. See Figure 3 for an illustration of the distance analysis performed. Users in the control group damaged critical structures on all 3 occasions. Critical structures were approached 5 of 9 times, and 3 of these structures were damaged (3/5 or 78% risk). The first 2 users damaged the sigmoid sinus and did not drill deep enough to reach the facial nerve and semicircular canals. The third student spared the sigmoid sinus and facial nerve but damaged the lateral and posterior semicircular canals. See Table 1 for an overview of the results of these experiments. Figure 5 illustrates the relation between the protective perimeter distance and the associated risk of damaging structures.

### Accuracy of Virtual Drilling

The software representation of the drilled cavities from the 6 lateral temporal bone approaches were compared with the post-operative real cavities through surface-to-surface error analysis (see Methods section). Detailed results per approach are provided in Table 2. The average mean difference between the virtually drilled cavities and the real cavities was  $0.4 \pm 0.7$  mm. The average maximum virtual underestimation and overestimation errors were  $2.8 \pm 0.1$  and  $3.3 \pm 0.4$  mm, respectively. The absolute maximum virtual underestimation and overestimation errors during all approaches were 3.0 and 3.6 mm, respectively. Critical structures receiving audiovisual warnings were not injured during drilling.

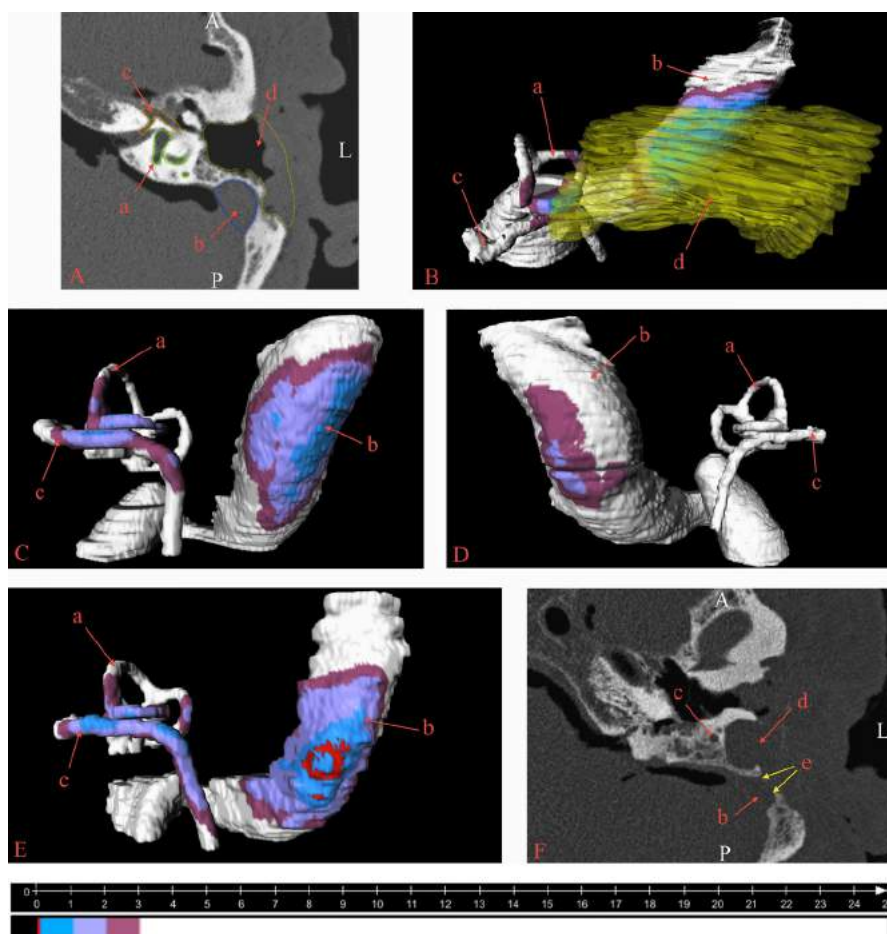


**Figure 4.3: Distance Analysis Results**

Results of the distance analysis performed on the inexperienced user mastoidectomy experiments. Figure annotations are displayed, designating (a) the semi-circular canals, (b) the sigmoid sinus, (c) the facial nerve, (d) the drill cavity, and (e) an area where the sigmoid sinus was damaged. (A) The critical structures and drill cavity were segmented manually from the postoperative computed tomographic scans. (B) The yellow cavity outline in (A) was converted into a 3D surface mesh and rendered in yellow (partially transparent). The critical structures were also converted to 3D surface meshes and rendered. Subsequently, the distances between the drill cavity and the critical structures were calculated, and these distances are displayed as colors on the critical structures. The legend for this color-coded distance is provided at the bottom of the Figure in millimeters. Red designates areas where the drill came so close that the structure was damaged. Blue designates areas where the student drilled closer than 1 mm to the structure. Light purple designates areas where the student approached the structure between 1 and 2 mm. Dark purple shows where the student's drill came within 2-3 mm in proximity of the structure. White represents areas where the drill cavity is more than 3 mm away from the structure. (C) Analysis of a procedure in which the student approached a large extent of the structures within EVADE's protective perimeter diameter of 3 mm. No structure was damaged. (D) Analysis of a mastoidectomy in which the student did not approach the semicircular canals closely. (E) Analysis of a procedure in which the sigmoid sinus was damaged by the student even though a 2-mm protective perimeter was imposed. (F) The damaged area of the sinus in (E) can also be seen on the computed tomographic scan (yellow arrows).

**Table 4.1: Mastoid Drilling Results**

<b>Group type</b>	<b>control group</b>			<b>1 mm protective perimeter</b>		
<b>Per Student</b>	1	2	3	4	5	6
SS approached	yes	yes	yes	1.3	0.0	0.0
SSC approached	no	no	yes	0.2	0.5	0.3
FN approached	no	no	yes	0.8	1.5	1.7
Fraction approached*	33%	33%	100%	66%	66%	66%
Structure damaged	yes	yes	yes	no	yes	yes
Damaged structure type	SS	SS	SCC	-	SS	SS
Fraction damaged*	100%	100%	33%	0%	50%	50%
<b>Per Group</b>	<b>control group</b>			<b>1 mm protective perimeter</b>		
Fraction approached **	56%			67%		
Total damaged structures	3			2		
Fraction damaged**	78%			33%		

Results of the unexperienced user mastoid drilling experiments, including the distance analysis results per student (top of table) and summary per group (bottom of table).

*Group type*: Type of group the student belongs too, i.e. a particular distance control protective perimeter group or control group.

*SS approached*: For the control group this parameter evaluates whether the sigmoid sinus was visually approached. For the distance control groups this parameter gives the minimum distance from the drill cavity to the sigmoid sinus in millimeters.

*SSC approached*: For the control group this parameter evaluates whether the semicircular canals were visually approached. For the distance control groups this parameter gives the minimum distance from the drill cavity to the semicircular canals in millimeters.

*FN approached*: For of the control group this parameter evaluates whether the facial nerve was visually approached. For the distance control groups this parameter gives the minimum distance from the drill cavity to the facial nerve in millimeters.

2 mm protective perimeter			3 mm protective perimeter		
7	8	9	10	11	12
1.5	0.0	1.2	0.7	0.3	1.7
4.3	1.1	0.6	0.9	0.9	0.3
2.7	0.7	1.9	2.2	1.0	1.6
33%	100%	100%	100%	100%	100%
no	yes	no	no	no	no
-	SS	-	-	-	-
0%	33%	0%	0%	0%	0%
2 mm protective perimeter			3 mm protective perimeter		
	78%			100%	
	1			0	
	11%			0%	

*Fraction approached:* The fraction (%) of all three structures (consisting of the sigmoid sinus, semicircular canals, and facial nerve) that was either approached visually in the control group, or to within the protective perimeter distance in the distance control groups. Results are given per student\* or per group\*\*.

*Structure damaged:* This parameter shows if any critical structure was damaged by the student.

*Damaged structure type:* If a structure was damaged by the student, this parameter gives the abbreviation of that particular structure (SS = sigmoid sinus, SSC = semicircular canals, FN = facial nerve). If no structure was damaged, this parameter yields a '-'.

*Fraction damaged:* For the control group, the fraction (%) of visually approached structures that were damaged. For the distance control groups, the fraction of structures approached to within the protective perimeter distance that were damaged. Results are given per student\* or per group\*\*.

*Total damaged structures:* The total number of damaged structures per group.

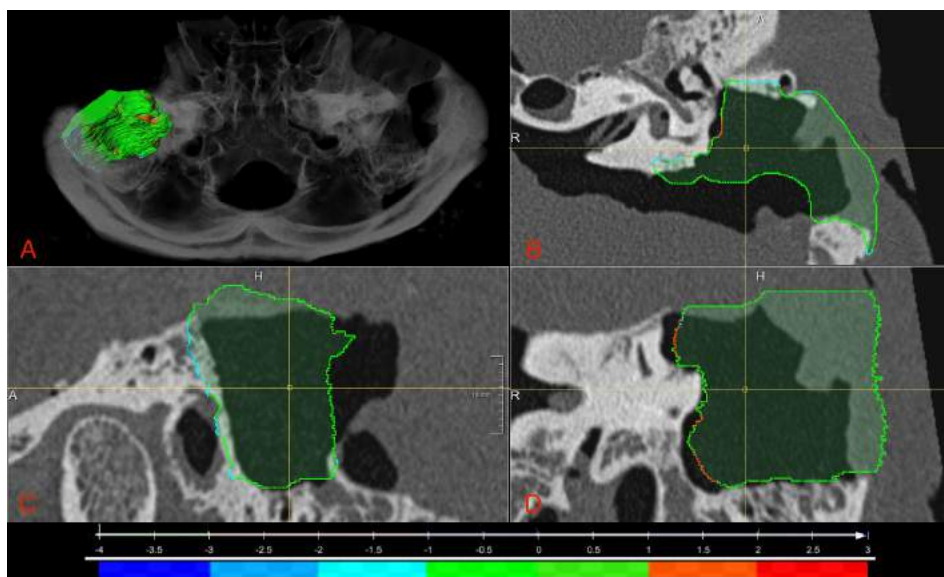


**Figure 4.4: Virtual Drilling Errors**

Illustration of drilling errors in the virtual drill cavity. Results are shown for the virtual versus real drill cavity surface-to-surface distance analysis of approach 5 (Table 1). (A) Translucent 3D rendering of high-resolution postoperative computed tomography (CT) of the temporal bone. The virtually drilled cavity is rendered within the right temporal bone. (B, C, D) Orthogonal sections through the postoperative CT and the drill cavity in the axial, sagittal, and coronal plane respectively. The drill cavity's surface is color-to-error coded. The legend for the color-to-error representation is provided at the bottom of the Figure. The green areas within the distance map denote errors of less than 1 mm. The orange areas represent virtual underestimation errors between 1 and 2 mm. The red areas represent areas of underestimation errors between 2 and 3 mm. The blue areas represent overestimation errors in a similar fashion.

### Clinical Feasibility

EVADE was used in the 3 clinical cases described in the Methods section. The patients' sigmoid sinuses, jugular bulbs, facial nerves, and semicircular canals were segmented preoperatively, which required approximately 30 minutes per patient. Setting up the necessary hardware in the operating room required approximately 30 minutes. The setup did not disturb the workflow of the surgeon, operating nurses, and anesthesia (Figure 6). During surgery, the surgeons could hear and see the audiovisual feedback and understand the information given by the system. Audiovisual warnings were given for the segmented structures mentioned previously. The protective perimeter was set to 3 mm for each of these structures. The surgeons found the provided audiovisual feedback useful because it helped them to maintain anatomic orientation during drilling. The distance control method was regarded as more useful than the virtual drilling method. Critical structures receiving audiovisual warnings were not injured during surgery. See Video 1 for an illustration of the distance control and virtual drilling methods in the operating theater.

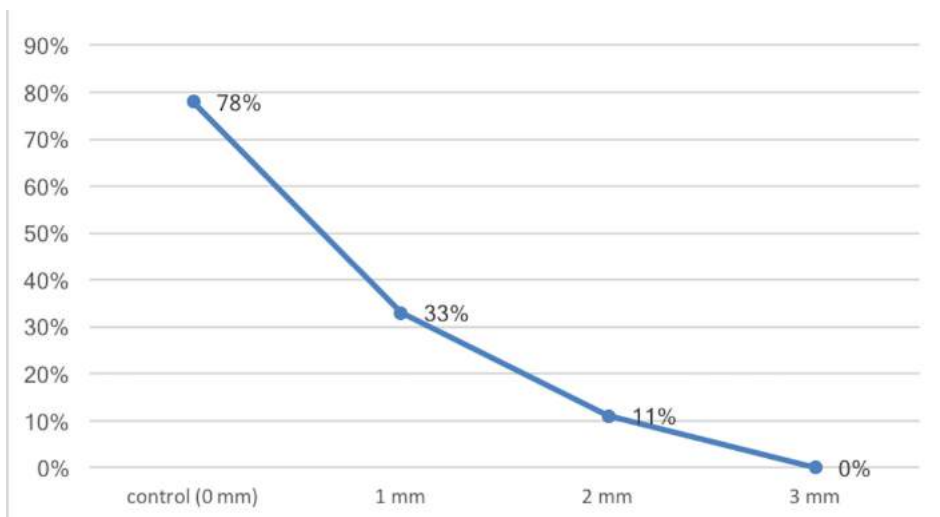


**Figure 4.5: Risk of Drill Damage as a Function of Protective Perimeter Distance**

Relation between the protective perimeter distance and the risk of a medical student damaging an approached critical structure during mastoidectomy on human cadaveric heads. On the y-axis the risk of drill damage (%) is depicted. The x-axis shows the associated protective perimeter distance from 0 mm in the control group to a maximum of 3 mm.

**Table 4.2: Virtual Drilling Accuracy**

Approach #	Approach Type	Mean Difference (mm)	Standard Deviation (mm)	Max Underestimation (mm)	Max Overestimation (mm)
1	Mastoidectomy	0.4	0.4	2.7	-2.5
2	Mastoidectomy	0.8	0.7	3.0	-3.6
3	Translabrynthine	0.4	0.5	2.9	-3.4
4	Translabrynthine	0.3	0.5	2.7	-3.6
5	Retrolabrynthine	0.4	0.5	2.8	-3.2
6	Retrolabrynthine	0.4	0.8	2.7	-3.6
<b>AVERAGE</b>		<b>0.4</b>	<b>0.7</b>	<b>2.8±0.1</b>	<b>-3.3±0.4</b>

Results of the virtual drilling cavity analysis showing the surface-to-surface differences between the virtually drilled cavities and the real cavities per approach performed.

*Approach Number:* Number of the surgical approach performed.

*Approach Type:* Type of surgical approach performed. A mastoidectomy classifies as a canal wall up cortical mastoidectomy.

*Mean Difference:* Mean distance of all calculated surface-to-surface distances between the virtual cavity and real cavity per approach.

*Standard Deviation:* Standard deviation of all calculated surface-to-surface distances between the virtual cavity and real cavity per approach.

*Maximum Underestimation:* Maximum surface-to-surface distance in which the virtual drill cavity is smaller than the real drill cavity, specified per approach.

*Maximum Overestimation:* Maximum surface-to-surface distance in which the virtual drill cavity is larger than the real drill cavity, specified per approach.

*Average:* Average of the values (with standard deviations) averaged over the six approaches.



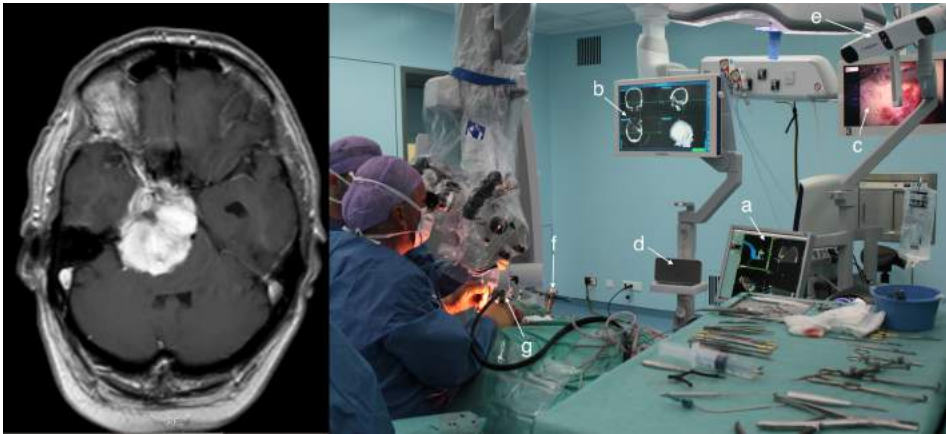


**Figure 4.6: Clinical Setup**

A clinical case and the intraoperative setup for EVADE. The left panel shows a T1-weighted gadolinium-enhanced axial magnetic resonance imaging scan of clinical test case 3. The right-sided petroclival meningioma was debulked through a combined retrolabyrinthine-middle fossa approach. The presented audiovisual feedback functions were used during drilling of the skull base. The right side of this Figure shows the intra-operative setting. Figure annotations designate (a) a computer screen showing the EVADE interface, (b) a screen showing the standard image guidance interface, (c) a screen showing the images from the microscope, (d) a speaker producing audio warnings, (e) the infrared camera of the navigation system, (f) the reference arc, and (g) the navigated drill with tracking frame attached.

#### **Video 4.1: Impression of Audiovisual Feedback Methods**

This video shows a neurosurgeon performing a right-sided combined retrolabyrinthine-middle fossa approach on a patient with petroclival meningioma (see Figure 6) while using the feedback functions of EVADE. It provides an impression of how the distance control and virtual drilling methods are used in the operating theatre.

Link: <https://doi.org/10.1016/j.wneu.2017.09.142>

## Discussion

This study evaluated two novel image guidance feedback methods that promise to improve surgery of the skull base: distance control and virtual drilling. Distance control image guidance reduces a surgeon's subjective workload required for drilling an approach through the lateral skull base surgery. [10] This could save surgeons precious mental energy needed for intracranial microsurgery (e.g., resection of a cerebellopontine angle tumor). Virtual drilling feedback helps the surgeon to improve the surgical approach by offering insight into the position and size of the drill cavity in relation to anatomic structures and underlying pathology, without requiring intraoperative imaging. [12,15]

Both feedback methods are already commercially available in some form. Karl Storz (Tuttlingen, Germany) has implemented distance control in their 2016 NAV1 navigation software, which is marketed specifically for endoscopic sinus and trans-sphenoidal surgery. BrainLab (Munich, Germany) offers Eraser, which can be used as a virtual drilling method. The results of this study are therefore relevant for neurosurgeons, otolaryngologists, and maxillofacial surgeons using this software. We anticipate that other manufacturers will release similar feedback methods soon.

This study sets a benchmark for distance control technology. It is, to our knowledge, the first investigation quantifying the effect of distance control on risk of damaging anatomically important structures of the skull base in a surgically realistic setting. Our data show an inversely proportional relationship between the protective perimeter distance and the risk of damage (Figure 5).

The risk was high (78%) in the control group, and it decreased to nonexistent (0%) in the 3-mm protective perimeter group. Assuming the quality of a mastoidectomy improves if more temporal bone structures are closely approached, it seems that the mastoidectomies in the protective perimeter distance control groups were of higher quality (67%-100% of structures approached) compared with the control group (56% approached).

In our opinion, these results suggest that even unskilled users can drill the skull base safely with a distance control system, if a protective perimeter distance of at least 3 mm is imposed. The results furthermore suggest that distance control is effective in reducing risks of iatrogenic injury to temporal bone structures from a navigated high-speed drill. It is important to realize that it is impossible to prove scientifically that new technology is 100% safe (one would

need an unlimited number of tests), and by no means do we claim here that the presented methods are infallible.

We chose to investigate risk reduction in a population of unexperienced users (medical students) with a similar level of training to ensure that subgroup results would not be biased by diverging surgical skills or anatomic knowledge, as would occur in a population of skull base surgeons with diverging ages, training, and skillsets. Another advantage of using unexperienced users was that we could measure a strong effect on risk, and consequently keep subgroups small. The disadvantage of this setup is that the quantified risk reductions cannot be translated directly to experienced users, such as skull base surgeons.

However, we believe that the presented risk quantification offers skull base surgeons important information on how to use distance control systems in practice. A protective perimeter distance of 3 mm or larger should be relatively safe in the hands of a skilled user, allowing the surgeon to drill quickly to preserve time and mental energy. A protective perimeter distance of 1 mm intrinsically (because of intrinsic spatial errors in image guidance) entails a higher risk of drill damage. In the hands of an experienced skull base surgeon, this risk might be acceptable if drilling is performed slowly and with focus. As with all technology, each surgeon must decide how to use it and make surgical decisions based on all available information (anatomic knowledge, previous experience, current view of the surgical field, sound of the drill while drilling, neuromonitoring, and image guidance). Distance control feedback may be a helpful addition to this armamentarium, especially in challenging cases, such as with altered anatomy or revision surgery.

Furthermore, our investigation of virtual drilling accuracy shows that virtual cavities can correspond to actual cavities, if care is taken to optimize navigation accuracy with bone-anchored head immobilization, rigid attachment of the reference frame, high-resolution isotropic CT images, bone-anchored fiducial markers, and optical tracking. The average maximum virtual overestimation and underestimation errors (of approximately 3 mm) were similar to the intrinsic maximum errors of tracking a drill tip in space, as published in our previous phantom study. [12] However, this time human cadaveric temporal bones with heterogeneous bone (e.g., cortex vs. trabeculae vs. the hard bone of the labyrinth) were drilled, and the surgeon used multiple drill bit types and sizes during each approach. Therefore, it seems that the use of different drill bits and heterogeneous human bone did not have a negative effect on the accuracy of virtual drilling. We suggest that the virtual drilling errors are a representation of the varying spatial accuracy inherent to an image guidance system, and not related to software implementation.

Overestimation errors of virtual drill cavities cause the system's monitor to display particular anatomy as absent, while it is still present within the operating field. Overestimation errors do not harbor direct risks for the patient; however, if these errors are large and frequent, they may provide unreliable information about the extent of bone drilling. On the other hand, underestimation errors could be directly dangerous for the patient because surgeons might get the impression from the system's monitor that they should drill further to arrive at a target, while in fact it has already been reached. Therefore, underestimation errors can contribute to iatrogenic injury of anatomic structures.

EVADe's design, which combines virtual drilling with distance control into one system, could prevent this type of iatrogenic injury, in theory. Effectively, any underestimation error occurring in the neighborhood of an anatomic structure can be "neutralized" by its protective perimeter and associated warning. Therefore, it is no coincidence that our finding of a "safe" 3-mm protective perimeter distance is approximately equal to the virtual drilling maximum underestimation error of  $2.8 \pm 0.1$  mm. This means that technical improvements in the spatial accuracy of image guidance systems might be able to decrease virtual drilling error and the required protective perimeter distance.

This study has several limitations. The cadaver and laboratory setting makes it difficult to directly extrapolate our cadaver results to surgery on patients. Our results do not demonstrate that distance control and virtual drilling are effective technologies for the experienced users for which they are intended. The efficacy of these methods for skull base surgeons will have to be demonstrated in a separate preclinical study. Moreover, our small sample size would make statistical analyses of the data unreliable; therefore, none were performed. Another limitation is the fact that drill cavity measurement inaccuracies were probably introduced into the virtual drill cavity error analysis. Two sources of error can be identified: the measurement error owing to scan resolution and the human error during manual segmentation of the cavities.

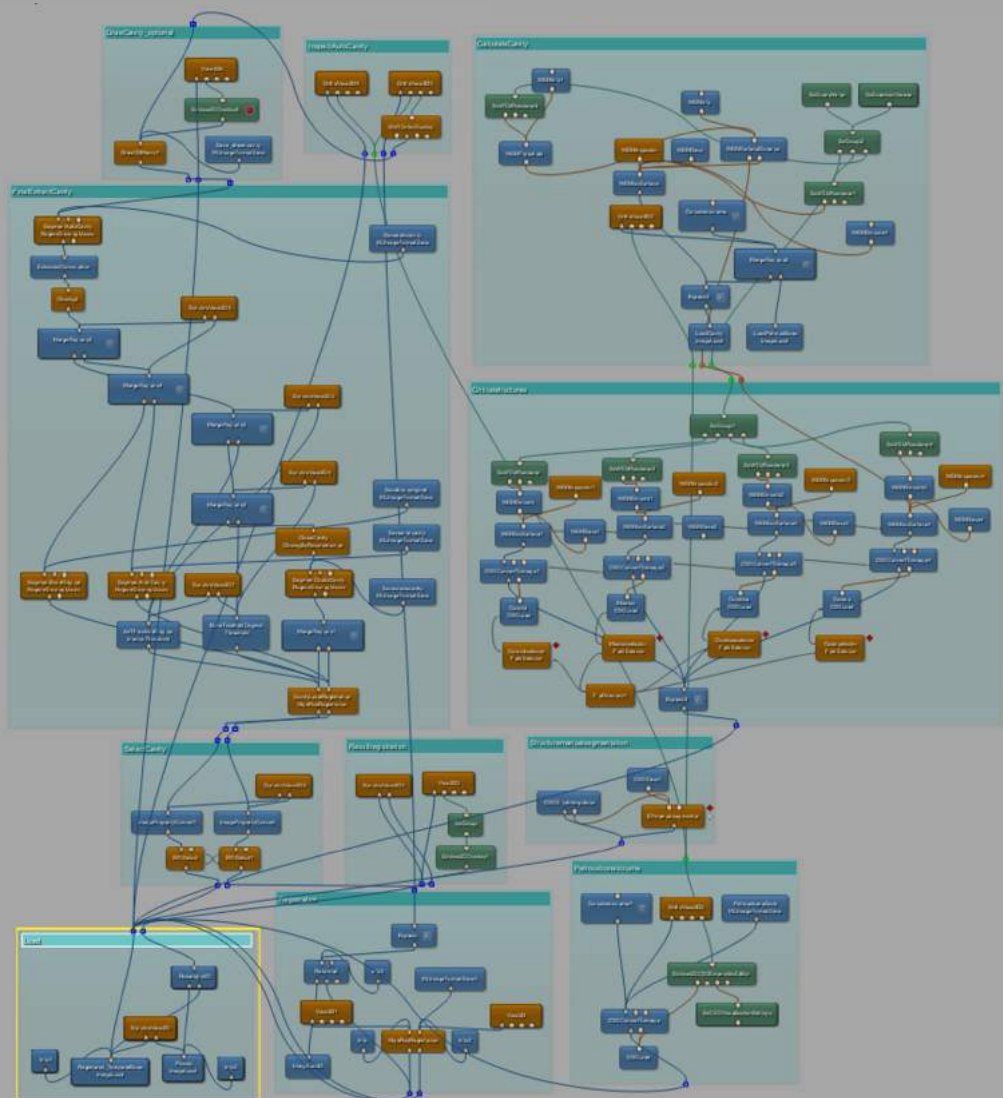
To our knowledge, we are the first group to demonstrate clinical feasibility of a combined distance control and virtual drilling system, which is more advanced compared with previous research modules [11,13] and currently available commercial products. We hope that this study inspires skull base surgeons to demand, and manufacturers to develop, similar systems in the near future. In any event, we hope that our research provides a better understanding of the possibilities and limitations of image guidance feedback technology.

## Conclusion

This article benchmarks the amount of risk reduction provided by distance control technology during drilling of the lateral skull base in a small population of surgically unexperienced users. Our data demonstrate the possible existence of an inversely proportional relationship between a set protective perimeter distance and the risk of drill damage. In this experimental setting, drill damage risk could be reduced to 0% by using a protective perimeter distance of 3 mm. Furthermore, we found that errors in virtual drilling reflect the intrinsic spatial errors of an image guidance system. Virtual drilling accuracy does not appear to depend on the heterogeneous density of human temporal bones and usage of multiple drill bit types and sizes. Finally, we report clinical feasibility of the combined distance control and virtual drilling system EVADE for lateral skull base surgery.

## References

1. Gharabaghi A, Rosahl SK, Feigl GC, Liebig T, Mirzayan JM, Heckl S, et al. Image-guided lateral suboccipital approach: part 1-individualized landmarks for surgical planning. *Neurosurgery*. 2008;62(3 suppl 1): 18-22-23.
2. Green JD Jr, Shelton C, Brackmann DE. Iatrogenic facial nerve injury during otologic surgery. *Laryngoscope*. 1994;104(8 Pt 1):922-926.
3. Nilssen EL, Wormald PJ. Facial nerve palsy in mastoid surgery. *J Laryngol Otol*. 1997;111:113-116.
4. Asma A, Marina MB, Mazita A, Fadzilah I, Mazlina S, Saim L. Iatrogenic facial nerve palsy: lessons to learn. *Singapore Med J*. 2009;50: 1154-1157.
5. Hohman MH, Bhama PK, Hadlock TA. Epidemiology of iatrogenic facial nerve injury: a decade of experience. *Laryngoscope*. 2014;124:260-265.
6. Ciric I, Zhao JC, Rosenblatt S, Wiet R, O'Shaughnessy B. Suboccipital retrosigmoid approach for removal of vestibular schwannomas: facial nerve function and hearing preservation. *Neurosurgery*. 2005;56:560-570 [discussion: 560- 570].
7. Hofer M, Grunert R, Dittrich E, Müller E, Möckel M, Koulechov K, et al. Surgery on the lateral skull base with the navigated controlled drill employed for a mastoidectomy (pre clinical evaluation). *Stud Health Technol Inform*. 2007;125: 179-184.
8. Strauss G, Koulechov K, Hofer M, Dittrich E, Grunert R, Moeckel H, et al. The navigation- controlled drill in temporal bone surgery: a feasibility study. *Laryngoscope*. 2007;117:434-441.
9. Hofer M, Dittrich E, Scholl C, Neumuth T, Strauss M, Dietz A, et al. First clinical evaluation of the navigated controlled drill at the lateral skull base. *Stud Health Technol Inform*. 2008;132:171-173.
10. Luz M, Manzey D, Modemann S, Strauss G. Less is sometimes more: a comparison of distance- control and navigated-control concepts of image-guided navigation support for surgeons. *Ergonomics*. 2015;58:383-393.
11. Strauß G, Schaller S, Zaminer B, Heininger S, Hofer M, Manzey D, et al. Klinische Erfahrungen mit einem Kollisionswarnsystem. *HNO*. 2011;59: 470-479.
12. Voormolen EHJ, Woerdeman PA, van Stralen M, Noordmans HJ, Viergever MA, Regli L, et al. Validation of exposure visualization and audible distance emission for navigated temporal bone drilling in phantoms. *PLoS One*. 2012;7:e41262.
13. Cho B, Oka M, Matsumoto N, Ouchida R, Hong J, Hashizume M. Warning navigation system using real-time safe region monitoring for otologic surgery. *Int J Comput Assist Radiol Surg*. 2012;8:395-405.
14. Woerdeman PA, Willems PWA, Noordmans HJ, Tulleken CAF, van der Sprenkel JWB. The impact of workflow and volumetric feedback on frameless image-guided neurosurgery. *Neurosurgery*. 2009; 64(suppl 3):ons170-ons175 [discussion: ons176].
15. Wurm J, Bohr C, Iro H, Bumm K. Intra-operative image update: first experiences with new software in computer-assisted sinus surgery. *Int J Med Robot*. 2008;4:202-209.
16. Klein S, Staring M, Murphy K, Viergever MA, Pluim JP. elastix: a toolbox for intensity-based medical image registration. *IEEE Trans Med Imag- ing*. 2010;29:196-205.
17. Voormolen EHJ, van Stralen M, Woerdeman PA, Pluim JP, Noordmans HJ, Viergever MA, et al. Determination of a facial nerve safety zone for navigated temporal bone surgery. *Neurosurgery*. 2012;70(1 Suppl Operative):50-60 [discussion: 60].



## **Distance Control and Virtual Drilling Improves Anatomical Orientation during Anterior Petrosectomy**

### ***Authors:***

Eduard H. J. Voormolen, Sander J. Diederer, Helene Cebula, Peter A. Woerdeman, Herke  
Jan Noordmans, Max A. Viergever, Pierre A. Robe, Sebastien Froelich, Luca Regli, Jan Willem  
Berkelbach van der Sprenkel

Submitted



## Abstract

**Object:** A combined drill distance control and virtual drilling image guidance feedback method was developed. The objective was to investigate whether usage of the proposed method, during anterior petrosectomy, would improve surgical orientation and objective surgical performance. The accuracy of virtual drilling, and the clinical practicability of the combined method, was also investigated.

### Methods:

In a simulated surgical setting using human cadavers, a trial was conducted with five expert skull base surgeons, from three different hospitals. They performed 10 anterior petrosectomy approaches, using either feedback methods or standard image guidance. Damage to critical structures was assessed. Operating time, drill cavity sizes, and proximity of postoperative drill cavities to the cochlea and the acoustic meatus, were measured. Questionnaires were obtained postoperatively. Errors in the virtual drill cavities as compared with actual postoperative cavities were calculated. In a clinical setup, the method was used during anterior petrosectomy.

### Results:

Surgeons rated their intraoperative orientation significantly better with feedback methods than with standard image guidance. During the cadaver trial, the cochlea was harmed on one occasion in the control group, while surgeons drilled closer to the cochlea and meatus without injuring them in the group using feedback. Virtual under- and overestimation errors were  $2.2 \pm 0.2$  and  $-3.0 \pm 0.6$  millimeters on average. The method functioned properly during the clinical setup.

### Conclusion:

The proposed feedback method improves orientation and surgical performance in an experimental setting. Errors in virtual drilling reflect spatial errors of the image guidance system. The method is clinically feasible during anterior petrosectomy.

## Introduction

Open microscopic anterior petrosectomy (AP) has become a standard neurosurgical procedure to approach intradural lesions such as brainstem cavernous malformations, petroclival meningiomas, posterior circulation aneurysms, and extradural lesions of the petrous apex. [1,2] AP requires drilling of the petrous bone in Kawase's triangle (or quadrangle). [3,10] One of its major complications is hearing loss caused by iatrogenic damage to the cochlea during the drilling part of the procedure. [5,8,11,17] Gross et al. reported a 12% incidence of hearing loss after AP to approach brainstem cavernous malformations. [7] This rate may be higher for other types of lesions and is probably dependent on the extent of exposure required. [8]

Several methods that aid in protection of the cochlea during AP, have been described previously. [2,5,6,9,11] Neurosurgical literature recommends to use anatomic landmarks (such as topographic features or anatomical extrapolations like the cochlear line and cochlear safety line) to localize the cochlea. [4,8,11] However, other studies show there is significant anatomic variability in the temporal bone, which potentially limits the applicability of these methods. [1,13] Therefore, a more reliable method, specified to the individual patient's anatomy, is needed.

Moreover, demand for good clinical outcomes after skull base surgery is currently increasing because of the effectiveness of less-invasive techniques such as radiosurgery. Therefore, aside from having extensive anatomical knowledge gained from cadaver dissections and surgical experience, modern skull base surgeons need to be optimally informed about each individual patient's anatomical variations during surgery.

Pre-operative imaging combined with intraoperative image guidance potentially provides an anatomically individualized method for designating the cochlea and other anatomical structures during AP. However, standard image guidance is as of yet unable to provide (real-time) feedback to indicate the location of these structures, while the surgeon is drilling the petrous apex.

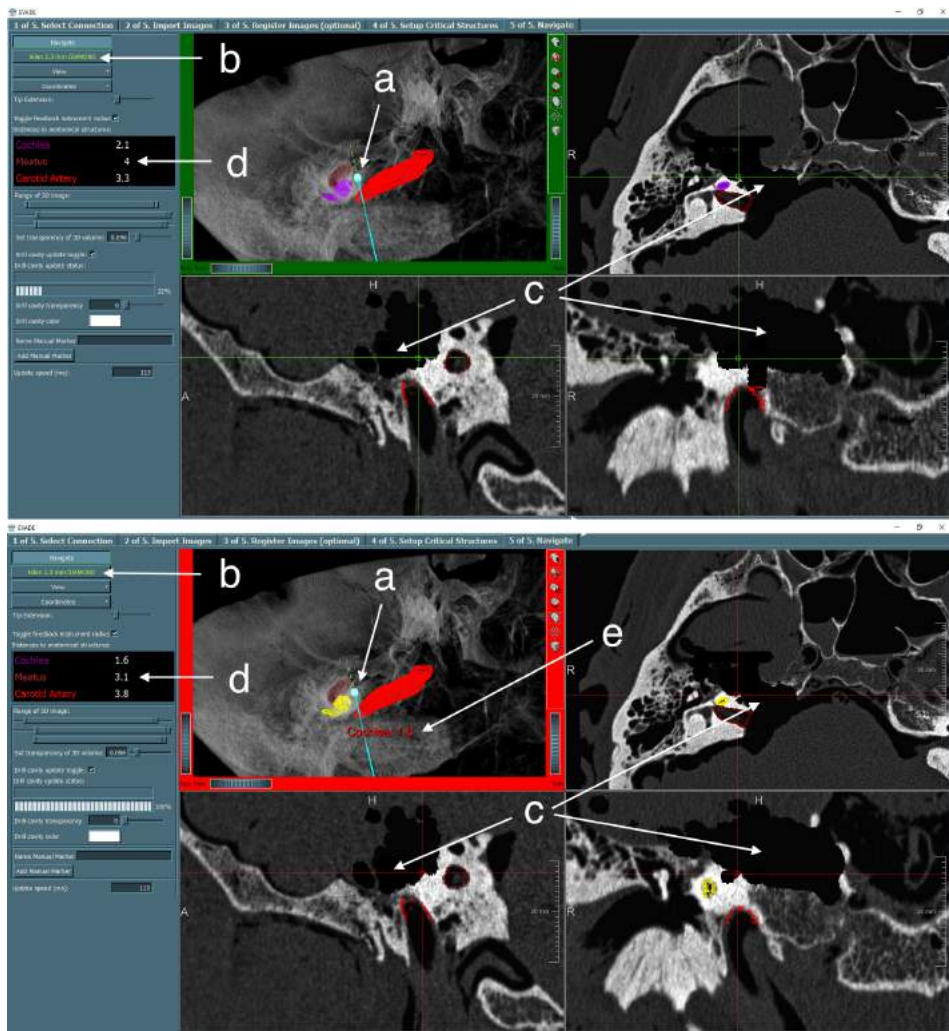


**Figure 5.1: The EVADE Interface**

The EVADE feedback interface is shown twice. The top image shows the interface under ‘normal’ conditions. The bottom frame shows the interface when it gives an audiovisual warning because the drill entered the protective perimeter of critical structures. Figure annotations (a–e) are displayed in white and are not part of the software. The cross designates the current position of the drill tip. The light blue shape at (a) represents the drill bit on the tip of the drill. The type and size of the drill bit can be selected at (b). The cochlea is shown in purple, the internal acoustic meatus in brown, and the carotid artery is outlined in red. The virtually drilled cavity is shown on the anatomical images in black (c). The current distances to anatomical structures are displayed in the textual information panel at (d). The bottom panel shows a moment during surgery when the distance to the cochlea is 1.8 mm from the drill bit which is below the set protective perimeter of 2.0 mm. Therefore, the system gives the surgeon a visual warning changing colors of the interface from green to red. Additionally, a text is displayed over the 3D rendering stating the name(s) of the structure(s) and the distance to this/these structure(s) at (e). Moreover, an audio warning is given at the same time.

Therefore, we developed a special software module (called exposure visualization and distance emission - EVADE) for this purpose. [14-16] The software augments image guided drilling during AP with distance control and virtual drilling feedback. Distance control continuously computes the distance between the drill tip and important structures (e.g. the cochlea, internal acoustic meatus, and internal carotid artery) and emits audiovisual warnings when the drill tip comes within a protective perimeter set at a certain distance around these structures. The warning includes a beep followed by a voice stating the name of the structure approached. Virtual drilling updates the pre-operative CT scan in near real time to show virtual bone drilling, enabling the surgeon to see the current extent of the drill cavity during surgery. See Figure 1.

Our hypothesis was that usage of the presented software improves the anatomical orientation of surgeons, thus reducing the risk of drill damage to anatomical structures during AP, while maintaining, or even improving surgical performance (for definition see Methods). The aim of this article was to investigate this hypothesis (i.e. the software's efficacy), and furthermore evaluate the accuracy and clinical feasibility of the software during AP. Efficacy was evaluated in a trial comparing surgical performance in a population of skull base surgeons performing AP either with standard image guidance and EVADE, or with just standard image guidance, in a cadaveric simulated surgical setting. Second, we researched whether virtual drilling feedback was accurate. Third, we investigated the clinical feasibility of the software during AP in a case of petroclival meningioma.

## Material and Methods

### Cadaver Heads

Five formalin fixed human cadaveric heads supplied by our institute's pathology department were used for this study. The cadaver heads were fitted with eight bone-mounted screw fiducial markers for registration purposes. They were placed 4 cm off midline along the convexity of the skull on both sides.

### Pre-operative Scans

Two computed tomography (CT) scans were acquired per head pre-operatively. One scan of lower resolution depicted the whole head including all fiducial markers; this scan was used for cadaver head-image registration for image guidance. A second high-resolution scan of the temporal bone anatomy was obtained to accurately segment petrous bone structures. Both scans were acquired on either a 64- or 256-slice Philips CT scanner. Scan parameters were set to 120 kVp, 200 mAs, with a voxel size of  $0.48 \times 0.48 \times 1.0 \text{ mm}^3$  for the image guidance scan and  $0.20 \times 0.20 \times 0.30 \text{ mm}^3$  for the temporal bone scan.

### Experimental Set-Up

Pre-operatively, the cochlea, internal acoustic meatus, and carotid artery were manually segmented (contours were drawn in the axial plane and subsequently checked in the sagittal and coronal planes) on the left and right sides by one of the researchers with extensive knowledge of radiological temporal bone anatomy. It took approximately 30 minutes to perform the segmentation per side. Next, the cadaver heads were fixed to the table using four table-mounted screws. See Figure 2. A reference frame (Medtronic Inc. Boulder CO, USA) was attached to the table. Each head was registered using four skull-fixed fiducial points (screws) to the pre-operatively acquired image guidance CT-scan. A SureTrak tracking frame (Medtronic Inc. Boulder CO, USA) was fixed to the drill and it was calibrated for image guidance.

Before the surgeons started their task, the heads were prepared in a standardized fashion: A curved skin incision over the ear, followed by a 5 by 5 cm temporal bone craniotomy was performed. Subsequently, the dura was peeled from the middle fossa and the middle meningeal artery was cut, exposing the greater superficial petrosal nerve (GSPN), foramen ovale, and mandibular nerve (V3). A spatula was positioned behind the petrous ridge to retract the temporal lobe from the skull base and expose the petrous apex.

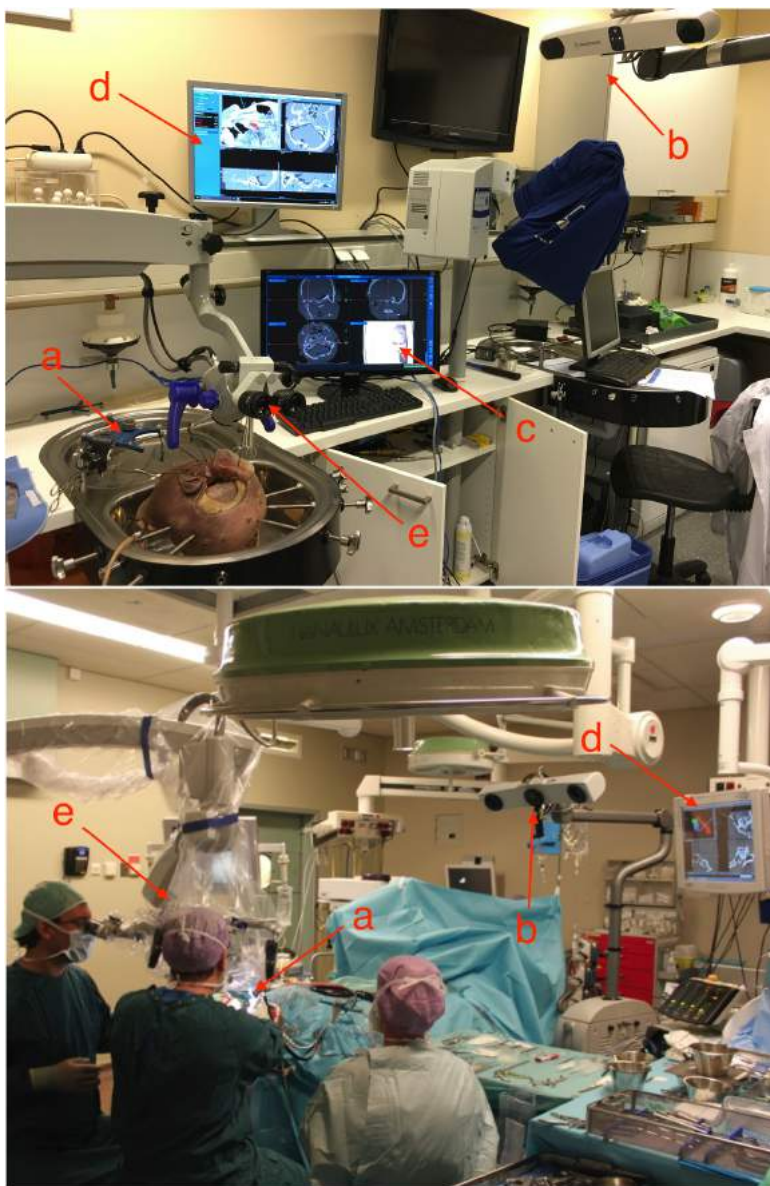


**Figure 5.2: Experimental Setup**

Illustration of the experimental cadaver and clinical setup. The upper frame shows the setup in the cadaver laboratory where a) designates the reference frame, b) the infrared camera of the image guidance system, c) the monitor displaying the standard image guidance interface, d) the monitor displaying the EVADE feedback software, e) the prepared cadaver head (start of the experiment), and f) the operating microscope.

The lower frame shows the setup in the operating room where a) designates the reference frame, b) the infrared camera of the image guidance system, c) the drill with attached SureTrak frame, d) the monitor displaying the EVADE feedback software, e) the operating microscope.

### Study Population

Five experienced Dutch skull base surgeons participated in the trial on a voluntary basis upon receiving an oral and/or written invitation by the main author (EV). Each surgeon had at least five years of experience in skull base surgery. The surgeons were based in three different university medical centers in the Netherlands with skull base reference clinics: the Erasmus University Medical Center, Rotterdam (1 surgeon); Leiden University Medical Center, Leiden (2 surgeons); University Medical Center Utrecht, Utrecht, The Netherlands (2 surgeons). The surgeons did not receive any financial or material compensation for participation in this study. A sixth separate skull base surgeon, and author of this manuscript, (LR) performed the clinical AP.

### Instructions and Task

All surgeons were introduced to the feedback functions of the EVADE image guidance software module via a standardized presentation approximately 30 minutes before the start of the experiment. The presentation instructed the surgeons about the experimental task. Their task was to make the largest possible bony exposure through the petrous apex, drilling as close as possible to the cochlea and meatus without injuring these structures. Surgeons were free to expand their exposures laterally. However, they were instructed to maintain the same kind of expansion for both approaches (on both sides). Moreover, surgeons were allowed to vary the protective perimeter value during the experiment. Completion of the task was defined from a surgeon perspective: the experiment ended when the surgeon believed that no more bone in the petrous apex could be drilled without injuring the cochlea or meatus.

### Trial Protocol

Ten anterior petrosectomy approaches were performed by five different skull base surgeons. Each surgeon performed two approaches on the same cadaver head on the same day. The first approach was performed using EVADE image guidance and standard image guidance and the second approach using standard image guidance. The anatomical side of the first approach (right or left) was decided by coin-toss. Two researchers (EV and SD/HC) were present during the experiments. Two digital stopwatches were used to measure the total operating time and the drill-on time. When the experiment finished, both researchers assessed drill cavities for iatrogenic damage to the meatus and cochlea. In addition, standardized questionnaires in which surgeons evaluated the presented feedback methods were obtained from the participants.

### Hardware and Software

Optical tracking was achieved with either a Stealth Treon or S7 navigation system (Medtronic Inc. Boulder CO, USA). The navigation machine was connected to a computer (Macbook



Pro, Apple Inc. Cupertino CA, USA) running Windows 7 (Microsoft Corp. Redmond WA, USA). The EVADE neuronavigation interface was used, which is a custom-made software program built using the MeVisLab Programming Environment versions 2.0 to 2.3.1 (MeVis Research, Bremen, Germany). StealthLink (Medtronic Inc. Boulder CO, USA) software enabled the EVADE interface to use the navigation coordinates provided by the image guidance system to calculate the drill position within the anatomical image. The position update speed of the system varies between 6-15 Hz in this setup.

#### AP Trial Outcome Measure Definitions

Post-operatively, the cadaver heads were re-scanned using CT (with the same scan parameters as the preoperative high resolution temporal bone CT). Subsequently, the post-operatively acquired temporal bone scans were registered to the corresponding pre-operative temporal bone scans. The drilled cavities were then delineated semi-automatically by an in-house algorithm developed and validated (data not shown) for this purpose. The relevant anatomical structures, being the cochlea, the internal acoustic meatus, the carotid artery, and the semicircular canals were delineated manually slice-by-slice on axial scans, and subsequently checked in three orthogonal directions and through 3D rendering. The drill cavity and anatomical structure segmentations were converted to 3D surface meshes without loss of resolution (i.e. with nodes at every voxel). For each of the ten approaches performed, the minimal unsigned Euclidian point-to-point distances between the meshes of the post-operative cavities and the anatomical structures were calculated. Furthermore, an axial maximum intensity projection (MIP) image, projecting the drill cavities and the segmented critical structures along the Z-direction, was computed for each anterior petrosectomy. In each MIP image, the area between the cochlea, meatus and drill cavity was calculated. This measure was called 'underused area'. We assume that a smaller underused area reflects a better surgical approach, because it means that more petrous bone has been removed close to the cochlea and meatus, thereby creating a larger exposure to the petroclival area. A value of zero represents an approach which follows the contours of the meatus and cochlea from anterior to posterior closely. See Figure 3 for an illustration of data analysis.

The following outcome measures were acquired and/or calculated as measures of surgical performance: total operating time, drill-on time, drill speed, cavity volume, iatrogenic damage to the cochlea/meatus, minimum and mean distance to cochlea/meatus, underused area, and standardized questionnaires.



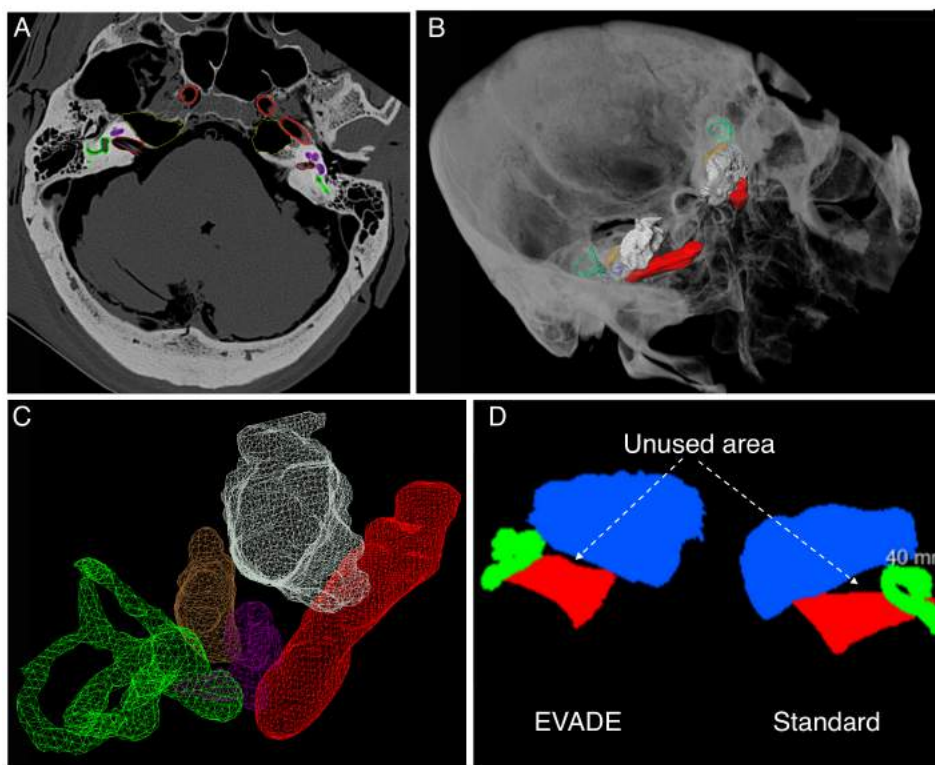


**Figure 5.3: Illustration of data analysis for the AP trial.**

Frame A shows an axial image of a registered temporal bone CT-scan in which anatomical structures were outlined by manual segmentation; red = carotid artery, purple = cochlea, brown = internal acoustic meatus, green = semicircular canals. Additionally, the two yellow outlines represent the left and right post-operative cavities segmented semi-automatically. Frame B is a 3D rendering showing a translucent temporal bone in which the structures and the drill cavities (in grey) described above are shown. Frame C shows an image zoomed in on the right side of the temporal bone to illustrate the 3D surface meshes of the drill cavity (in grey) and the anatomical structures (same color definitions as in frame B), which were generated to measure Euclidian distances. Frame D shows the result of one of the maximum intensity projections along the Z-axis. The drill cavity is shown in blue, the cochlea in green, and the internal acoustic meatus in red. The 'underused area' is the designated black space between the structures.

Total operating time is defined as the time taken from the first moment the surgeons looked through the microscope until the time the surgeon declared the task was complete. Drill-on time is defined as the time the drill was used to drill bone during the experiment. Drill speed is defined as the drill-on time divided by the drill cavity volume. Iatrogenic damage to the cochlea was defined as compromise of the structural integrity of the cochlea visible under the microscope and/or on the post-operative CT-scan. Iatrogenic damage to the meatus was defined as unintentional opening of the dura of the meatus with the drill, visible under the microscope. Statistical analysis was conducted with student's T-tests.

### Questionnaires

Standardized questionnaires were given to the surgeons in written form directly after the experiment ended. Each questionnaire contained five questions and required answers to be given on a five-point scale. The surgeons received instructions about the meaning of the scale. A student's T-test was applied to the data.

### Accuracy of Virtual Drilling

Under- and overestimation errors of the virtual cavities as compared with postoperative drill cavities were assessed. The mean and signed maximum Euclidian surface-to-surface distances (i.e. the errors) between EVADE's 'virtually' drilled cavity and the real cavity were calculated. The resulting surface-to-surface distances are a measure of the virtual drilling error. If the distance is zero, there is perfect overlap and the virtual drilling corresponds exactly to the real drilling. If the distance is non-zero, EVADE either overestimated or underestimated the virtual cavity compared with reality. The mean distance, standard deviation, maximum underestimation error and maximum overestimation error were calculated per approach.

### Clinical Case

In the operating room in the University Medical Center Utrecht an anterior petrosectomy approach was performed. Ethics approval from the hospital's medical review board to conduct this study was obtained. Patient-image registration was performed in the same way as for the cadaver trial. Two CT-scans (using similar scan parameters) with four bone-anchored skull fiducial markers were obtained pre-operatively. During this experiment, it was evaluated whether the software was working properly and whether the audiovisual information was received by the surgeon per-operatively. In addition, the surgeon was given a standardized questionnaire post-operatively.

## Results

### AP Trial Results

The total time needed to complete the AP task was on average 7 minutes longer (on a total of 74 minutes) in the group using EVADE compared with the control group ( $p = 0.69$ ). The drill-on time, the drill cavity volumes and the drill speed were similar in both groups. Surgeons using EVADE approached the cochlea on average 1 mm closer, as average minimum distances were  $1.1 \pm 0.7$  mm in the feedback group compared with  $2.2 \pm 1.4$  mm in the control group ( $p = 0.19$ ). The meatus was approached on average 0.8 mm closer in the group using EVADE (minimum distances of  $0.2 \pm 0.4$  mm vs  $1.0 \pm 1.2$  mm  $p = 0.21$ ). The data for the carotid artery and semicircular canals were calculated but are not reported here, because they were similar between groups. The 'underused area' (see Methods: AP Trial Outcome Measure Definitions) was  $0.1 \pm 0.1$  mm<sup>2</sup> in the EVADE group and  $0.9 \pm 1.2$  mm<sup>2</sup> in the control group ( $p = 0.22$ ). The basal turn of the cochlea was inadvertently opened by the drill on one occasion in the control group. The cochlea and meatus were not injured in the feedback group. See Table 1 for a group-wise comparison of outcome measures.

**Table 5.1: Outcomes of the AP trial**

Outcome Measure	EVADE	Standard	P-value
Total Time (h:m)	01:17±00:22	01:10±00:27	0.69
Petrous Bone Volume (cc)	5.1±1.24	5.3±1.6	0.85
Drill Time (h:m)	00:21:±00:05	00:21:±00:04	0.83
Drill speed (cc/min)	0.08±0.03	0.07±0.02	0.58
Total Cavity Volume (cc)	1.51±0.49	1.47±0.62	0.92
Underused Area (mm <sup>2</sup> )	0.1±0.1	0.9±1.2	0.22
Cochlea			
Injured	0/5	1/5	-
Minimal Distance (mm)	1.1±0.7	2.2±1.36	0.19
Meatus			
Injured	0/5	0/5	-
Minimal Distance (mm)	0.2±0.4	1.0±1.2	0.21

See the Methods section for definitions.

**Table 5.2: Outcomes of the Questionnaires per Skull Base Surgeon**

Surgeon #	Setting	Safety	Visual Feedback	Audio Feedback	Use Clinically?	Anatomical Orientation	
						EVADE	Standard
1	Laboratory	5	3	5	1(Yes)	5	5
2	Laboratory	5	2	5	1(Yes)	5	3
3	Laboratory	4	4	5	1(Yes)	4	3
4	Laboratory	4	3	5	1(Yes)	4	3
5	Laboratory	5	4	5	1(Yes)	5	3
6	Clinical	5	3	5	-	-	-
<b>AVERAGE</b>		<b>4.7</b>	<b>3.2</b>	<b>5</b>	<b>5/5</b>	<b>4.6*</b>	<b>3.4*</b>

Setting: 'Laboratory' if the surgeon performed simulated APs on a cadaver head in the laboratory, 'Clinical' if the surgeon performed AP on a patient in the operating room.

Safety: Answer to the question – How safe do you think EVADE is? (very safe: 5 ; not safe at all : 1)

Visual Feedback: Answer to the question - How well does EVADE's visual feedback help you to locate important anatomical structures? (a lot: 5 ; not at all: 1)

Audio Feedback: Answer to the question - How well does EVADE's audio feedback help you to locate important anatomical structures? (a lot: 5 ; not at all: 1)

Use Clinically?: Answer to the question – Would you use EVADE to perform an AP on a clinical case? (yes: 1 ; no: 0)

EVADE: Answer to the question – How was your anatomical orientation during the AP performed with EVADE? (very good: 5 ; very bad: 1)

Standard: Answer to the question – How was your anatomical orientation during the AP performed with standard image guidance? (very good: 5 ; very bad: 1)

\* Statistically significant difference between EVADE feedback and standard image guidance ( $p = 0.03$ )

Surgeons rated EVADE feedback as very safe (4.6/5). They rated the usefulness of the module's visual feedback in locating anatomical structures as average (3.2/5), and the audio distance feedback as excellent (5.0/5). Surgeons rated their intra-operative anatomical orientation statistically significantly better with the feedback system as compared to standard image guidance (4.6/5 vs 3.4/5  $p = 0.03$ ). See Table 2 for detailed results of the questionnaire.

#### Accuracy of Virtual Drilling

The virtually drilled cavities from five anterior petrosectomies were compared with the post-operative real cavities through surface-to-surface error analysis (see methods). The average mean difference between the virtually drilled cavities and the real cavities was  $0.2 \pm 0.1$  mm. Virtual drill cavity maximum under - and overestimation errors were on average  $2.2 \pm 0.2$  and  $3.0 \pm 0.6$  millimeters, respectively. The absolute maximum virtual under - and overestimation errors during all approaches were 2.4 and 3.6 mm respectively.

### Clinical Feasibility

A 36-year-old woman presented with dysarthria, an ataxic gait and intermittent diplopia on the basis of a left-sided petroclival meningeoma. She underwent a gross total resection (Simpson grade II) via an AP. Setup of the image guidance system hardware in the operating room required approximately 15 minutes of additional time. The software functioned properly during surgery: the surgeon could hear and see the audiovisual feedback given by the system. The protective perimeter was initially set to 3.0 mm and subsequently adjusted by the surgeon to 2.0 mm intra-operatively for the cochlea, internal acoustic meatus and carotid artery structures. The surgeon reported in the standardized questionnaire that the provided audiovisual feedback helped to improve his surgical orientation (see Table 1). Anatomical structures receiving distance control were not injured during this case.

## Discussion

We evaluated the effectiveness of an image guided feedback implementation combining distance control and virtual drilling feedback. As we hypothesized, our results demonstrate that this type of feedback improves skull base surgeons' anatomical orientation. Additionally, we are the first group to show that image guidance feedback might boost surgical performance of skull base surgeons by allowing them to 'optimize' their drill cavity. This is reflected by the fact that the cochlea and meatus were approached closer on average without being damaged, and the fact that the 'underused area' was smaller in the feedback group compared with the control group. Our other hypothesis was that usage of feedback reduces the risk of harming the cochlea. The cochlea was unintentionally injured on one occasion in the control group of this trial. This amounts to an incidence of 10%, which is a statistic that corresponds to the incidence reported in the literature. [7]

However, because of a small population size, this study cannot unequivocally claim that usage of feedback diminishes risk of drill damage to the cochlea or improves surgical performance. A statistically sufficient sample size would require 146 skull base surgeons (group 1 incidence 10%; group 2 incidence 0%; alpha 0.05; power 0.8). Unfortunately, it was not feasible to include this relatively large number of surgeons within acceptable time frames, given the paucity of trained skull base surgeons in Europe. Since we would not be able to show more than trends toward a protective effect, we stopped data collection at that point.

The cadaver setup of this research provided the advantage to minimize bias in ways that would be difficult to achieve in a clinical setting. For example, assuming left and right symmetry in the human head, bias due to anatomical variations between the control and intervention group was minimized. Moreover, memory bias in favor of EVADE was eliminated, since each trial surgeon always performed the first AP of the experiment with EVADE and afterwards with standard image guidance. In fact, it might be that our results are biased towards favoring the control group.

Previously, we found that the maximum 'intrinsic' target registration error of current image guidance systems is approximately 3.0 mm when using a navigated drill.[16] Furthermore, we demonstrated that virtual drilling during lateral temporal bone approaches had maximum errors ranging between 2.5 - 3.6 mm. [14] The accuracy results presented here (2.4 - 3.6 mm for AP virtual drilling) support our hypothesis that errors do not depend on the approach type, but rather reflect the intrinsic spatial errors of the image guidance system. Note that the

EVADE method is designed to neutralize these spatial errors in virtual drilling per-operatively with distance control (i.e. setting the protective perimeter value between 2-3 mm).

This study has several limitations. First, because of its cadaver and laboratory setting, it is impossible to extrapolate trial results to the clinical situation, although we here demonstrate clinical feasibility of the feedback system for AP. Second, it is important to emphasize that the feedback module will work properly only if anatomical structures have been delineated accurately in individualized pre-operative scans, and care is taken to accurately perform the patient-image registration with bone anchored fiducial markers.

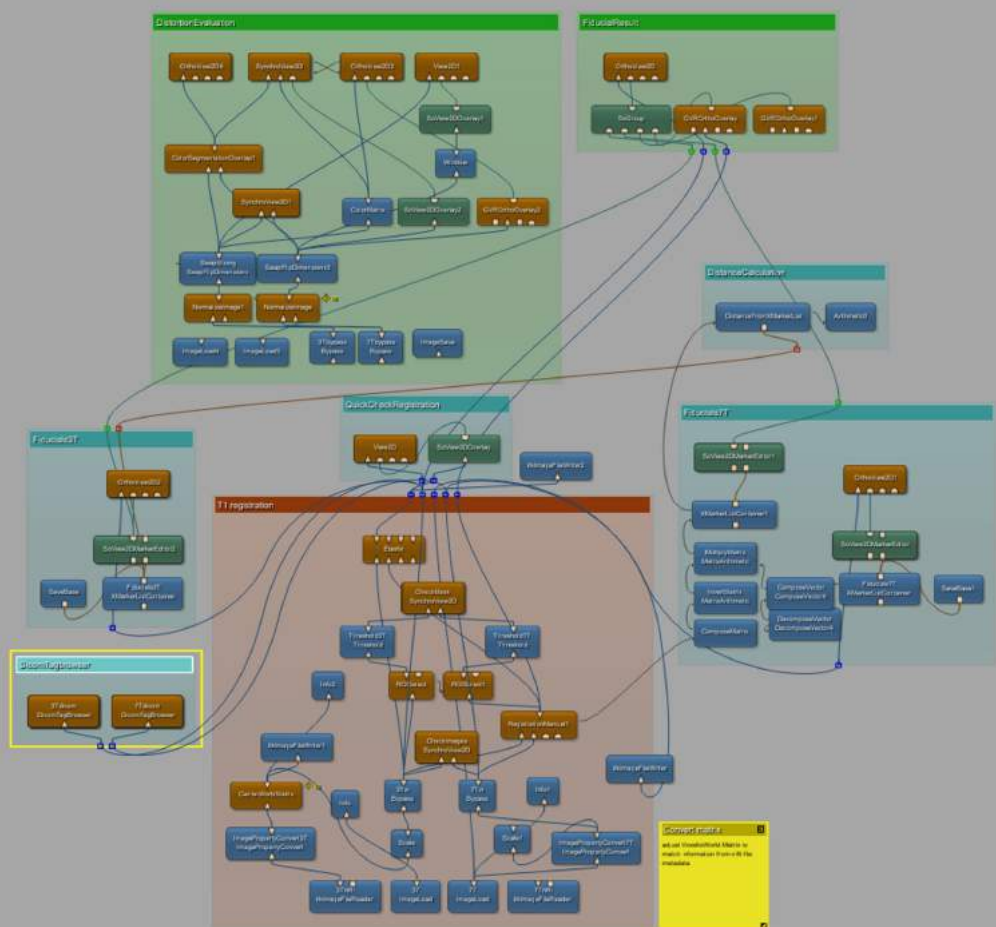
## **Conclusion**

In a population of experienced skull base surgeons, the addition of virtual drilling and particularly of drill distance control feedback during image-guided petrous apex drilling improves anatomical orientation, at least in an experimental setting. Moreover, there are trends in our data pointing towards an effect of this feedback to reduce the risk of accidentally drilling the cochlea and to improve surgical performance. Furthermore, this study shows that, during AP, errors in virtual drilling reflect the intrinsic spatial errors of an image guidance system. The presented image guidance feedback setup for AP is clinically feasible.

## References

1. Adams Pérez J, Rassier Isolan G, Pires de Aguiar PH, Antunes AM: Volumetry and Analysis of Anatomical Variants of the Anterior Portion of the Petrous Apex Outlined by the Kawase Triangle Using Computed Tomography. *J Neurol Surg Part B Skull Base* 75:147–151, 2014
2. Aslan A, Balyan FR, Taibah A, Sanna M: Anatomic relationships between surgical landmarks in type b and type c infratemporal fossa approaches. *Eur Arch Oto-Rhino-Laryngol Off J Eur Fed Oto-Rhino-Laryngol Soc EUFOS Affil Ger Soc Oto-Rhino-Laryngol - Head Neck Surg* 255:259–264, 1998
3. Borghei-Razavi H, Tomio R, Fereshtehnejad S-M, Shibao S, Schick U, Toda M, et al: Anterior petrosal approach: The safety of Kawase triangle as an anatomical landmark for anterior petrosectomy in petroclival meningiomas. *Clin Neurol Neurosurg* 139:282–287, 2015
4. Diaz Day J: The middle fossa approach and extended middle fossa approach: technique and operative nuances. *Neurosurgery* 70:192–201, 2012
5. Forbes JA, Rivas A, Tsai B, Ehtesham M, Zuckerman S, Wanna G, et al: Microsurgical Localization of the Cochlea in the Extended Middle Fossa Approach. *J Neurol Surg Part B Skull Base* 73:410–414, 2012
6. Fukuda H, Evins AI, Burrell JC, Medda A, Iwasaki K, Stieg PE, et al: Partial Anterior Petrosectomies for Upper Basilar Artery Trunk Aneurysms: A Cadaveric and Clinical Study. *World Neurosurg* 82:1113–1119, 2014
7. Gross BA, Dunn IF, Du R, Al-Mefty O: Petrosal approaches to brainstem cavernous malformations. *Neurosurg Focus* 33:E10, 2012
8. Guo X, Tabani H, Griswold D, Tayebi Meybodi A, Gonzalez Sanchez JJ, Lawton MT, et al: Hearing Preservation During Anterior Petrosectomy: The “Cochlear Safety Line.” *World Neurosurg* 99:618–622, 2017
9. Hsu FPK, Anderson GJ, Dogan A, Finizio J, Noguchi A, Liu KC, et al: Extended middle fossa approach: quantitative analysis of petroclival exposure and surgical freedom as a function of successive temporal bone removal by using frameless stereotaxy. *J Neurosurg* 100:695–699, 2004
10. Kawase T, Shiobara R, Taya S: Anterior transpetrosal-transtentorial approach for sphenopetroclival meningiomas: surgical method and results in 10 patients. *Neurosurgery* 28:869–875–876, 1991
11. Kim SM, Lee HY, Kim HK, Zabramski JM: Cochlear line: a novel landmark for hearing preservation using the anterior petrosal approach. *J Neurosurg* 123:9–13, 2015
12. Van Gompel JJ, Alikhani P, Tabor MH, van Loveren HR, Agazzi S, Froelich S, et al: Anterior inferior petrosectomy: defining the role of endonasal endoscopic techniques for petrous apex approaches. *J Neurosurg* 120:1321–1325, 2014
13. Villavicencio AT, Leveque JC, Bulsara KR, Friedman AH, Gray L: Three-dimensional computed tomographic cranial base measurements for improvement of surgical approaches to the petrous carotid artery and apex regions. *Neurosurgery* 49:342–352–353, 2001
14. Voormolen EHJ, Diederens S, van Stralen M, Woerdeman PA, Noordmans HJ, Viergever MA, et al: Benchmarking Distance Control and Virtual Drilling for Lateral Skull Base Surgery. *World Neurosurg* 109:e217–e228, 2018
15. Voormolen EHJ, van Stralen M, Woerdeman PA, Pluim JPW, Noordmans HJ, Viergever MA, et al: Determination of a facial nerve safety zone for navigated temporal bone surgery. *Neurosurgery* 70:50–60; discussion 60, 2012
16. Voormolen EHJ, Woerdeman PA, van Stralen M, Noordmans HJ, Viergever MA, Regli L, et al: Validation of exposure visualization and audible distance emission for navigated temporal bone drilling in phantoms. *PloS One* 7:e41262, 2012
17. Wang J, Yoshioka F, Joo W, Komune N, Quilis-Quesada V, Rhoton AL: The cochlea in skull base surgery: an anatomy study. *J Neurosurg* 125:1–11, 2016





# **Implications of Extracranial Distortion in Ultra-High Field MRI for Image-Guided Cranial Neurosurgery**

***Authors:***

Eduard H. Voormolen, Sander J. Diederer, Peter A. Woerdeman,  
Jan Willem Berkelbach van der Sprenkel, Herke Jan Noordmans, Max A. Viergever,  
Peter R. Luijten, Hans Hoogduin, Pierre A. Robe

Submitted

## Abstract

### Background:

Ultra-high-field 7.0 tesla (7T) magnetic resonance imaging (MRI) of the brain is attractive for image guidance during neurosurgery because of its high tissue contrast and detailed vessel visualization. However, high-field MRI is prone to distortion artifacts, which may compromise image guidance. Here we investigate intracranial and extracranial (skin) distortions in 7T MRI scans.

### Methods:

Five patients (group A) with and five patients (group B) without skin-adhesive fiducials received magnetization-prepared T1-weighted 7T MRI and standard 3T MRI scans. The 7T and 3T images were rigidly co-registered and compared. Intracranial distortions were evaluated qualitatively, whereas shifts at the skin surface and shifts of the center positions of skin-adhesive fiducials were measured quantitatively. Moreover, we present an illustrative case of an ultra-high-field image-guided skull base meningioma resection.

### Results:

We found excellent *intracranial* correspondence between 3T and 7T MRI scans. However, the average maximum skin shift was  $6.8 \pm 2.0$  mm in group A, and  $5.2 \pm 0.9$  mm in group B. The average maximum difference between the skin-adhesive fiducial positions was  $5.6 \pm 3.1$  mm in group B. In our tumor resection case, the skull base meningioma blood supply could be targeted early thanks to 7T image guidance, which made subsequent tumor removal straightforward.

### Conclusion:

There are no visible *intracranial* distortions in magnetization-prepared T1-weighted 7T MRI cranial images. However, we found considerable *extracranial* shifts, regardless of the presence of skin-adhesive fiducials. These extracranial shifts render 7T images unreliable for patient-to-image registration. We recommend to perform patient-to-image registration on a routine (CT or 3T MR) image, and subsequently co-register the 7T MR image with the routine image on the image guidance machine, until this issue is resolved.

## Introduction

Ultra-high-field MR scanners are becoming more widely available, and ultra-high-field scans are increasingly used in neurosurgery [2,5,10]. One of the main advantages of scanning at ultra-high fields, is that high-resolution images with high signal-to-noise ratio can be acquired within clinically acceptable timeframes. Furthermore, image contrast between different tissue types is enhanced as compared with scans acquired at lower field strengths, for example between parenchyma and blood (allowing imaging of blood vessels in great detail) [6,7] and between tissues of different iron and protein content (e.g., glioma and healthy parenchyma) [9,12]. These characteristics could make ultra-high-field images attractive for image guidance during resection of brain tumors (see Figure 1).

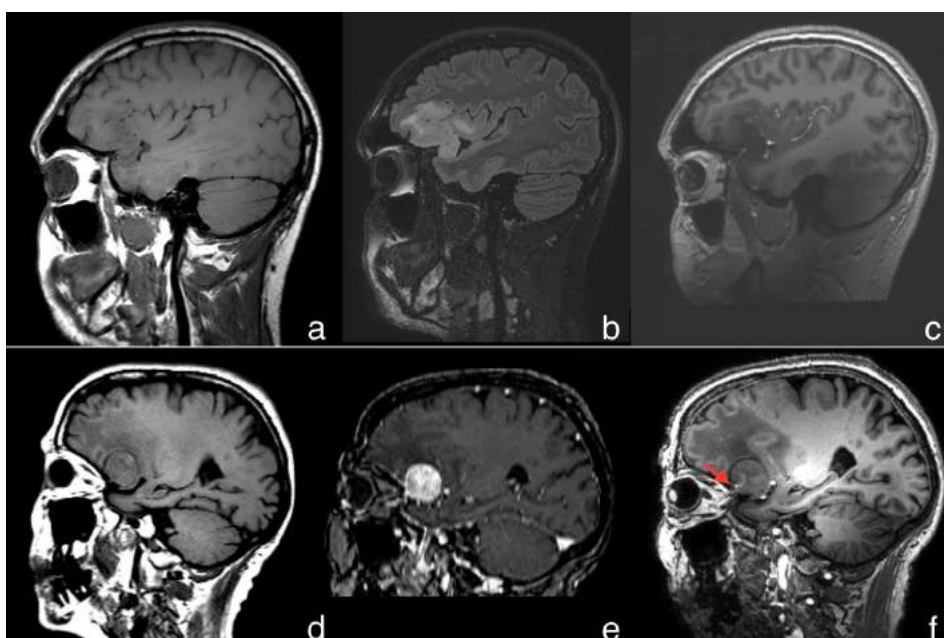


**Figure 6.1: Potential of 7T MRI for neurosurgical image guidance**

The top row (a,b,c) shows sagittal MR images of a patient with a left-sided insular glioma. Frames 1a and 1b depict the 3T T1-weighted and T2-FLAIR image, respectively. Figure 1c shows the T1-weighted 7T image. Note that this image visualizes the tumor more clearly than the 3T T1-weighted image; it is almost comparable with the 3T FLAIR image. Additionally, the 7T image distinctly shows the insular vessels.

The bottom row (d,e,f,) shows sagittal MR images of a different patient with a left-sided sphenoid wing meningioma, whose case is described in this article (Case 2). Frames 1d and 1e show a 3T T1-weighted image without and with gadolinium enhancement, respectively. Figure 1f shows the T1-weighted 7T scan. Both 3T images fail to clearly visualize a major arterial feeding vessel which can be seen vascularizing the tumor on the 7T image (red arrow).

MR images acquired using ultra-high-field scanners may, however, suffer from artifacts that violate the assumptions of spatial encoding, causing positional distortions that may compromise the spatial accuracy needed for image guidance. [1,3,5,11] Distortions can be categorized as originating from hardware or resulting from tissue characteristics. Intracranial distortions have been analyzed previously: Hardware-related distortions in 7T MRI are below voxel size and do not significantly contribute to inaccuracies during image-guided procedures. [3] With respect to artifacts caused by patient tissue characteristics, 7T MR images of the brain in Parkinson patients have comparable distortions to those observed on routine 1.5 T MRI. [5] Moreover, 7T MR images of patients with skull base tumors have been used for image guidance previously, without being hampered by intracranial artifacts that affected clinical utility. [2]

Based on these reports, we attempted to use a T1-weighted 7T MRI scan for image guidance with skin-adhesive fiducial-based patient-to-image registration in a case of glioma surgery (see Box 1 for a full case description). This procedure was performed with a back-up 3T MRI based image guidance system. To our surprise and in contrast with the abovementioned reports, tracking inaccuracies during image guidance rendered the 7T data useless.

This led us to investigate both *extracranial* and *intracranial* positional distortions at ultra-high MRI field strengths. We report here on the measured shifts in the positions of extracranial and intracranial elements on 7T MRI scans as compared with standard 3T MRI scans, and assess whether the presence of skin-adhesive fiducial markers influences these distortions.

#### **Box 1**

##### *Case 1: Suboptimal experience with ultra-highfield MR image guidance*

A 65-year-old female presented with a six-week history of dysphasia and progressive cognitive decline. Imaging studies found a left parietal mass with ring enhancement suspect of a high grade intra-axial tumor. She underwent an ultra-high-field MRI. An awake resection (in park bench position) with bipolar cortical stimulation was performed with the aid of image guidance with standard contrast-enhanced T1-weighted 3T MRI and T1-weighted non-contrast 7T MRI running simultaneously on two separate image guidance machines. 3T MRI fiducial registration error (FRE) and 7T FRE were respectively 1.9 mm and 3.5 mm. During surgery we found the target registration error in the ultra-high-field MR image guidance to be much greater than 3.5 mm. Therefore, image guidance with the 7T MRI was deemed unreliable and was discontinued. Maximal safe resection was achieved under 3T image guidance and neuromonitoring, and pathologic review revealed a glioblastoma multiforme WHO grade IV. There were no post-operative complications.

## Material & Methods

### *Subjects*

To assess intracranial distortion, shifts at the skin surface, and shifts in center positions of skin-adhesive fiducials, MRI data from ten subjects were used. Five patients without skin-adhesive fiducials were assigned to group A, and five patients with in total 33 skin-adhesive fiducials were assigned to group B. Furthermore, we present a surgical case with a left lateral sphenoid wing meningioma, who was operated using two image guidance systems: one loaded with 3T MR images, used to perform the procedure, and one loaded with 7T MR images, for investigative use (see Box 2). All subjects received both magnetization-prepared T1-weighted 7T MRI and standard 3T MRI scans.

The scans of the patients in group A were obtained from an anonymized research database (prospectively gathered at our institution). These five patients were diagnosed with WHO grade II gliomas. Demographics for the five consecutive patients with skin-adhesive fiducials in group B can be found in Table 1. Approval for this study was obtained from the Institutional Review Board at the University Medical Center Utrecht.

### *MRI Scan Parameters*

Patients received either a gadolinium-enhanced or a non-contrast T1-weighted 3T MRI scan, and a non-contrast T1-weighted 7T MRI scan. In group A the 3T and 7T MRI scans were obtained within four weeks from each other. In group B, both scans were obtained on the same day. Scan parameters were identical in group A and group B. Parameters for the 3D sagittal magnetization-prepared turbo field echo 3T scan were: Field of View (FOV) 256x256x192 mm<sup>3</sup> (matrix of 256x256x192), inversion time 960 ms, echo train length 232, readout repetition time (TR) 7.93 ms, echo time (TE) 4.5 ms, bandwidth 241 Hz/pixel, flip angle 8 degrees. The 7T scan parameters of the 3D sagittal magnetization-prepared turbo field echo sequence were: FOV 256x256x200 mm<sup>3</sup> (matrix of 256x256x200), inversion time 1200 ms, echo train length 256, readout TR 9 ms, TE 2.0 ms, bandwidth 506.3 Hz/pixel, flip angle 8 degrees. Total imaging times: 6m44s and 9m36s for 3T and 7T, respectively. Prior to the acquisition at 7T a B0-field map was acquired. The area of the brain of this map was used for 3<sup>rd</sup> order B0 shimming. At 3T the standard autoshim method of the scanner was used for linear shimming.

### *3T and 7T MRI Co-Registration*

Image-to-image co-registration was performed using a two-step semi-automated method implemented in the MeVisLab visual programming environment (MeVisLab 2.6, MeVis Research,

Bremen, Germany; [www.mevislab.de](http://www.mevislab.de)). The first step was a manual 6 degrees of freedom (DOF) linear registration without scaling to produce a coarse alignment of the images. The second step was an automatic linear transformation of the regions of interest based on mutual information cost optimization. The automatic co-registration step was performed with the use of the open source toolbox Elastix.[8] In this fashion, the ultra-high-field images were rigidly transformed (i.e. transformation without scaling or deformation) and overlaid on the 3T images for each subject.

### *Intracranial Distortion Evaluation*

Qualitative evaluation of image distortion of intracranial tissue was performed on the co-registered 3T and 7T MR images by two neurosurgeons (EV, PR). Two different methods were used.

First, color-coded difference images were generated based on image intensities from both images. Second, checkerboard views were made and the overlap of the images was estimated in three orthogonal directions (Figure 2). Both methods were used simultaneously. The difference image was used to screen for potential regions of distortion (it has a very high sensitivity for differences between images) and all these regions were then meticulously evaluated with the checkerboard view; making use of windowing, panning and zooming and varying the size of the checkered squares. We made sure that differences in the images did not represent differences in biological information (e.g. blood vessels). Different brain regions (ventricles, brain lobe cortices, and brain tumors) were evaluated systematically and the extents of non-overlap (i.e. shifts) were noted (Table 1).

### *Shifts in Skin Surface*

3T and co-registered 7T images were analyzed using the same BrainVoyager (BrainVoyager 20.6, Brain innovations, Maastricht, the Netherlands) workflow. The built-in region growing algorithm (thresholded at the image intensity of the skin) was used to segment the cranium from the background. Background voxels were set to 0. A mesh was iteratively morphed to find the surface of the cranium with the following parameters: smoothing force of 0.07, border control of 1.0, surface finding force of 0.3, finding intensity of the lowest image intensity of the skin; interpolation was set to trilinear (see Figure 3a). The meshes were then imported into the MeVisLab programming environment and analyzed further (see Figure 3b).

A region of interest (ROI) was imposed on the mesh, containing the convexity of the head, the orbit and nasal root, because this area is utilized as matching surface for most surface-based

(i.e. skin tracing) patient-to-image registration algorithms (see Figure 3c). Next, the unsigned Euclidian distance between 3T and 7T meshes was calculated for every node in the ROI and statistics (mean, standard deviation, maximum) were given. A color-to-distance coded mesh was generated (see Figure 3d). We validated this method on additional data by comparing 3T MRI with CT images: skin shifts yielded maxima of below 2.0 mm (data not shown).

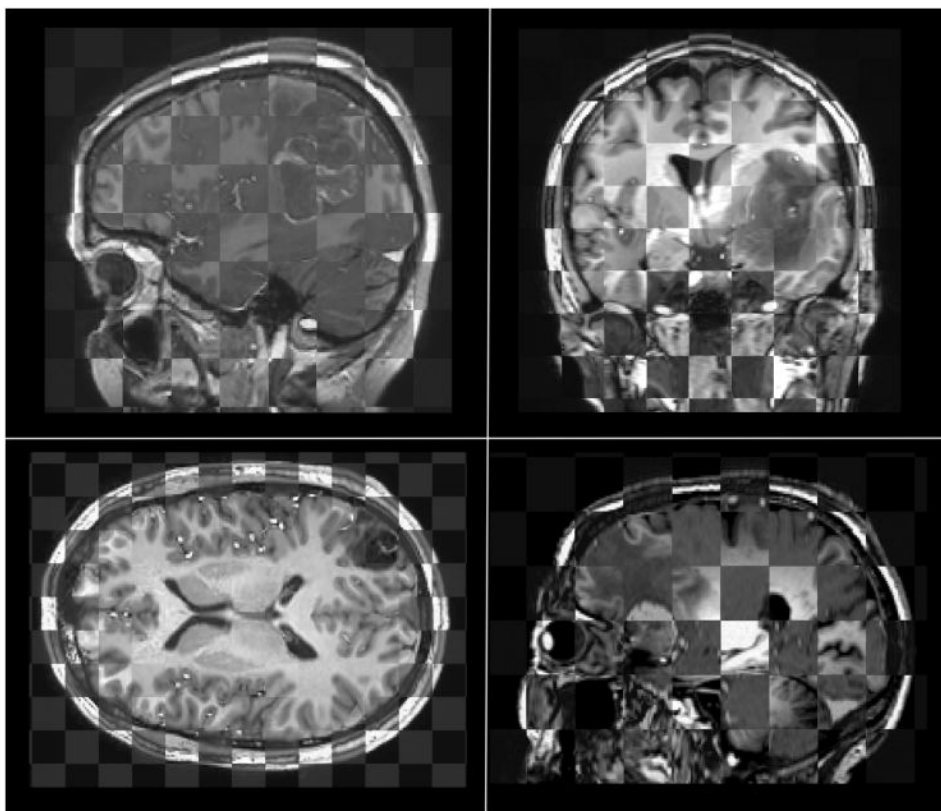


**Figure 6.2: 3T and 7T MR Image Overlap**

Checkerboard images of four different cases displaying excellent overlap, also in areas of tumor.

#### *Shifts in Skin-Adhesive Fiducials*

The center points of all skin-adhesive fiducial markers (Medtronic, USA) were designated by a neurosurgeon (EV) both on 3T and 7T MRI scans of five patients before co-registration. After co-registration, the center points were subjected to the same transformation function as the images. Subsequently, the Euclidian distance between the 3T and the 7T position for each center point was calculated in a custom-implemented method in the MeVisLab programming environment.



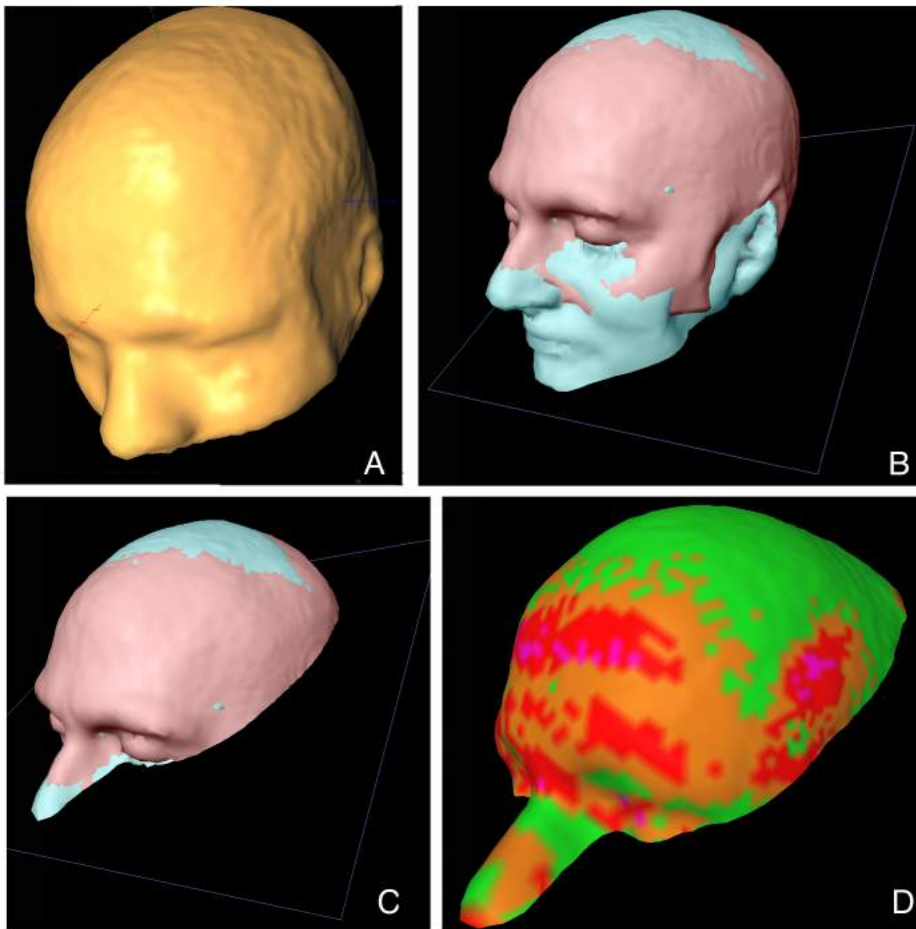


**Figure 6.3: Illustration of the surface skin shift analysis**

Frame A shows a rendering of the generated skin surface mesh of a 7T image (see Methods for details). Frame B shows renderings of the 3T mesh (in blue) and 7T mesh (in red) projected on top of each other. The 3T and 7T mesh ROIs (showing the parts of the skin surface most commonly used for surface-based patient-image registration: the forehead, orbit, and nasal root) are depicted in Frame C. Frame D shows a rendering of the color-to-distortion mesh (green < 2.0 mm; orange 2-3 mm, red 3-4 mm, and purple >4 mm shifts).

### *Surgical Cases*

Intra-operative image guidance was performed with a Medtronic Stealth Treon system (Medtronic Surgical Navigation, Louisville CO, USA). Surgeries were performed according to hospital protocol and standard microsurgical techniques. A Mayfield head clamp (Integra LifeSciences, Saint-Priest, France) was utilized for fixation of the head in all cases and in the meningioma case a Budde Halo retractor system (Integra LifeSciences, Saint-Priest, France) was used.

## Results

### *Intracranial Distortion Evaluation*

No intracranial supra-voxel distortions were found in the 7T MRI scans of group B (Table 1). We found no intracranial distortions around brain tumors. In group A, there were two cases where the medulla oblongata appeared to be shifted by one voxel in the 7T MRI compared with the 3T MRI scan.

### *Skin Shift Evaluation*

The overall mean shift of skin surface in group A was  $1.5 \pm 1.1$  mm, and the average maximum shift was  $6.8 \pm 2.0$  mm. The maximum shift found in group A was 9.1 mm. In group B, the overall mean shift was  $1.3 \pm 0.7$  mm, and the average maximum shift corresponded to  $5.2 \pm 0.9$  mm. The maximum shift in group B was 6.1 mm. Group differences were not statistically significant. The skin shift averaged over both groups was  $1.4 \pm 0.9$  mm with an average maximum shift of  $6.1 \pm 1.6$  mm. See Table 1 for details.

### *Shift in Skin-Adhesive Fiducials*

We analyzed the shift in skin-adhesive fiducials in group B over a total of 33 fiducials. The average shift was  $3.2 \pm 1.7$  mm and the average maximum shift  $5.6 \pm 3.1$  mm. The absolute maximum fiducial shift found was 9.4 mm. See Table 1 for results per case.

#### **Box 2**

##### *Case 2: Benefit of ultra-highfield (7T) MR image guidance*

A 74-year old female presented with a four-year history of progressive short term memory problems and a six-month history of progressive headaches. Imaging studies revealed a solid enhancing tumor at the left lateral sphenoid wing, suspect for meningioma. It was decided to perform a resection. The patient underwent an ultra-high-field MRI. Before surgery, the T1-weighted 7T MRI was fused with a standard 3T MRI on the navigation machine. Since there was no gadolinium enhancement of tumor tissue, but vessels were readily visualized on the 7T MRI, we could easily localize the major arterial feeder; a branch of the middle meningeal artery (Figure 1e). After patient-to-image registration, the FRE measured 2.3 mm. We used image guidance to direct our craniotomy and guide the subsequent drilling of the sphenoid wing to explore the feeding branch first. It was localized (Figure 4) and cauterized. Afterwards, an 'en bloc' resection of the tumor was achieved with minimal blood loss. There was no post-operative complication. Pathology showed a meningioma WHO grade I.

Table 6.1: Demographics and Results

Case	Sex	Age	Gr	Pathology			Gad	Fid
					Lobe	Side		
1	n/a	n/a	A	low grade glioma	occipital	L	no	no
2	n/a	n/a	A	low grade glioma	temporal	L	no	no
3	n/a	n/a	A	low grade glioma	insula	L	no	no
4	n/a	n/a	A	low grade glioma	temporal	R	no	no
5	n/a	n/a	A	low grade glioma	occipital	L	no	no
Group Mean								
6	F	82	B	neurocognitive	n/a	n/a	no	yes
7	F	75	B	neurocognitive	n/a	n/a	no	yes
8	F	74	B	meningeoma	sphenoid	L	yes	yes
9	M	25	B	low grade glioma	insula	L	yes	yes
10	F	65	B	high grade glioma	parietal	L	yes	yes
Group Mean								
Overall Mean								

This table shows the demographics of our study population, and the results of the intracranial and extracranial distortion evaluation per group (A and B) and per case.

Fid. Shift (mm)			Skin Shift (mm)			Spatial Shift At (# of voxels):							
Mean	SD	Max	Mean	SD	Max	Mid	Fro	Par	Tem	Occ	Pos	T.	
n/a	n/a	n/a	1,5	1,0	4,6	0	0	0	0	0	1	0	
n/a	n/a	n/a	1,7	1,2	8,8	0	0	0	0	0	1	0	
n/a	n/a	n/a	2,1	1,3	9,1	0	0	0	0	0	0	0	
n/a	n/a	n/a	1,1	0,9	5,2	0	0	0	0	0	0	0	
n/a	n/a	n/a	1,2	1,0	6,5	0	0	0	0	0	0	0	
<b>n/a</b>	<b>n/a</b>	<b>n/a</b>	<b>1,5</b>	<b>1,1</b>	<b>6,8</b>								
2,7	1,5	4,5	1,1	0,7	5,2	0	0	0	0	0	0	n/a	
1,5	0,7	2,5	1,0	0,5	3,9	0	0	0	0	0	0	n/a	
5,2	2,7	8,4	1,6	1,0	6,1	0	0	0	0	0	0	0	
3,6	3,2	9,4	1,1	0,7	6,0	0	0	0	0	0	0	0	
3,0	0,5	3,5	1,8	0,7	4,9	0	0	0	0	0	0	0	
<b>3,2</b>	<b>1,7</b>	<b>5,6</b>	<b>1,3</b>	<b>0,7</b>	<b>5,2</b>								
			<b>1,4</b>	<b>0,9</b>	<b>6,1</b>								

Legend:

Gr = group membership

Gad = administration of gadolineum

Fid = presence of skin adhesive fiducials

Fid. Shift = spatial shift in skin adhesive fiducials measured

SD = standard deviation

Mid = midbrain and ventricles

Fro = frontal lobe

Par = parietal lobe

Tem = temporal lobe

Occ = occipital lobe

Pos = posterior fossa

T. = tumor

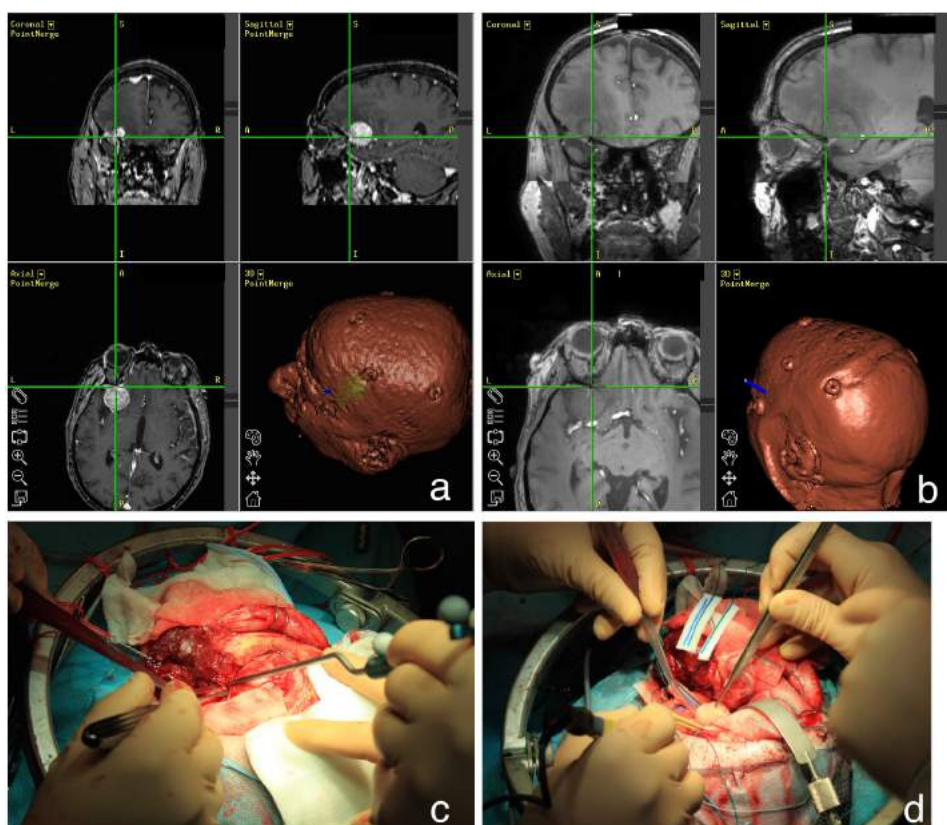


**Figure 6.4: Clinical Potential of 7T MRI-Based Image Guidance**

Perioperative images of the meningeoma case (described in Box 2). Frame a shows the gadolinium-enhanced 3T MR image guidance image. Frame b shows the corresponding (co-registered) 7T MR image. Frame C shows the image guidance tool pointed at the drilled sphenoid wing at the location shown in frame A and frame B. Note that it is impossible to discern an arterial feeder in the 3T MR image due to contrast enhancement, while 7T MRI shows the vessel clearly. Frame D shows that after ligation of the feeder the tumor lost its main blood supply and could be removed en-bloc straightforwardly.

## Discussion

This study indicates that ultra-high-field MRI can be used safely for cranial image guidance during brain tumor resection, provided the image is *not* used as a basis for patient-to-image registration. The reason that we conducted this study was the fact we found 7T MRI to yield major image guidance inaccuracies in our glioma case (as described in Box 1), while prior studies reassured us that geometric distortions in 7T MRI should be minimal [3,5], and 7T images could be utilized for image guidance [2].

We hypothesized that the observed inaccuracy was due to the skin-adhesive fiducials of our patient. Perhaps the fatty substance in the fiducials caused significant geometric distortions owing to the high magnetic field. Therefore, we investigated whether significant intracranial and extracranial (skin) shifts were present in our 7T data, and if these distortions were influenced by the presence of skin-adhesive fiducial markers.

We used qualitative methods to search for intracranial distortions; very similar to the way a neurosurgeon or radiation-oncologist in the clinic would evaluate images. Looking specifically at *intracranial* distortions, we confirm that the extent of these distortions in magnetization-prepared T1-weighted 7T MRI scans in neurosurgical patients with and without skin-adhesive fiducials appear to be of sub-voxel magnitude in comparison with 3T MRI scans. Since 3T MRI is regularly used for clinical image guidance, this finding implies that ultra-high-field MRI should be similarly suited for this purpose, in keeping with previous reports [2-5]. Since this finding held true in both patient groups (A and B), we also demonstrated that application of skin-adhesive fiducials does not significantly distort intracranial contents locally. We however did observe slight positional shifts of the medulla oblongata in two patients in group A. Since these images overlapped very well for other parts of the brain, image-to-image registration inaccuracy is unlikely. While motion artifacts caused by different head positions between scans may be the explanation for these shifts, we cannot exclude that the multiple tissue interfaces present in this area of the brain might have induced additional distortions. So, caution remains warranted for the use of 7T-MR images for navigation in posterior fossa surgery.

We also observed that *extracranial* distortions can reach considerable amplitudes in 7T MR images. We found shifts in the position of the skin surface of up to approximately 9 mm in 7T MRI scans compared with 3T MRI. These skin shifts were generally most profound around the lower forehead and orbit (see Figure 2D), which are locations typically used in most surface

matching patient-to-image registration algorithms. Moreover, we observed that skin-adhesive fiducials could shift up to approximately 9 mm as well.

Generally, at the skin surface, there is a high chance that susceptibility artifacts occur, because of the air-skin interface and because of the distance from the gradient center. [4,11] However, our high scanning bandwidth of 500 Hz/voxel should make the occurrence of susceptibility artifacts less likely. Therefore, an alternative explanation for the extracranial distortions could be that we used 3<sup>rd</sup> order B0 shimming which is known to cause B0 offsets at the level of the skin. Another possible factor contributing to skin distortion might be displacement of the skin during positioning of the head in the 7T scanner, as a result of the tighter head coil. More research is needed to elucidate the specific cause(s) of extracranial distortions, so as to arrive at a protocol suitable for image guidance.

In summary, we must conclude that it is presently not reliable to use ultra-high-field MRI for patient-to-image registration, either with skin surface matching or with skin-adhesive fiducial point matching algorithms. However, 7T MRI scans can still be used for image guidance as we demonstrated in Case 2, by fusing the images on the image guidance machine with another reliable image, be it 3T MRI (as we did) or CT (as described by others [2,5]).

## Conclusion

This study demonstrates that no significant *intracranial* supratentorial geometric distortion is present in T1-weighted 7T brain MR images as compared with 3T T1-weighted scans of patients with skin-adhesive fiducials. Accordingly, it seems feasible to use such scans for intraoperative image guidance.

However, extracranial distortions occur on 7T MRI scans in terms of skin surface shifts and shifts in center positions of skin-adhesive fiducials. These shifts can lead to unacceptably high patient-to-image registration inaccuracies if the 7T MR image is used as a basis for registration.

Therefore, we recommend performing the patient-to-image registration on the basis of a routine (CT or 3T MR) image, and subsequently co-registering the 7T MR image with this routine image on the image guidance machine. This method was successfully used in the skull base meningioma case, where the ability to navigate on ultra-high-field MRI aided tumor resection.

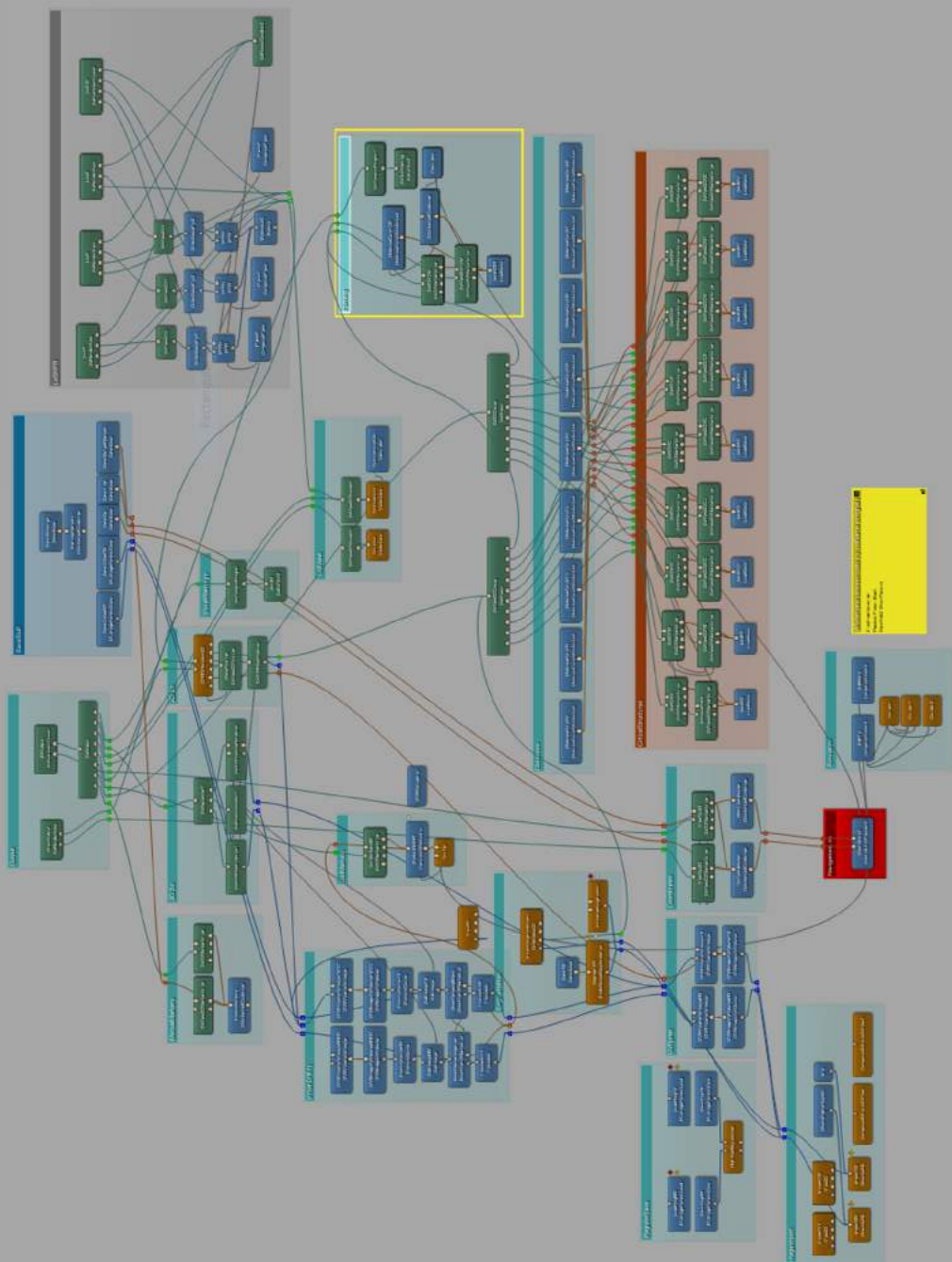
## References

1. Archip N, Clatz O, Whalen SBS, DiMaio SP, Black PMMD, Jolesz FAMD, Golby AMD, Warfield SK (2008) Compensation of Geometric Distortion Effects on Intraoperative Magnetic Resonance Imaging for Enhanced Visualization in Image-Guided Neurosurgery. *Neurosurgery* 62(3):209–216
2. Barrett TF, Dyvorne HA, Padormo F, Pawha PS, Delman BN, Shrivastava RK, Balchandani P (2017) First Application of 7-T Magnetic Resonance Imaging in Endoscopic Endonasal Surgery of Skull Base Tumors. *World Neurosurg* 103:600–610
3. Dammann P, Kraff O, Wrede KH, Özkan N, Orzada S, Meuller OM, Sandalcioğlu IE, Sure U, Gizewski ER, Ladd ME, Gasser T (2011) Evaluation of Hardware-related Geometrical Distortion in Structural MRI at 7 Tesla for Image-guided Applications in Neurosurgery. *Acad Radiol* 18(7):910–916
4. Dean D, Kamath J, Duerk JL, Ganz E (1998) Validation of object-induced MR distortion correction for frameless stereotactic neurosurgery. *IEEE Trans Med Imaging* 17(5):810–816
5. Duchin Y, Abosch A, Yacoub E, Sapiro G, Harel N (2012) Feasibility of Using Ultra-High Field (7 T) MRI for Clinical Surgical Targeting. *PLoS ONE* 7(5):e37328
6. Harteveld AA, De Cockler LIL, Dieleman N, van der Kolk AG, Zwanenburg JJM, Robe PA, Luijten PR, Hendrikse J (2015) High-resolution postcontrast time-of-flight MR angiography of intracranial perforators at 7.0 Tesla. *PLoS One* 10(3):e0121051
7. Kang C-K, Park C-A, Lee DS, Lee Y-B, Park C-W, Kim Y-B, Cho Z-H (2015) Velocity measurement of microvessels using phase-contrast magnetic resonance angiography at 7 tesla MRI. *Magn Reson Med*
8. Klein S, Staring M, Murphy K, Viergever MA, Pluim JP (2010) elastix: a toolbox for intensity-based medical image registration. *IEEE Trans Med Imaging* 29(1):196–205
9. Li Y, Larson P, Chen AP, Lupo JM, Ozhinsky E, Kelley D, Chang SM, Nelson SJ (2015) Short-echo three-dimensional H-1 MR spectroscopic imaging of patients with glioma at 7 tesla for characterization of differences in metabolite levels. *J Magn Reson Imaging* 41(5):1332–1341
10. Noebauer-Huhmann I-M, Szomolanyi P, Kronnerwetter C, Widhalm G, Weber M, Nemec S, Juras V, Ladd ME, Prayer D, Trattnig S (2015) Brain tumours at 7T MRI compared to 3T—contrast effect after half and full standard contrast agent dose: initial results. *Eur Radiol* 25(1):106–112
11. Wang H, Balter J, Cao Y (2013) Patient-induced susceptibility effect on geometric distortion of clinical brain MRI for radiation treatment planning on a 3T scanner. *Phys Med Biol* 58(3):465
12. Zaiss M, Windschuh J, Paech D, Meissner JE, Burth S, Schmitt B, Kickingereder P, Wiestler B, Wick W, Bendszus M, Schlemmer HP, Ladd ME, Bachert P, Radbruch A (2015) Relaxation-compensated CEST-MRI of the human brain at 7 T: Unbiased insight into NOE and amide signal changes in human glioblastoma. *NeuroImage* 112:180–188

## Acknowledgements

We kindly acknowledge Fredy Visser, of Philips Healthcare, Best, The Netherlands, for his help in acquiring the 7T images.





# 7

## **Summary & Discussion**

### **'A Manifesto for Computer Assisted Surgery of the Skull Base'**

The goal of this discussion is to describe guiding principles to achieve what I believe to be important aims in the field of Computer-Assisted Surgery of the Skull Base (CASSB), summarize my own contributions to the field, and identify a number of specific technological features that need to be developed (Table 2). My hypothesis is that a further development of CASSB will lead to improvements in four domains: clinical outcomes, research, training, and quality assurance, on which I will elaborate below.

I will explain the reasons why changes from the status quo are necessary, and describe the format of necessary changes for the near and distant future. For sake of clarity, this description has been categorized into the nine principal components of CASSB (see Table 1).

### 1. Preoperative Imaging

My proposition is that skull base specialists need to view images as a digital representation of patients: i.e. a digital patient model or medical avatar.

We need to improve image quality to increase the realism of the medical avatar, which will become crucial in CASSB, as I will explain below. To specify, with 'quality', I mean the spatial resolution, contrast between tissue types and pathology, but also the geometric accuracy of images.

Ultra-high field (7T) MRI is such a promising imaging technology capable of increasing resolution and contrast. For instance, it can be used to improve skull base surgery by enhanced localization of important blood vessels of skull base tumors (see box 2 of Chapter 6). However, as is shown in Chapter 6, we found extracranial geometrical shifts in the position of the skin and skin-adhesive fiducials in magnetization-prepared T1-weighted 7T MRI cranial images of up to 9 mm. Such extensive shifts render these images unreliable for patient-to-image registration. Fortunately, we found no visible intracranial distortions. Therefore, I conclude that 7T MR images can be used for CASSB with the following work-around: the patient-to-image registration should be performed on a routine (CT or MR) image, which is subsequently co-registered to the 7T MR image on the image guidance machine. Nevertheless, more research is needed to improve the geometric accuracy of these ultra-high field MR images.

Furthermore, images constituting the medical avatar should be stored, normalized to a standard 3D space to render them comparable, and (semi-)automatic algorithms should segment all relevant anatomical structures within these scans. This thesis provides an example of a segmentation algorithm in Chapter 2, which describes the development and evaluation of Nerve-

Click for semi-automatic segmentation of the intra-temporal facial nerve centerline from high resolution CT images. NerveClick's accuracy was evaluated in healthy, neuro-otologic and neurosurgical patients. Surgeons using NerveClick could segment facial nerve centerlines fast and with high accuracy (with a mean maximum error of  $0.44 \pm 0.23$  mm). Further research is needed to implement a fully automatic algorithm, which not only segments the facial nerve, but includes all important normal anatomical structures of the skull base such as large veins (e.g. transverse and sigmoid sinuses), arteries (e.g. internal carotid arteries) and other cranial nerves (e.g. the optic nerves).

Moreover, beside images and segmentations, we need to be able to store spatial information about treatment simulation and execution into the same normalized space. Furthermore, one could also store basic clinical parameters (e.g. age, sex, pre-operative performance score) and outcome parameters into this database (mortality, post-operative performance scores, hospital stay length, etc.). In any case, the information should be stored in a new type of unified data standard (similar to e.g. DICOM). The conceptualized comprehensive radio-anatomical, treatment simulation and execution database will be one of the key features for the envisioned computer assisted future. I coin the term Medical Avatar Archive (MARCH) for this database.

## 2. Decision making

Nowadays, once a patient presents with symptomatic skull base disease, he/she is discussed in a joint meeting of the skull base group and general treatment plans are decided upon. The decision boils down to surgery, radiation therapy or a combination of these modalities. Treatment decisions are made during oral discussions based on the combined experience of the group. A strong skewing might exist towards the strongest (or the most senior) opinion in the group, which may or may not be the best option. Experience is a very important factor in medicine, but even the best surgeon suffers from human biases and non-medical (i.e. political or financial) motivations. I believe that in the future, we should base decisions on more objective information, such as an array of different simulated surgical approaches, dosimetric plans (e.g. linear accelerator vs. gamma knife), and combined plans generated with assistance of a computer on the digital patient model. Further down the road, we should additionally compare a new case to previous similar cases within a MARCH in terms of clinical outcome.

## 3. Treatment planning

Currently, once a decision for surgical treatment has been made, skull base surgeons study scans of the patient preoperatively and conjure a specific surgical plan in their minds. These

plans are sometimes discussed on a general level (e.g. between neurosurgeons and otolaryngologists) if a multi-disciplinary approach is necessary. The workflow of formulating surgical plans should become more objective in the future. Therefore, I believe we should further develop realistic (virtual) surgical simulators that allow surgeons to accurately simulate different skull base approaches in a step by step fashion. The simulations should be presentable and easily understandable for use during discussions in skull base meetings. Moreover, they should be able to interface with radiation oncology planning software. Additionally, simulators should allow surgeons to define optimal patient positions during each surgical step. The plans need to be storable in a MARCH, and exportable to image guidance machines. In the long run, machine learning algorithms might learn to make treatment plans based on training on large (and continuously updating) national/international MARCHes. I will call these machine learning algorithms 'virtual treatment planners' (VTP). Of course, plans generated by the VTPs should always be scrutinized by the entire skull base team, and any adaptations should be fed back to the VTP to improve the algorithm.

#### 4. Patient-Image Registration

The two most commonly used methods for patient-to-image registration in skull base surgery are fiducial-based localization (either skin adhesive markers or bone anchored screws) and skin surface registration. Superior accuracy is achieved by utilizing bone anchored fiducials. However, the disadvantage is that placing these fiducials under local anesthetic entails slight discomfort for the patients and requires more complex logistics. Moreover, usually bone-anchored fiducials contain metal which might affect image quality in MRI. Therefore, I believe that future developments should strongly focus on using intra-operative imaging as a means to achieve similar highly accurate patient-image registration. Another option would be to explore a combination of skin surface based or skin adhesive marker-based registration, and locally optimizing it by using bone surfaces of the skull base, during surgery.

#### 5. Patient positioning

A robotic patient positioning system (e.g. a robotic couch) needs to be developed to adjust the patient's head to the optimal position (enabling good visualization and ergonomics for the surgeon/surgical robot while crossing a minimal amount of neurovascular structures) during each step of the planned treatment.

#### 6. Execution of surgery

Currently, there is no objective way to compare the surgical methods of one surgeon to another. Moreover, there is a large variation in treatment methods (in types of approaches

utilized, but even in the amount of radiosurgery applied) between different skull base groups, even within the same geographical area. I believe one of the possible causes of this phenomenon, is that skull base surgery is heavily based upon historical schools of training. Today, there are many different schools of training in the world which sometimes adhere to opposing methods. Variations in treatment methods inherently mean that some patients receive suboptimal care. Unfortunately, since skull base surgeries are low volume and technically complex treatments, we are unable to correlate treatment variations with patient outcome at the moment. Also, during surgery, there are no patient specific quality assurance or safety checks in place, except for the accreditation received by the surgeons from their school of training. I believe we need to improve these issues to become future proof as a profession.

Therefore, in the very near future, surgeons should start to routinely document their surgical steps (from incision until closure) in terms of 3D positional coordinate sets with an image guidance system. Note that this is already technically possible with conventional image guidance machines. In the more distant future, surgeons should actively try to adhere to the steps formulated in the treatment plan. Eventually, I envision human operated- or (semi-)autonomous robots take over the execution of (some) steps as formulated in the treatment plan (e.g. skull base drilling).

## 7. Image Guidance

Currently, image guidance gives passive feedback. The surgeon uses image guidance to check his/her anatomical position for reassurance. This thesis describes methods to advance image guidance to give active feedback.

Chapter 3-5 describe the development and validation of new software, called EVADE, which is an acronym for exposure visualization and audible distance emission. It is specifically designed for active image guidance during drilling of the (lateral) skull base. EVADE updates the prior image and visualizes the bone drilling process during skull base surgery virtually in (near) real-time, without need for intra-operative imaging. This functionality is also known as 'virtual drilling'. Furthermore, the software continuously calculates the distance from the drill tip to segmented normal anatomical structures (e.g. the facial nerve) and produces audiovisual warnings if the surgeon drills in too close vicinity. This feature is called 'distance control'.

An important concept we introduced in Chapter 2 is the 'safety zone', 'safety mantle' or 'protective perimeter', which the EVADE software can establish around segmented structures. It allows for compensation of intrinsic spatial errors and latency in an image guidance

system. As is demonstrated in Chapter 3, the maximum amount of spatial error during tracking of a drill, in a clinical optical image guidance system, employing anchored fiducial (screw) based patient-image registration on a high-resolution CT-image, is approximately 3 mm.

This finding led to the following premise about virtual drilling: Virtual drilling is accurate if its maximum errors are around 3 mm. Since in that case, errors just represent the intrinsic spatial errors of the image guidance system. In this thesis, the accuracy of virtual drilling was evaluated with phantom models (Chapter 3) and with cadaver heads during different lateral skull base approaches: mastoidectomy, retro-mastoid and translabyrinthine approach (Chapter 4), and anterior petrosectomy (Chapter 5). The observed average maximum errors during all experiments ranged from 2.5-3.3 mm. Therefore, I conclude that the implementation of EVADE's virtual drilling is accurate.

Furthermore, the finding of a 3 mm intrinsic image guidance spatial error led to a premise about distance control: Distance control reduces the risk of iatrogenic drill damage to normal anatomical structures if the protective perimeter distance is above 3 mm.

Chapter 4 investigates the risk reduction provided by EVADE's distance control feature during drilling of the lateral skull base. The risk of drill damage could be reduced to 0% by using a protective perimeter distance of 3 mm. Moreover, if this distance is lowered under 3 mm, there is an inversely proportional relationship between the set distance and the risk of drill damage. Therefore, my conclusion is that EVADE's distance control protects normal anatomical structures from iatrogenic damage during drilling of the skull base.

The next question is whether EVADE's virtual drilling and distance control features are beneficial to the patient. Chapters 3 and 5 describe trials which compare EVADE with standard passive image guidance in terms of 'surgical orientation' and damage to structures. Chapter 3 describes a trial in which mastoidectomies were performed on phantom models. Surgeons felt better orientated and thought they had improved (modeled) tumor exposure, while less (modeled) normal anatomical structures were damaged, when using EVADE. Chapter 5 discusses a trial during which expert skull base surgeons from three different hospitals, performed anterior petrosectomies on human cadaver heads. Again, surgeons rated their intraoperative orientation statistically significantly better while using EVADE, compared with standard image guidance. Moreover, EVADE reduced the risk of drill damage to the cochlea, and even optimized the bony approach through the petrous bone. Therefore, I conclude that

EVADE has clinical potential. Additionally, Chapter 4 and 5 prove that EVADE is clinically feasible. Therefore, in the near future, a randomized clinical trial is needed to confirm the promise of this technology.

Furthermore, the accuracy of image guidance needs to be improved from 3 mm to sub-millimeter accuracy. Tracking of surgical tools needs to become as unobtrusive as possible. Instead of just a drill, all surgical instruments (knife, endoscope, rongeur, ultrasonic aspirator, suction, retractors, micro-instruments) should be tracked in real time during surgery. Then, image guidance will be able to document all surgical steps with accuracy and minimal effort on the part of the surgeon.

Further down the road, image guidance might evolve into a medical quality assurance officer which will check that surgeons adhere to the treatment plan. If deviation from the plan is necessary due to unforeseen circumstances (as may often be the case in these complex surgeries), then the image guidance machine will be able to tap into MARCH information from previous cases which might have had the same situation and ask a VTP for advice on the optimal way to proceed.

#### 8. Role of intraoperative imaging

If available, intraoperative imaging is now used in a relatively small number of cases at the surgeon's discretion. More intra-operative imaging is necessary to further computer assisted surgery, especially simulation software and patient-image registration. Therefore, I believe surgeons should start to perform intraoperative imaging as much as clinically acceptable and possible. Even in the distant future, intra-operative imaging will remain important to update the image guidance at predetermined points during surgery (e.g. after opening the dura or after significant tumor removal) to ensure accurate step-by-step guidance and quality assurance. Moreover, it will be especially valuable once an unforeseen situation occurs during treatment. All intraoperative images should be directly imported into a MARCH and they should be accessible to a VTP, since changes in the anatomy might call for an adaptation of the treatment plan.

#### 9. Imaging Follow Up

Imaging should be performed for every skull base case at the end of surgery and then at regular intervals as disease specific protocols dictate. The follow-up imaging should be stored in a MARCH, including automatic volumetric segmentation of the remaining pathology. In this way, growth of pathology or recurrence can be objectified and quantified. Treatment effects



(e.g. volume of debulking, or tumor shrinkage after radiosurgery) can be obtained from this information and stored as an outcome measure in the MARCH.

Obstructing Forces

The necessary developments outlined above are not brand-new ideas. Other researchers and manufacturers have tried to implement some of these technologies in the clinic in the past, but unfortunately failed. I identify three types of obstructions for innovation. First, attaining consent for testing new technologies clinically (e.g. to prove clinical efficacy), involves too many rules and regulations (local, national, CE/FDA). Therefore, sometimes it can simply require too many resources from a research group to get a new technology clinically approved for testing.

Second, manufacturers invest in technology from a commercial perspective. So, if the economic gains appear small (e.g. small market, high initial investments needed) then beneficial innovations will just not be further developed.

Table 7.1: Current State and Future of CASSB

#	Component	Current
1	Preoperative Imaging	a set of scans, usually only pathology is segmented
2	Treatment planning	Surgeons study scan and make specific surgical plan in their minds
3	Decision making	team: overall treatment plan based on verbal information
4	Patient-Image Registration	fiducials, skin surface matching
5	Patient positioning	surgeons position patient
6	Execution of surgery	surgeons perform treatment
7	Image Guidance	passive to reassure surgeon
8	Intraoperative imaging	when available at surgeon' discretion
9	Follow-up Imaging	manual measurements of remaining/recurrent pathology

This table categorizes the current status and necessary changes for the near and far future per component of CASSB.

Third, evidence-based medicine (EBM), although a clinically beneficial breakthrough in its own right, has become a blockade for technical innovation, because regulating bodies and (some) medical doctors rely too heavily on proving technology is effective on a large scale before it can be adopted in the clinic. For some of the technologies described above, it might be too resource or logistically intensive to prove clinical efficacy by EBM standards.

In fact, these three obstructing forces operate in a vicious circle to stall innovation: regulating bodies/the medical community only accept technology which is 'proven' to be effective, rules and regulations make it harder to prove this, which causes the commercial attractiveness of investing in technology to decline.

However, I believe these difficulties might be overcome in the future, if the advantages of the described innovations are clear to all involved parties: patients, researchers, the medical community, regulating bodies, and manufacturers.

Near Future	Distant Future
rough digital model of the patient, semi-automated segmentation of anatomic structures (NerveClick)	High quality medical avatar, automated segmentation of all relevant anatomic structures stored in MARCH
surgery is simulated by surgeons and presented to team	an array of different surgical and dosimetric plans are computer generated by VTPs
team decision based on comparison of different digital treatment plans	team decision based on different digital VTP generated treatment plans and historical results from a MARCH
fiducials, intraoperative imaging	intraoperative imaging
surgeon's positions patient into position derived from planning system	patient is positioned into optimal position for each step by an automatic patient positioning system
surgeons perform treatment and documents steps	surgeon and/or robot performs treatment on step-by-step basis
active assistant, documenter of surgical procedure in space (e.g. EVADE)	active assistant, documenter, quality assurance officer
as much as possible to improve planning system	at multiple predetermined checkpoints, for quality assurance
semi-automatic volumetric segmentation of remaining/recurrent pathology	automatic volumetric segmentation of pathology, stored in MARCH as outcome

## **Hypothesized advantages**

### **Clinical Outcomes**

I envision these developments will improve the clinical outcomes of patients with skull base disease because of two factors. First, decision making in the skull base team will be improved because it will be founded on a comparison of objective patient-specific treatment plans and relevant historical results. Second, planning will probably improve the overall outcomes of surgery in itself, especially if planning is combined with robotic positioning and a quality assurance system to confirm that the plan is executed accordingly. Also, risks will further be minimized by optimally combining surgery with radiosurgery. Furthermore, in the more distant future, if improved treatments become available, they might be 'downloaded' into a VTP and conferred to surgeons and/or surgical robots by use of the image guidance computer, which might speed up the spread of new treatments.

### **Research**

Furthermore, these measures will improve skull base research. If treatments are documented spatially in combination with outcome measures it becomes easier to adequately evaluate variations in surgical methods. Moreover, trials could formulate spatial specifications on surgical approaches (in a similar manner as contemporary trials in radiation oncology specify dosage) which could be effected in treatment planning software and preoperatively by active image guidance assistants. This would lead to decreased heterogeneity and assure quality, while evaluating new (surgical) treatments.

### **Training**

Surgical training would be improved if skull base trainees could formulate treatment plans and compare these plans to the plans of their supervisors or eventually VTPs. During surgery trainees would be able to carefully follow steps put forward by image guidance, acquiring surgical skills while maintaining safety for the patient. Moreover, once large internationally shared MARCHes are available, skull base trainees have the condensed knowledge of many surgeons available for study.

### **Quality assurance**

The topic of objective quality assurance in (skull base) surgery is uncharted territory. It might be relatively insignificant at the moment, but I think it will become more important in the future since patients and insurers will demand it. Therefore, skull base specialists should strive to develop appropriate quality assurance measures and regulations first, before an external official body does it, and perhaps dictates inappropriate and unwanted procedures.

My major proposition is that the computer should, through the innovations outlined above, be included as a ‘member’ of the skull base team. Therefore, this thesis is meant to stimulate clinical skull base specialists to demand, and researchers and manufacturers to design, the technologies summarized in Table 2. Besides showcasing some of my own scientific contributions to guidance and imaging, hopefully, this thesis will act as a means to focus research efforts within the field of CASSB and advance it for the benefit of our patients.

**Table 7.2: Necessary Innovations**

#	Technology Type
1	High definition geometrically accurate images to serve as a medical avatar
2	Automatic segmentation algorithms to segment anatomical structures and pathology
3	A standard format to store information as basis of a MARCH, containing: <ul style="list-style-type: none"> <li>- normalized preoperative images</li> <li>- segmented anatomical structures</li> <li>- treatment plans</li> <li>-treatment execution information</li> <li>- clinical outcome measures</li> <li>- intraoperative images</li> <li>- normalized postoperative follow up images</li> </ul>
4	Surgical simulator to define treatment plans
5	Robotic patient positioning system to improve intraoperative positioning
6	Active image guidance assistants documenting surgical steps and conveying treatment plans to surgeons
7	Quality assurance/safety software to check if treatment plans are executed according to the treatment plan
8	Intraoperative imaging which is fast and easy
9	Automatic spatial designation (i.e. segmentation) of (remaining or recurrent) pathology in follow up images

Summarizes necessary innovations researchers and industry in the field should focus on to achieve the envisioned future benefits of CASSB.



# Appendix

**Nederlandse Samenvatting**

**List of Publications**

**Dankwoord**

**Curriculum Vitae**



## Nederlandse Samenvatting

### Hoofdstuk 1: Algemene inleiding

In de algemene inleiding van dit proefschrift getiteld "Computer Geassisteerde Schedelbasis Chirurgie: Bijdragen aan Beeldgeleiding en Beeldvorming" werd de hoofddoelstelling verwoord, namelijk: de kwaliteit van zorg voor patiënten met schedelbasis tumoren verbeteren, door het verder ontwikkelen van Computer Geassisteerde Schedelbasis Chirurgie (CGSC).

In het algemeen kan onderzoek op het gebied van CGSC worden onderverdeeld in negen verschillende richtingen:

- 1) Preoperatieve beeldvorming
- 2) Planning
- 3) Besluitvorming
- 4) Patiënt-beeld registratie
- 5) Patiënt positionering
- 6) Opereren
- 7) Beeldgeleiding
- 8) Intra-operatieve beeldvorming
- 9) Follow-up beeldvorming

Het wetenschappelijke doel van dit proefschrift is om verbeteringen te presenteren in preoperatieve beeldvorming en beeldgeleiding.

### Hoofdstuk 2: Bijdrage aan Computertomografie (CT) Beeldvorming

Hoofdstuk 2 beschrijft de ontwikkeling en evaluatie van het 'NerveClick' algoritme voor semi-automatische segmentatie van de aangezichtszenuw middellijn in hoge resolutie CT-beelden van het os temporale. NerveClick is speciaal ontwikkeld om te gebruiken bij beeldgeleiding tijdens schedelbasisoperaties. De nauwkeurigheid van de software werd geëvalueerd bij gezonde, neuro-otologische en neurochirurgische patiënten. Chirurgen die NerveClick gebruikten, konden de middellijnen van gezichtszenuwen snel en met hoge nauwkeurigheid segmenteren (gemiddelde maximale fout van  $0,44 \pm 0,23$  mm).



### **Hoofdstuk 3 tot en met 5: Bijdragen aan Beeldgeleiding**

Hoofdstuk 3-5 beschrijft de ontwikkeling en validatie van nieuwe software, EVADE genaamd, wat een afkorting is voor 'Exposure Visualization & Audible Distance Emission'. De software is specifiek ontworpen voor actieve beeldgeleiding tijdens het boren van de (laterale) schedelbasis. EVADE werkt het eerdere beeld bij en visualiseert het botboorproces tijdens schedelbasisoperaties in realtime, zonder gebruik te maken van intra-operatieve beeldvorming. Deze functionaliteit wordt 'virtueel boren' genoemd. Daarnaast berekent de software continu de afstand van de boorpunt tot gesegmenteerde normale anatomische structuren (bijvoorbeeld de aangezichtszenuw) en produceert deze audiovisuele waarschuwingen als de chirurg te dicht in de buurt boort. Deze functie heet 'afstandscontrole'.

Een belangrijk concept dat reeds in hoofdstuk 2 werd geïntroduceerd, is de 'veiligheidszone', die de EVADE-software instelt rond gesegmenteerde structuren. De veiligheidszone is bedoeld om ruimtelijke fouten en latentie van een beeldgeleidingssysteem te compenseren. Zoals aangetoond in hoofdstuk 3, is de maximale ruimtelijke fout van een optisch beeldgeleidingssysteem, gebruikmakende van botschroefjes als ijkpunten voor de patiënt-beeldregistratie van een hoge resolutie CT-beeld, ongeveer 3 mm.

Deze bevinding leidde tot het volgende uitgangspunt voor virtueel boren: virtueel boren wordt nauwkeurig geacht als de maximale fout rond de 3 mm is. Aangezien in dat geval de fout alleen de intrinsieke ruimtelijke onnauwkeurigheid van het beeldgeleidingssysteem weergeeft.

In dit proefschrift werd de nauwkeurigheid van virtueel boren geëvalueerd in fantoommodellen (Hoofdstuk 3) en in kadaverhoofden tijdens verschillende laterale schedelbasisbenaderingen: mastoïdeectomie, retromastoïde en translabirintische benadering (Hoofdstuk 4) en anterieure petrosectomie (Hoofdstuk 5). De waargenomen gemiddelde maximale fouten tijdens alle experimenten varieerden van 2,5-3,3 mm. Zodoende concludeer ik dat de implementatie van EVADE's virtuele boringen nauwkeurig is.

Verder leidde de bevinding van een intrinsieke ruimtelijke fout van 3 mm tot een premisse over afstandscontrole: afstandscontrole vermindert het risico van boorschade aan normale anatomische structuren als de veiligheidszone groter is dan 3 mm.

Hoofdstuk 4 onderzoekt de risicoreductie die geboden wordt door afstandscontrole tijdens het uitboren van de laterale schedelbasis. Het risico van boorschade blijkt te kunnen worden verminderd tot 0% door een veiligheidszone van 3 mm te gebruiken. Indien de veiligheidszone onder de 3 mm wordt ingesteld, is er een omgekeerd evenredige relatie tussen de ingestelde afstand en het risico van boorschade. Daarom concludeer ik dat de afstandscontrole functie van EVADE normale anatomische structuren beschermt tegen iatrogene schade tijdens het uitboren van de schedelbasis.

De vraag is of de virtueel boren en afstandscontrole functies gunstig zijn voor de patiënt. Hoofdstukken 3 en 5 beschrijven proeven die EVADE vergelijken met standaard (passieve) beeldgeleiding op het gebied van 'chirurgische oriëntatie' en boorschade. Hoofdstuk 3 beschrijft een studie waarin mastoïdectomieën werden uitgevoerd op fantoommodellen. Chirurgen waren beter georiënteerd, terwijl minder (gemodelleerde) normale anatomische structuren beschadigd werden, bij gebruik van EVADE. Hoofdstuk 5 beschrijft een proef waarbij deskundige schedelbasischirurgen uit drie verschillende ziekenhuizen anterieure petrosectomieën uitvoerden op kadaverhoofden. Het bleek dat chirurgen hun intra-operatieve oriëntatie statistisch significant beter vonden tijdens gebruik van EVADE in vergelijking tot standaard beeldgeleiding. Bovendien reduceerde EVADE het risico op boorschade aan het slakkenhuis en lijkt het de vorm van de benige benadering door het os petrosum te optimaliseren. Daarom concludeer ik dat EVADE klinisch potentieel heeft. Bovendien bewijzen Hoofdstuk 4 en 5 dat EVADE klinisch haalbaar is. Daarom is in de nabije toekomst een gerandomiseerde klinische studie nodig om de belofte van deze technologie te bevestigen.

## **Hoofdstuk 6: Bijdrage aan Magnetische Resonantie Beeldvorming (MRI)**

MRI met ultrahoog veld (7 Tesla) is een veelbelovende nieuwe beeldtechnologie die de resolutie en contrast van medische beelden kan verhogen. Voor schedelbasischirurgie kunnen dit soort MR beelden verbeterde lokalisatie van belangrijke bloedvaten van schedelbasistumoren bewerkstelligen (zie kader 2 van hoofdstuk 6). Echter, zoals in hoofdstuk 6 wordt aangetoond, zijn er extracraniële geometrische verschuivingen in de positie van de huid- en huidfiducials tot wel 9 mm aangetroffen in magnetisatie-voorbereide T1-gewogen 7T MR beelden van het cranium. Dergelijke grove verschuivingen maken deze beelden eigenlijk ongeschikt voor patiënt-beeldregistratie en dus niet bruikbaar voor computer geassisteerde chirurgie. Aan de andere kant werden er geen intracraniale verstoringen van de beelden gevonden. Daarom concludeer ik dat 7T MR beelden toch kunnen worden gebruikt voor CGSC met de

volgende work-around: de patiënt-beeldregistratie zal moeten worden uitgevoerd op een routine (CT of MR) beeld, waarop vervolgens de 7T MR afbeelding wordt geregistreerd. Er is meer onderzoek nodig om de geometrische nauwkeurigheid van deze 7T MR-beelden te verbeteren.

## **Hoofdstuk 7: Discussie & Samenvatting -- 'Een manifest voor computer geassisteerde schedelbasis chirurgie'**

Dit hoofdstuk presenteert een aantal principes die mijns inziens zouden moeten worden gehanteerd om belangrijke doelen van CGSC in de toekomst te bewerkstelligen. Specifieke technologieën die nog ontwikkeld moeten worden, worden beschreven en gecategoriseerd volgens de negen onderzoeksrichtingen van CGSC (zie boven). Daarnaast vat dit hoofdstuk mijn eigen bijdragen aan het veld samen (zie boven). Hopelijk dient dit proefschrift als een middel om de onderzoeksinspanningen op het gebied van CGSC te focuseren en te bevorderen, ten behoeve van onze patiënten.

## List of Publications

### This thesis:

**Voormolen, Eduard H**, Marijn van Stralen, Peter A Woerdeman, Josien P W Pluim, Herke Jan Noordmans, Max A Viergever, Luca Regli, en Jan Willem Berkelbach van der Sprenkel. "Determination of a Facial Nerve Safety Zone for Navigated Temporal Bone Surgery". *Neurosurgery* 70, nr. 1 Suppl Operative (maart 2012): 50–60; discussion 60.

**Voormolen, Eduard H**, Peter A Woerdeman, Marijn van Stralen, Herke Jan Noordmans, Max A Viergever, Luca Regli, en Jan Willem Berkelbach van der Sprenkel. "Validation of Exposure Visualization and Audible Distance Emission for Navigated Temporal Bone Drilling in Phantoms". *PloS One* 7, nr. 7 (2012): e41262.

**Voormolen, Eduard H**, Sander Diederer, Marijn van Stralen, Peter A Woerdeman, Herke Jan Noordmans, Max A Viergever, Luca Regli, Pierre A Robe, en Jan Willem Berkelbach van der Sprenkel. "Benchmarking Distance Control and Virtual Drilling for Lateral Skull Base Surgery". *World Neurosurgery* 109 (januari 2018): e217–28.

**Voormolen, Eduard H**, Sander Diederer, Helene Cebula, Peter A Woerdeman, Herke Jan Noordmans, Max A Viergever, Pierre A Robe, Sebastien Froelich, Luca Regli en Jan Willem Berkelbach van der Sprenkel. "Distance Control and Virtual Drilling Improves Anatomical Orientation during Anterior Petrosectomy" *Submitted*

**Voormolen, Eduard H**, Sander Diederer, Peter A Woerdeman, Jan Willem Berkelbach van der Sprenkel, Herke Jan Noordmans, Max A Viergever, Peter Luijten, Hans Hoogduin, en Pierre A Robe "Implications of Extracranial Distortion in Ultra-High Field MRI for Image-Guided Cranial Neurosurgery" *Submitted*

## Other publications:

**Voormolen, Eduard H**, Abdelkarime Khodadade Jahrome, Lambertus W Bartels, Frans L Moll, Willem P Mali, en Peter J Blankestijn. "Nonmaturation of Arm Arteriovenous Fistulas for Hemodialysis Access: A Systematic Review of Risk Factors and Results of Early Treatment". *Journal of Vascular Surgery* 49, nr. 5 (mei 2009): 1325–36.

Gragnaniello, Cristian, Remi Nader, Tristan van Doormaal, Mahmoud Kamel, **Eduard H Voormolen**, Giovanni Lasio, Emad Aboud, Luca Regli, Cornelius A F Tulleken, en Ossama Al-Mefty. "Skull Base Tumor Model". *Journal of Neurosurgery* 113, nr. 5 (november 2010): 1106–11.

**Voormolen, Eduard H**, Corie Wei, Eva W C Chow, Anne S Bassett, David J Mikulis, en Adrian P Crawley. "Voxel-Based Morphometry and Automated Lobar Volumetry: The Trade-off between Spatial Scale and Statistical Correction". *NeuroImage* 49, nr. 1 (1 januari 2010): 587–96.

Chow, Eva W C, Andrew Ho, Corie Wei, **Eduard H Voormolen**, Adrian P Crawley, en Anne S Bassett. "Association of Schizophrenia in 22q11.2 Deletion Syndrome and Gray Matter Volumetric Deficits in the Superior Temporal Gyrus". *The American Journal of Psychiatry* 168, nr. 5 (mei 2011): 522–29.

**Voormolen, Eduard H**, Sebastien Froelich, Peter A Woerdeman, Jan Willem Berkelbach van der Sprenkel, Weibel Braunius, en Luca Regli. "Surgical Instrument Tracking Optimizes Trans-Sphenoidal Endoscopic Treatment of Petrous Apex Cholesterol Granuloma". *Journal of Neurological Surgery. Part A, Central European Neurosurgery* 74, nr. 2 (maart 2013): 109–12.

Khlebnikov, Vitaliy, Daniel Polders, Jeroen Hendrikse, Pierre A Robe, **Eduard H Voormolen**, Peter R Luijten, Dennis W J Klomp, en Hans Hoogduin. "Amide Proton Transfer (APT) Imaging of Brain Tumors at 7 T: The Role of Tissue Water T1-Relaxation Properties". *Magnetic Resonance in Medicine* 77, nr. 4 (april 2017): 1525–32.

Sadik, Zjiwar H A, **Eduard H Voormolen**, Paul R A M Depauw, Bachtiar Burhani, Willy-Anne Nieuwlaat, Jeroen Verheul, Sieger Leenstra, Ruth E M Fleischeuer, en Patrick E. J. Hanssens. "Treatment of Nonfunctional Pituitary Adenoma Postoperative Remnants: Adjuvant or Delayed Gamma Knife Radiosurgery?" *World Neurosurgery* 100 (april 2017): 361–68.

## Dankwoord

Alle mensen die hebben bijgedragen aan dit proefschrift wil ik ontzettend bedanken. Een aantal mensen wil ik graag noemen:

**Prof. dr. P. Robe**, beste Pierre, je ongebreidelde enthousiasme en stimulerende advies over ons onderzoek zijn doorslaggevend geweest. Door jou heb ik dit proefschrift af kunnen maken. Ik bewonder je wilskracht, je 'shotgun approach' qua onderzoek, en hoe je je leven toewijdt aan ons mooie vak neurochirurgie. Dank voor de mogelijkheid die je voor mij creëerde, om een radiochirurgie stage in Columbus te volgen. Ook wil ik je hartelijk bedanken voor wat je voor mijn familie hebt betekend. Ik hoop nog veel van je te leren, en nog een keer samen eindelijk dat rondje golf te spelen op Durbuy...

**Prof. dr. M. A. Viergever**, beste Max, dank voor het vertrouwen dat je in mij gesteld hebt de afgelopen jaren. Je sturing was essentieel. Ik ben er trots op dat je mij hebt opgeleid als Biomedical Image Sciences student. Hierdoor is dit boekje een unieke mix geworden van beeldverwerking en neurochirurgie. Ik hoop in de toekomst dit soort multidisciplinair onderzoek te blijven doen en hierdoor een klein onderdeel te mogen zijn van jouw scientific legacy in de beeldverwerking.

**Dr. J.W. Berkelbach van der Sprenkel**, beste Jan Willem, wij hebben van het begin af aan een klik gehad. Jij zag iets in mij toen ik als student bij je kwam en vertelde dat ik neurochirurg wilde worden en ook wel even de neuronavigatie wilde verbeteren. Dit boekje is het resultaat van jouw vooruitstrevende ideeën. Je liet mij heel vrij in de uitvoering en het is gelukt: we hebben software gemaakt en toegepast op onze patiënten in de operatiekamer. Ik ben heel blij dat je naast mijn copromotor ook mijn opleider bent. Bovenal ben ik echt trots dat je aan mij jouw uitgebreide schedelbasischirurgie ervaring wilt doorgeven. Het was voor mij heel speciaal om je ook buiten werk om te mogen leren kennen als aimabele vader, en toegewijde partner van Marloes. Hoogtepunt voor mij was het bezoek aan jullie prachtige wijngaard in Toscane. Ik hoop dat we in de toekomst nog vele glazen uit Piebertie mogen drinken...het liefst na een lange dag samen opereren aan de schedelbasis.

**Dr. H.J. Noordmans**, beste Herke Jan, ik wil je bedanken voor je hoog-technische inbreng vanuit het oogpunt van de klinische fysica, zonder welke dit project niet had kunnen slagen. Je scherpe feedback op onze stukken heeft ook veel geholpen. Je hield goed in de gaten dat de boel niet te 'commercieel' werd opgeschreven. Desalniettemin, kon je commercieel vermaak

ook goed waarderen, zag ik, toen wij samen in Disney World Florida waren voor een congres. We gaan elkaar vast nog veel spreken voor het vervolgonderzoek wat uit dit boekje vloeit.

**Prof. dr. R. Stokroos, Prof. dr. P. Luijten, Prof. dr. C. Terhaard, en Prof. dr. W. Peul**, bedankt voor de tijd en moeite die jullie genomen hebben om mijn proefschrift te beoordelen. Ik ben er zeer trots op om straks in het historische Academieggebouw van gedachten te mogen wisselen.

**Prof. dr. S. Froelich**, dear Sébastien, thank you for taking the time to assess my thesis. It absolutely is a great honor for me to become your skull base fellow at l'hôpital Lariboisière in Paris. I hope to learn from your elegant anatomical dissection techniques, and the much-needed nuance you bring to the field. My family and I are looking forward to this fantastic adventure.

**Dr. M. van Stralen**, beste Marijn, jij hebt mij werkelijk ontzettend veel geholpen met dit project. Eindeloze uren koffietjes drinken en discussiëren over hoe we de software moesten vormgeven. Jij hebt mij alle fijne kneepjes van C++, python en MeVisLab geleerd. Altijd als ik een probleem had met het programmeren dan stond jij voor me klaar. Zonder jou waren er geen nieuwe algoritmen geweest, en dus ook geen promotie. Door mijn klinische verplichtingen ben ik je de laatste tijd, tot mijn spijt, uit het oog verloren. Ik hoop dat we de banden weer kunnen aanhalen. Misschien is het weer tijd voor biertjes in Bremen?

**Dr. P.A. Woerdeman**, beste Peter, het was jij die me enthousiast maakte voor computer geassisteerde neurochirurgie. Toen ik in Utrecht begon, ging jij promoveren op dit onderwerp. Ik ben trots dat ik in jouw voetsporen mag treden met dit boekje. Je hebt me geholpen om dit project op te starten, en ook weer de laatste tijd om het goed af te sluiten. Ik bewonder je keuze voor de kinderneurochirurgie, maar hoop stiekem dat we samen in de toekomst nog meer onderzoek mogen doen op het gebied van beeld-geleid opereren.

**Prof. dr. L. Regli**, dear Luca, you were the role-model that made me want to become a neurosurgeon. Thank you for accepting me as your resident in Utrecht. Thank you for your support of this research project from the very start. I have learned a great deal from your meta-vision while addressing clinical problems, and from observing your meticulous surgical technique in the operating theatre. It was hard for me when you left, but it is my dream to work with you again in the future, either in the OR, or on the buckelpiste, but preferably both. Thank you for inspiring me!

**Drs. S. Diederer**, beste Sander, de grap dat jij een soort jonge versie bent van mij, snijdt nu ik erover nadenk wel hout, en daar ben ik supertrots op. Je bent mijn Equites-maatje, lid, collega AIOS, en nu ook bekeerd tot beeldverwerking-onderzoeker. Je hebt mij, eerst als mijn student, en later als onderzoeksmaatje veel geholpen met de stukken in dit proefschrift. Belangrijker nog, toen ik mijn knie had gebroken, heb jij mij de trap op gesjouwd. Hoe was ik anders boven gekomen? Ik bewonder je praktische creativiteit, en je interesse in zo een beetje alles. Ik zal altijd proberen je te helpen waar nodig. Hoop dat we samen blijven, opereren, meten, schrijven, programmeren en natuurlijk...peren.

**Prof. dr. R. Bleys**, beste Ronald, ik wil je hartelijk bedanken voor het feit dat ik altijd bij de afdeling anatomie mocht binnenwandelen met het verzoek voor een hoofd voor mijn onderzoek...en dat ik deze dan ook direct kreeg! Ik realiseer me goed dat jij ons hiermee mogelijkheden gaf, welke op maar weinig plekken op de wereld bestaan.

**Dr. T. van Doormaal**, beste Tristan, wat kijk ik tegen jou op. Toen ik net bij de neurochirurgie begon, introduceerde je me op het lab van BTI/ELANA. Mede door jou kon ik daar de experimenten uitvoeren die dit proefschrift mogelijk hebben gemaakt. Over de jaren heen, heb ik jou, Maartje, en je drie kleine dames, steeds beter mogen leren kennen. Maar onze tijd samen in Columbus was met name speciaal voor me: bestralen, crossfitten, levensbeschouwing, repeat. En dan AMRAP in drie maanden. Ik bewonder je moed en mondigheid, en je operatieve skills. Je weet het, ik kocht je huis over met de hoop dat er een beetje van jouw neurochirurgische eigenschappen via de muren op mij af stralen.

**Claartje Beks-Ypma, en het Brain Technology Institute team**, dank voor de geweldige tijd in jullie state-of-the-art onderzoeksinstituut. Wat is dat een inspirerende omgeving voor een onderzoeker! Bedankt voor de gezelligheid, kansen, en steun. Ik wil speciaal bedanken: Felix von Coerper, Rutger Tulleken, Saskia Redegeld, Glenn Bronkers, Rick Mansvelt Beck, André van Dieren, en Sander van Thoor. De naam-stoeltjes voor onze tweeling worden nog veelvuldig gebruikt!

**Prof. dr. C. Tulleken**, beste professor, u bent de godfather van de Utrechtse neurochirurgie. Het was een eer dat ik u, na uw pensioen, toch heb mogen meemaken op BTI/ELANA. Zo bijzonder was het, dat U altijd geïnteresseerd was in mij en mijn onderzoek. Dank dat u mij heeft onderwezen in zowel micro-vasculaire anastomose technieken, als Spinoza.



**Dr. H. Thomeer**, beste Hans, wat is het een ontzettend geweldig dat wij elkaar gevonden hebben in de passie voor schedelbasis chirurgie. Ik weet zeker dat onze pa's trots zijn op wat we al bereikt hebben! Het lijkt me fantastisch om onze samenwerking tot een nog veel hoger niveau te tillen in de toekomst, zowel professioneel als privé.

**Dr. D. Blakaj**, dear Duk, thank you for your hospitality and guidance during my time in Columbus, OH. It was a great honor to learn from such a gifted and open-minded radiation oncologist. But it was even nicer that you showed us around town and that I had the pleasure to get to know your wonderful family. Let's keep in touch, and I hope to continue to count on you for game tickets! Go Crew!

**Studenten**, beste Jeroen van Norden en Oscar Jimenez del Toro, dank voor jullie inzet voor mijn onderzoek. Dank Jeroen, voor je bijdrage aan de kadaver experimenten. Thanks Oscar, for your work on semi-automated segmentation of the sigmoid sinus.

**Stafleden neurochirurgie van het UMC Utrecht**, graag wil ik jullie allemaal bedanken voor de fantastische klinische opleiding die jullie mij geven. Ik heb een zeer goede theoretische achtergrond gekregen, en van een ieder heb ik truckjes voor in mijn chirurgisch repertoire afgekeken. Ik ben er trots op om te zeggen dat ik in Utrecht ben opgeleid.

**Dr. K. Han**, beste Sen, jou wil ik graag apart noemen. Je bent een inspiratie voor mij als neurochirurgisch 'alleskunner', maar vooral als mens. Ik hoop ooit mijn leven net zo mooi in balans te krijgen als jij. Dank voor wat je hebt gedaan voor mij en mijn familie. Jouw absolute rust als het even lastig is tijdens een operatie, en daarbij de befaamde woorden 'beetje surgical, even wachten' zal ik nooit vergeten.

**Albi van Angelen**, bedankt voor alles wat je voor mij hebt gedaan Albi. Je was voor mij altijd een soort zorgzame moeder binnen la familia der Utrechtse neurochirurgie.

**Stafleden neurochirurgie van het St. Elisabeth Ziekenhuis Tilburg**, jullie hebben mij enorm veel geleerd op neurochirurgisch en intermenselijk vlak, in de anderhalf jaar dat ik bij jullie mocht werken. Jullie hielpen mij om chirurgisch zelfvertrouwen te ontwikkelen. Het is inspirerend om te zien hoe jullie vakgroep samenwerkt, en het vak neurochirurgie verder brengt. Zeker qua schedelbasischirurgie, vind ik jullie vooruitstrevend en toonaangevend.

**Collega assistenten, PA-ers, verpleegkundigen, operatie assistenten, en overige medewerkers** van het cluster Neurologie & Neurochirurgie van het UMC Utrecht en van het St. Elisabeth Ziekenhuis Tilburg, ik wil jullie bedanken voor de zeer prettige samenwerking de afgelopen jaren.

**Vrienden van de KGB, MGA, Equites, en jaarclub Steiger**, dank voor jullie geduld met deze te vaak afwezige man. Jullie hebben mij geïnspireerd, gevormd en gemaakt. Weet dat jullie vriendschap heel speciaal is voor mij. Ik sta altijd voor jullie klaar.

**Georg Krijgh en Lucas de Breed**, het is eervol om met zulke succesvolle en trouwe vrienden aan mijn zijde dit proefschrift te mogen verdedigen. De periode die we samen beleefden in I-House in UC Berkeley, is een van de meest vormende geweest in mijn leven. Dat we elkaar de afgelopen jaren iets minder frequent gezien hebben heeft nul relevantie. Want dat wij er straks weer met z'n drieën staan vind ik super 'Vo.

**Erik en Monique, en Caspar, Harmen, Edith, Iris, en Dominique**, bedankt voor jullie interesse in mijn onderzoek, en met name bedankt dat ik een deel mocht worden van jullie hele bijzondere gezin. Ik ben zo blij met de van Munster-package deal, waardoor ik vijf fantastische broers en zussen erbij kreeg! De reis naar Lapland was een hoogtepunt. Carpe diem, want het glas is half vol.

**Nora**, mijn lieve organizoes, je hebt het steeds voor mij opgenomen, en je hebt gezorgd dat je puberende broertje op het rechte pad bleef. Ik ben zo blij dat jij een mooie eigen familie met Alexandr hebt gekregen, en je daarbij ook nog de uitdagende academische carrière kan hebben die je graag wilde. Milan, Oscar, en ook Christiaan, jullie zijn supercoole gasten! Ik zie ernaar uit om nog vele vuurtjes te stoken in Korytná samen met jullie!

**Papa en Mama**, mijn parental units, wat hebben jullie mij een enorm stimulerende multiculturele opvoeding gegeven waarin de mogelijkheden om mijzelf te ontwikkelen nagenoeg onbeperkt waren. Mama, ik ben blij met jouw sturende opvoeding en gepassioneerde levensadviezen vanuit het Tsjechische perspectief. Papa, je leerde me Hollandse nuchterheid en vooral: zelf keuzes maken. Ik kan met trots zeggen dat ik gekozen heb voor jouw vak. Papa en Mama, dank dat jullie mij altijd intens gestimuleerd hebben om een carrière na te streven, maar vooral ook geleerd hebben dat familie het allerbelangrijkste is in het leven.

**Isabelle, Victor en Maximus**, jullie zijn mijn koekie, mijn apie, en ons C-tje! Supertrots ben ik dat jullie mijn genen bij jullie dragen.

**Lieve Daphne**, jij bent degene van wie ik het allermeeft heb geleerd. Technisch gesproken ben jij mijn mooiste wifi, en het allerbeste moederbord dat er bestaat voor onze drie bits. Kristalhelder is het, dat ik het leven samen met jou ga sjeffen, want wij hebben synergie. Laten we elkaar blijven uitdagen tot we een oud opaatje/omaaatje zijn, en uiteindelijk samen vergaan tot sterrenstof.

## Curriculum Vitae



Eduard Voormolen was born on 21<sup>st</sup> of February, 1983 in Leiden, the Netherlands. After finishing a Dutch-English bilingual Gymnasium high school program at the Rijnlands Lyceum, Oegstgeest in 2001, he continued his undergraduate education at University College Utrecht (UCU) from 2001 to 2004, during which he enrolled as a foreign exchange student at University of California, Berkeley CA, in the United States. Furthermore, during his time at UCU, the author spent 4 months at the Toronto Western Hospital in Toronto, Canada to perform research on voxel-based morphometry. A 4-year accelerated medical school program SUMMA (Selective Utrecht Medical Masters), was started at the University of Utrecht in 2004. In 2006 Eduard also enrolled in the master program biomedical image sciences (BIS) at the University of Utrecht. SUMMA and BIS were successfully completed in 2009 and 2010.

Plans to become an interventional radiologist were made, and a research project investigating new MRI techniques for imaging blood flow in arteriovenous grafts for renal dialysis was initiated at the department of Radiology of the UMC Utrecht. However, during his clinical rotation as an intern at the department of Neurosurgery, Eduard was inspired to become a neurosurgeon. A personal grant from the Alexandre Suerman foundation was obtained for a research project at the department of Neurosurgery and Image Sciences Institute about computer-assisted skull base surgery, which culminated into the current thesis. A MD-PhD grant was received from ZonMW (The Netherlands Organization for Health Research and Development), and neurosurgical residency under the supervision of Prof. L. Regli was started in December 2011. Besides receiving education in neurosurgery at the UMC Utrecht (training supervisor: Dr. J.W. Berkelbach van der Sprenkel) and St. Elisabeth Hospital, Tilburg (training supervisor: Dr. G. Beute), the author was trained (and certified) in stereotactic radiosurgery at the James Cancer Hospital, Wexner Medical Center, Columbus OH, in the United States (training supervisors: Dr. D. Blakaj and Prof. A. Chakravarti). He will complete his neurosurgical residency at the end of 2018 under the supervision of Prof. P.A. Robe at the UMC Utrecht. Eduard is married to Daphne Voormolen-van Munster. He has a daughter (Isabelle) and two sons (Victor and Maximus).

```

#-----
#!           Macro module EVADE
#/*!
# \file      Evade.py
# \author    ehjvoormolen
# \date      2018-07-10
# */
#-----

def navigate():
    structures = getstructures()
    boolupdate = 0
    boolnav = 0
    boolpointer = 1
    boolnowarnings = 1
    homingvalue = "none"
    while (ctx.field("Navigate").value == 1):
        ctx.field("StealthLink2.getInstrument").touch()
        #check if tool is visible
        if ctx.field("StealthLink2.toolStatus").value == 0:#0 !!! voor klinisch gebruik
            #boolupdate = 1 --> check if tool is far away from anatomy in the future then up-
            date the 3D drilling
            # calculate distances
            #print max(getdistances(structures))
            if getwarnings(getdistances(structures)):
                boolnowarnings = 0
            else: boolnowarnings = 1
            #homingvalue = homing(ctx.field("Calculator.resultVector1").value, ctx.field("HOM-
            sensitivity").value, homingvalue)
            # put green cross in postion
            ctx.field("ShowPosition.worldPosition").value = ctx.field("StealthLink2.instrument-
            Tip").value
            # ctx.field("ViewScan2D.worldPosition").value = ctx.field("StealthLink2.instrument-
            Tip").value
            # put vectorline in position
            ctx.field("ToolView.start").value = ctx.field("StealthLink2.instrumentTip").value
            ctx.field("ToolView.end").value = ctx.field("StealthLink2.instrumentHind").value
            # put tip extension in position
            ctx.field("TipExtensionCalc.v1").value = ctx.field("StealthLink2.instrumentTip").
            value
            ctx.field("TipExtensionCalc.v2").value = ctx.field("StealthLink2.instrumentHind").
            value
            ctx.field("TipExtension.end").value = ctx.field("StealthLink2.instrumentTip").value
            # perform virtual drilling
            ctx.field("MarkerDrillHB Vector Start Position").value = ctx.field("StealthLink2

```

